HEINRICH HEINE
UNIVERSITÄT
DÜSSELDORF

Ultrafast relaxation dynamics of carotenoid excited states

Inaugural-Dissertation

zur Erlangung des Doktorgrades
der Mathematisch-Naturwissenschaftlichen Fakultät
der Heinrich-Heine-Universität Düsseldorf

vorgelegt von

Evgeny Evgenievich Ostroumov
aus Moskau, Russland

Düsseldorf/Mülheim an der Ruhr, Juli 2010

aus dem Max-Planck-Institut für Bioanorganische Chemie, Mülheim an der Ruhr

Gedruckt mit der Genehmigung der
Mathematisch-Naturwissenschaftlichen Fakultät der
Heinrich-Heine-Universität Düsseldorf

Referent: Prof. Dr. Alfred R. Holzwarth
Koreferent: Prof. Dr. Georg Pretzler

Tag der mündlichen Prüfung: 8 Juli 2010

All truths are easy to understand
once they are discovered;
the point is to discover them.

Galileo Galilei

CONTENTS

Abbreviations

BNI	benzonitrile
DADS	decay-associated difference spectra
DAS	decay-associated spectra
DEE	diethyl ether
DFT	density functional theory
ESA	excited state absorption
FC	Frank-Condon
GB	ground state bleaching
HEX	n-hexane
IC	internal conversion
ICT	intramolecular charge transfer state
IRF	instrument response function
ISRS	impulsive stimulated Raman scattering
LFD	lifetime density maps
MEM	maximum entropy method
MO	molecular orbital
MRCI	multireference configuration interaction approach
MTHF	methyltetrahydrofuran
RC	reaction coordinate
SADS	species-associated difference spectra
SAS	species-associated spectra
SE	stimulated emission
TA	transient absorption

Chapter 1

Introduction

1.1 Overview and discovery

Carotenoids belong to a very abundant family of pigments in nature. They are responsible not only for the bright orange/red coloring of plants (e.g. fruits, flowers, stems), but also for diverse colors of insect bodies, skin and feathers of birds, skin and flesh of fish. Although carotenoids can be synthesized only by plants and microorganisms, they are found in all living organisms often via food uptake. Carotenoids have multiple vital functions. As an efficient light-harvesters present in almost all photosynthetic organisms they absorb light in the visible spectral range and transfer the excitation energy to the chlorophylls. Carotenoids can act as antioxidants: they prevent singlet oxygen formation and in this respect inhibit the destructive oxidation of biological macromolecules. Oxidation processes are known to affect the structure and function of proteins, lipids and DNA. Thus, carotenoids, as antioxidants, play an important role in protection of the organism against cancer and some other diseases. Moreover, β-carotene and other carotenoids with unsubstituted β-ring are the main source for vitamin A synthesis, which is essential for the normal growth and development of the immune system and vision. Carotenoids are also used in nature to stabilize the structure of proteins and are important building blocks in protein macromolecules.

The first carotene molecule was isolated from carrot roots in 1831 by H. Wackenroder (see (Govindjee, 1999) for a review). In 1837 xanthophylls as yellow pigments were reported by Berzelius who observed them in the autumn leaves. Officially the class of carotenoids received its name in 1911 from M.S. Tswett, who was able for the first time to isolate and purify the xanthophylls and carotenes using chromatography. The chemical structure of β-carotene was determined in 1931 by P. Karrer and for this work he received a Nobel Prize in 1937. In the crystalline form carotenoid molecules were obtained in 1950. More than 700 naturally occurring carotenoids were isolated since the discovery of carotenes in 1837 and substantial knowledge on their structure and function in plants and animal tissues has since been accumulated (G. Britton et al., 2004). However, despite the intense research in many fields of science, the electronic structure of carotenoids and the mechanisms of energy transfer and antioxidative action still remain uncertain.

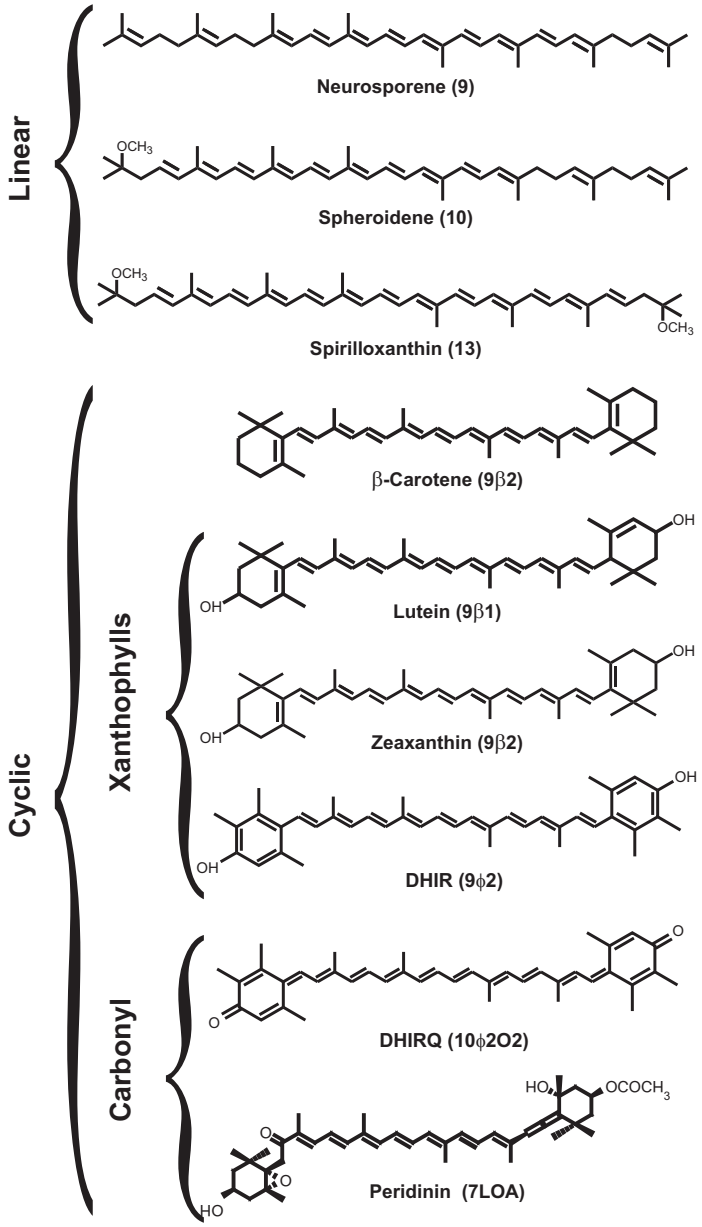

Figure 1.1. Molecular structures of selected carotenoids. The classification is shown on the left side. Notations: number - conjugation length of the linear chain, β – conjugation in the end rings, ϕ – conjugation in aryl rung, O – conjugation in the carbonyl, L – lactone ring, A – conjugation in the allene moiety (IUPAC/IUB, 1975).

1.2 Chemical structure and electronic properties

The spectroscopic features and electronic properties of carotenoids are defined by their molecular structure and can vary substantially (Fig. 1.1). The 'core' element of a carotenoid molecule is a symmetrical tetraterpene skeleton formed by linkage of two 20-carbon units. In many carotenoids the end groups are modified into rings at one or both ends giving monocyclic or dicyclic carotenoids. The oxygen-containing carotenoids belong to a separate sub-class of xanthophylls.

The main spectroscopic properties of carotenoids are defined by the backbone consisting of the conjugated system of C=C double bonds and can be well modeled by linear polyenes. Linear polyenes belong to the same C_{2h} point symmetry group and are more suitable for theoretical studies because of their simpler structure. Here C_2 refers to a twofold rotation symmetry around an axis perpendicular to the molecular plane, and *h* refers to the σ_h operation, i.e. reflection across the molecular plane.

The electronic states of polyenes can be described based on the molecular symmetry group by four irreducible representations: A_g, A_u, B_g, B_u (see Table 1.1). Here 'A' and 'B' refer to symmetric and antisymmetric representations with respect to the 180° rotation operation (C_2), while 'u' and 'g' refer to symmetric and antisymmetric representations with respect to the inversion operation (*i*, combination of C_2 and σ_h operations). Double occupation of each molecular orbital leads to a wavefunction that is necessarily symmetric under the mirror plane reflection operation (σ_h=1) and therefore only two representations, namely A_g or B_u (rows 1 and 4 in Table 1.1) are possible. Since pairwise filling leads to a symmetric wavefunction with respect to both the C_2 and *i* operations (C_2=1, *i*=1), the ground state is always an A_g state (row 1 in Table 1.1). In addition to the symmetry notations the state labels for polyenes usually carry '+' and '-' superscripts, which denotes the pseudoparity character as introduced by Pariser (R. Pariser, 1956). The order of the states of the same symmetry is labeled by a number in front of the symmetry symbol and the singlet (triplet) character is denoted by superscript number respectively. According to these rules the ground singlet state (S_0) is labeled as $1^1A_g^-$ - first (ground) singlet state symmetric with respect to the C_2, *i* and σ_h operations (row 1 in Table 1.1) and has a negative pseudoparity sign. In a similar manner the first excited singlet state (S_1) in carotenoids and long polyenes has the same symmetry as the ground state and is labeled $2^1A_g^-$, whereas the second excited state (S_2) is often the $1^1B_u^+$ state.

Table 1.1 C_{2h} symmetry table for notation of electronic states of linear polyenes. E – identity operator, C_2 – rotation by 180^0 operator, *i* – inversion operator, σ_h - mirror plane reflection operator.

C_{2h}	E	C_2	*i*	σ_h
A_g	1	1	1	1
B_g	1	-1	1	-1
A_u	1	1	-1	-1
B_u	1	-1	-1	1

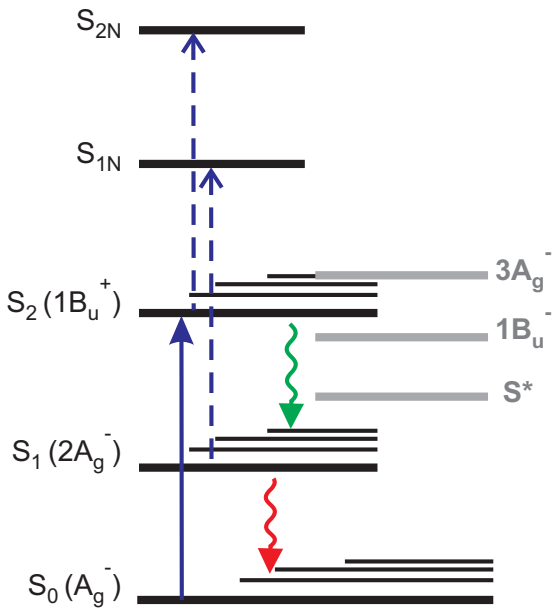

Figure 1.2. Typical energy level scheme of a carotenoid molecule. Straight solid arrow – ground state absorption transition, dashed straight arrows – excited-state absorption, wavy arrows – internal conversion and dissipation. Grey levels – electronic 'dark' states.

Transitions between electronic states are defined by the optical selection rules, which state that if the transition moment function (product of the wave-functions of the two states and the transition moment operator, e.g. A_g*μ*B_u) is symmetric then the transition is allowed, otherwise it is forbidden. The transition dipole moment has a vector form μ={x,y,z}. The coordinates are shown in Table 1.1 (see last column). The symmetry of a transition (and therefore its allowedeness) is defined as

$$A_g \cdot \mu \cdot B_u = (1 \quad 1 \quad 1 \quad 1) * \begin{pmatrix} 1 & -1 & -1 & 1 \\ 1 & -1 & -1 & 1 \\ 1 & 1 & -1 & -1 \end{pmatrix} * (1 \quad -1 \quad -1 \quad 1) = \begin{pmatrix} A_g \\ A_g \\ B_g \end{pmatrix}, \qquad (1.1)$$

From this equation it follows that for all three coordinates of the transition moment operator μ the product is symmetric ('*g*' - gerade) and therefore the transition is allowed. Similarly one can show that generally transitions between states with the same symmetry are forbidden (e.g. S_0-S_1), and with different symmetry – are allowed (e.g. S_0-S_2, see Fig. 1.3). The S_0-S_2 transition in carotenoids has a well known intense absorption band in the blue-green spectral range and because of this transition carotenoids have their well known yellow-red color. Forbidden states, i.e. states that can not be observed via light absorption from the ground state (like the S_1 state, see Fig. 1.2) are often called in the literature as 'dark states'.

1.3 Quantum chemical calculations

The strong S_0-S_2 transition is of a π-π^* type and can be well described by simple molecular orbital theory (MO) or by the free-electron model (B.E. Kohler and I.D.W. Samuel, 1995; R.L. Christensen, 1999). These simple models are based on the Hartree-Fock (HF) approach which treats the molecule as a system consisting of single electrons where each of the electrons moves independently in an average field of the other electrons and nuclei. Within the HF approach the many-body problem is transformed to a set of single-particle equations (HF equations). The HF approach is the simplest approximation of the general electronic Schrödinger equation. It can explain, for instance, the bathochromic shift (to longer wavelengths) of the S_0-S_2 transition for carotenoids (and polyenes) with increasing conjugation length. However methods based on the HF approach cannot take into account the correlation between electrons, and therefore, many spectroscopic effects cannot be reproduced.

The configuration interaction approach (CI) is method that makes it possible to take into account the electron-electron correlation. However the limitations of the method allow to use it for ground-state calculations only (with a few exceptions). For excited-state calculations the multireference configuration interaction approach (MRCI) is used. Here in addition to singly excited configurations (HOMO-1$\rightarrow$LUMO and HOMO$\rightarrow$LUMO+1) the doubly (HOMO,HOMO $\rightarrow$LUMO,LUMO etc.) and higher order excited configurations are included. The MRCI approach describes more correctly the properties of the low lying electronic states (e.g. state ordering of the $E(2^1A_g^-)<E(1^1B_u^+)$ states). However calculations based on CI as well as MRCI methods are very time consuming (P. Tavan and K. Schulten, 1986).

The density functional theory (DFT) approach has a completely different concept and has proven to be a reliable and inexpensive method (R.G. Parr and W. Yang, 1989; R.M. Dreizler and E.K.U. Gross, 1990). In the DFT approach any multibody system can be defined in the form of an electronic density functional. The drawback of the method is that the construction of a functional is rather empirical: functional is ether obtained by fitting to the experimental data or is modeled on the basis of *a priory* knowledge of the system features. The DFT is based on the Hohenberg-Kohn theorems. The first theorem states that the electron density and the external potential containing the electron-nuclei attraction (and any additional magnetic/electric field) are mapped one-to-one. The second theorem guarantees the existence of the variational principle for electron densities such that the electronic energy of a system calculated with a trial density is always higher than the total energy obtained with the exact density. The Kohn-Sham formalism within the DFT approach allows to transfer a static many-

electron problem to a set of fictitious single electron problems, in which each electron moves in an effective potential. In contrast to the HF approach, the interaction between electrons within the Kohn-Sham formalism can be taken into account via exchange-correlation terms in a functional. However, since the exact form of these terms is not known, approximations to the functional have to be made. With the advance of DFT methods many of exchange-correlation functionals have been introduced.

The essence of the DFT approach is such that the system has a definite state only at the lowest energy, thus the DFT approach is normally applied for ground state calculations. However, it can also be used for calculating particular excited state if certain constraints are introduced (e.g. spin multiplicity, irreducible representation of the excited state). As another method for calculations of electronically excited states without constraints the time-dependent DFT (TDDFT) was introduced (E.K.U. Gross and W. Kohn, 1990; M.A.L. Marques and E.K.U. Gross, 2004). It is based on the same Hohenberg-Kohn theorems reformulated in a time-dependent manner. The main disadvantage of the TDDFT approach is the single excitation basis giving strong deviations when double or higher excitations contribute, especially in large molecules (long polyenes and carotenoids (C.-P. Hsu et al., 2001; A. Dreuw and M. Head-Gordon, 2005)). To solve this problem combined DFT/CI and DFT/MRCI methods have been implemented (S. Grimme, 1996; S. Grimme and M. Waletzke, 1999)]. The main idea behind this combined approach is the use of information about dynamical electron correlation from DFT and the treatment of nondynamical effects by CI methods.

Recently the DFT/MRCI method was applied to linear polyenes, β-carotenes (N=3..11) and complex phenolic carotenoids (C.M. Marian and N. Gilka, 2008; M. Kleinschmidt et al., 2009; C.M. Marian et al., 2009). This combined approach for the first time reproduces well the state ordering and energy gap between different electronic states including the so-called ‘dark states’, which have pronounced double excitation character. The absolute values of excitation energies of the states tend to be underestimated by the method by 0.1-0.5 eV (800-4000 cm^{-1}) however (A. Dreuw and M. Head-Gordon, 2005; C.M. Marian and N. Gilka, 2008).

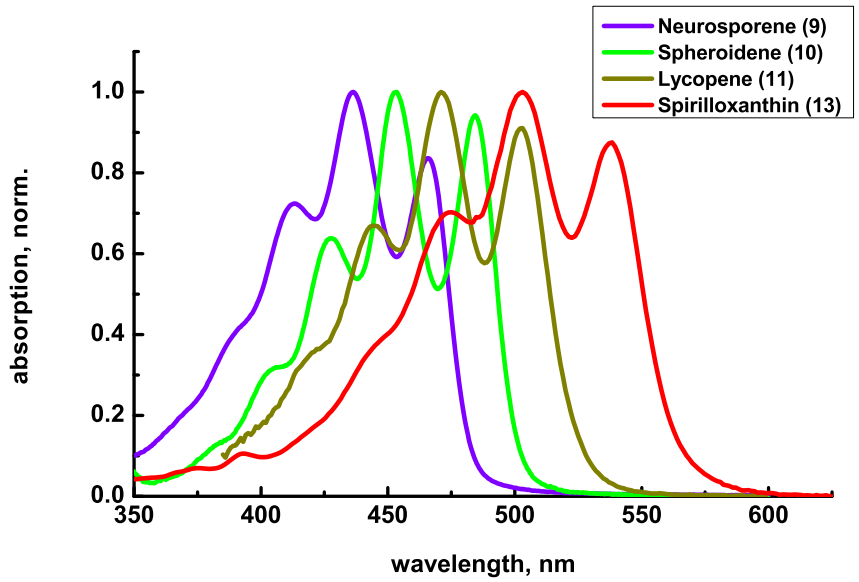

Figure 1.3. Typical absorption spectra of carotenoids with conjugation length N=9..13.

1.4 S_1 state of carotenoids

The transition between the ground state and the first excited state in carotenoids (and polyenes) is one-photon forbidden and therefore the S_1 state can not be observed directly by its absorption or fluorescence. A number of different techniques were applied to determine the energy and lifetime of the S_1 state. The fluorescence (R. Fujii et al., 2001; R. Fujii et al., 2001), resonance Raman (T. Sashima et al., 1998) (T. Sashima et al., 2000) and femtosecond S_1-S_2 transient absorption (T. Polivka et al., 2002; T. Polivka et al., 2002) studies showed that the S_1 energy is located between 11000 cm^{-1} (N>13) and 16000 cm^{-1} (N<9) (for a review see (T. Polivka and V. Sundström, 2004)). Although the values resulting from different methods can vary, the general tendency of the experimentally determined S_1 energies is in agreement with the energy gap law.

Transient absorption spectroscopy is the most popular and powerful method in studies of carotenoid relaxation dynamics. This method reveals the well known S_1-S_N ESA band in the 500-650 nm spectral range. Often vibrational cooling within the S_1 state with a lifetime below 1 ps can be observed in the transient absorption data. The measurements of the decay of the relaxed ESA signal of the S_1 state gave lifetimes between 1.4 ps for spirilloxanthin (N=13) (C.C. Gradinaru et al., 2001) and 35 ps for neoxanthin (N=8) (H.A. Frank et al., 2000). The S_1 lifetime follows the energy gap law (V. Chynwat and H.A. Frank, 1995) and can rise above 400 ps for shorter carotenoid homologs (P.O. Andersson et al., 1995) as well as

decrease below 1 ps for synthetic long-chain carotenoids (P.O. Andersson and T. Gillbro, 1995). In cases when the backbone of the molecule deviates from the ideal polyene, for instance, when complex end groups with a conjugation inside affect the polyene chain of the carotenoid, a notion of "effective" conjugation length n_{eff} is introduced (H.A. Frank et al., 1996; H.A. Frank et al., 2000; D. Kosumi et al., 2009), and the S_1 lifetime follows this n_{eff} values.

1.5 S_2 state of carotenoids

The main absorption band of carotenoids is located in the blue-green spectral range and has the three-peak profile (Fig. 1.3). This absorption band is solely due to the S_0-S_2 transition and the peak sequence reflects the vibrational structure of the system of conjugated carbon double bonds. Their spacing corresponds to the average of the two vibrational stretching modes – 1150 cm^{-1} (C-C) and 1600 cm^{-1} (C=C) (T. Polivka and V. Sundström, 2004). The position of this absorption band in carotenoids depends mainly on the conjugation length and is well described by the asymptotic dependence E=A+B/N, where E – energy of the transition, N – number of conjugated double bonds, A and B – additional parameters (P.O. Andersson and T. Gillbro, 1995). Additionally, the absorption band experiences up to 40 nm red shift in solvents with high refractive index (P.O. Andersson et al., 1991). The broadening and resolution of the bands is defined by the presence of non-bonded interactions between the methyl groups of the β-ionone or other type end rings with hydrogen atoms of the polyene chain (R.L. Christensen and B.E. Kohler, 1973; R. Hemley and B.E. Kohler, 1977).

Due to the very high internal conversion (IC) rate from the S_2 state to the S_1 state, no or only a very weak fluorescence is observed in carotenoids. Fluorescence up-conversion has revealed the lifetime of the S_2 state generally to be below 300 fs (A.N. MacPherson and T. Gillbro, 1998; S. Akimoto et al., 1999; S. Akimoto et al., 2000). The dependence of the τ_{S2} on the conjugation length is in accordance with the energy gap law for carotenoids with N<8. In longer carotenoids an inverse dependence is observed, i.e. the lifetime decreases with an increase of the conjugation length (S. Akimoto et al., 1999; T. Ritz et al., 2000). This effect is often explained by the appearance of other singlet states ('dark' states, see below) located for long carotenoids between the S_2 and S_1 states.

1.6 'Dark states' of carotenoids

In addition to the S_1 and S_2 excited states, additional low-lying states are discussed in the literature (for a review see (T. Polivka and V. Sundström, 2009)). In 1987 the localization of states with $1^1B_u^-$ and $3^1A_g^-$ symmetries below the S_2 state was predicted for carotenoids

with N≥9 and 13 respectively (Fig. 1.2) (P. Tavan and K. Schulten, 1987). The first experimental observation of these states (T. Sashima et al., 1999; R. Fujii et al., 2001) was based on the results obtained in Koyama's group using resonance Raman and steady-state fluorescence spectroscopy. Later, signatures of these states were found by time-resolved spectroscopy (on the time-scale of 300 fs and 40 fs) and were ascribed to the $1^1B_u^-$ and $3^1A_g^-$ states respectively (M. Ikuta et al., 2006). However these results were questioned by other groups (T. Buckup et al., 2006; D.M. Niedzwiedzki et al., 2006).

Another dark state, the S* state has been observed on the picosecond time scale. It was first observed in spirilloxanthin containing light-harvesting I (LHI) protein of *Rhodospirillum rubrum* (C.C. Gradinaru et al., 2001). This state was reported to act as an intermediate in the ultrafast formation of the triplet state of the carotenoid (E. Papagiannakis et al., 2002; E. Papagiannakis et al., 2003). An ESA band blue-shifted from the normal S_1-S_{1N} ESA band with ~6 ps lifetime was assigned to this S* state. The following experiments on isolated carotenoids have made the picture more complicated. In (D.S. Larsen et al., 2003) a similar signal labeled as $S^‡$ with a lifetime >50 ps was reported for β-carotene. The hypothesis of this new excited electronic state in isolated carotenoids was questioned by Wohlleben et al. (W. Wohlleben et al., 2004; T. Buckup et al., 2006). These authors applying the so-called Pump-Deplete-Probe technique a 10 ps signal in β-carotene and a 6 ps signal in carotenoids with N≥11 ascribed to a vibrationally hot-S_0 state populated via stimulated Raman scattering from the S_2 state. Another hypothesis for the S* state was suggested by H. Frank, where the role of cis- isomers was discussed and the characteristic blue-shifted signal of 2-5 ps in different carotenoids was ascribed to the S_1 state of the cis- isomer (D.M. Niedzwiedzki et al., 2006; D. Niedzwiedzki et al., 2007). More methods were applied to this problem (E. Papagiannakis et al., 2006; N. Christensson et al., 2009) but the origin of the positive shoulder on the short-wavelength side of the S_1-S_N ESA band remained unclear and controversial.

1.7 Charge transfer state of carotenoids

The group of carbonyl carotenoids plays an important role in a number of photosynthetic antenna systems from marine organisms (H.A. Frank, 1999; E. Papagiannakis et al., 2005; G. Guglielmi et al., 2005; T. Polivka et al., 2007). These carotenoids show unusual spectroscopic features and attracted substantial attention during the last decade. Peridinin and fucoxanthin, two members of this group, are known to be efficient light harvesters and their energy transfer efficiency to chlorophyll is approaching 100% (T.W. Goodwin, 1980; G. Britton et al., 1998). The main distinction of these carotenoids is the strong dependence of their spectral properties on the environment. The absorption of peridinin

in n-hexane shows the usual three peak structure. However in polar methanol the absorption band is strongly broadened and structureless (J.A. Bautista et al., 1999). The S_1 lifetime of peridinin decreases from 161 ps in nonpolar n-hexane to 12 ps in methanol. Similar effects were observed in other carotenoids containing carbonyl functional groups (H.A. Frank et al., 2000). The shortening of the lifetime and changes in the steady-state and transient spectra (D. Zigmantas et al., 2001) were ascribed to an intramolecular charge transfer (ICT) state which is formed between the carbonyl group and the carbon-carbon π-electron system. According to this explanation upon excitation a charge redistribution occurs and electron density shifts from the donor (conjugated carbon-carbon system) to the acceptor (carbonyl group). The stabilization of the negative charge on the keto groups in highly polar solvents leads to a multi-conformation state of the carotenoid and causes broadening and loss of the vibrational band structure. The stabilization of the ICT state also lowers its energy and therefore makes it an efficient quencher of the S_1 state via IC, which substantially shortens the S_1 lifetime. The picture is further complicated by the suggested strong mixing of the S_1 state and the ICT state. Despite intense studies of carbonyl carotenoids, especially peridinin, the exact electronic nature of the ICT state and its dynamics remained unclear.

1.8 Goals and structure of the work

The functions of carotenoids are very diverse and many of them are defined by their electronic excited state properties. Active research of carotenoids caring out since the middle of the last century in different branches of biology, chemistry and physics. However, despite of substantial efforts and multiple approaches the electronic structure and energy conversion processes in carotenoids remain unclear. In this field of particular interest are the so-called 'dark states' and their possible contribution to the relaxation dynamics in carotenoids. The main aim of this work was a systematic study of relaxation processes in carotenoids on the femtosecond and picosecond time-scales. The main questions raised in this work are:

i) What is the excited state ordering in carotenoids with N>9?

ii) What are the relaxation processes occurring during first 200-400 fs after excitation into the strong absorbing (S_2) state? Do the optically forbidden states take part in the excited state relaxation dynamics of carotenoids with conjugation length N>9, and what is their possible role?

iii) What are the origin, properties and functions of the S* state occurring on the picosecond time-scale in protein-bound and isolated carotenoids?

iv) What effects do carbonyl groups have on the electronic properties of carotenoids? What is the mechanism and role of the intramolecular charge transfer (ICT) states?

In order to answer these questions we have studied the excited state dynamics for a number of isolated carotenoids under a range of experimental conditions. Femtosecond transient absorption spectroscopy was applied to measure the relaxation dynamics and various theoretical models and approaches were used in the analysis of the experimental data. The results and interpretations were also checked by advanced quantum chemical calculations (in collaboration with the group of Prof. C. Marian).

In **Chapter 1** a general introduction to carotenoids spectroscopy is presented. The problem of the dark states and the main literature references in the field are summarized.

Chapter 2 gives a short description of experimental techniques, the data analysis algorithms and the sample preparation procedures that were used in the present work.

In **Chapter 3** the femtosecond relaxation dynamics of β-carotene and lutein is described. A target analysis together with quantum chemical calculations, performed by our collaborators in the Institute of Theoretical Chemistry, provided a proof for the localization of the 'dark $1B_u^-$ state' in the vicinity of the initially excited $1B_u^+$ (S_2) state. A system of optical Bloch equations used in the analysis algorithm gives an insight into the coherent behavior of the electronically excited states and provides an explanation for the oscillatory character of the experimental decays.

Chapter 4 presents a deeper study of the coherent behavior of the initially excited states using the Redfield theory approach in its general form. An assignment of the states in the model to the physical electronic states in carotenoids is suggested. Energies of the states, inter-state coupling strengths, and coupling to the bath (spectral density) from the transient absorption kinetics are studied.

Chapter 5 addresses the 'S* state' problem in β-carotene. A systematic study of β-carotene transient absorption decays measured on the picosecond timescale at different excitation wavelengths and pulse intensities allowed to explain the main features of the relaxation dynamics and to exclude the existing inconsistent models. It is concluded that the 'S* state' as such does not exist. It rather represents the vibrationally excited S_1 state.

In **Chapter 6** the study of the synthetic carbonyl carotenoid DHIRQ by transient absorption spectroscopy and quantum chemical calculations is presented. The effect of the carbonyl groups on the electronic properties and relaxation dynamics of this carotenoid is discussed. A drastic change in the decay lifetime and the system of electronic levels caused by

longer conjugation length and emergence of the intra-molecular charge transfer (ICT) state, respectively, are reported. DHIRQ is shown to be the carotenoid with the shortest lifetime (0.4 ps) observed so far.

Chapter 2

Materials and Methods

2.1 Transient absorption

Time-resolved spectroscopy is a widely used tool in solid state physics, chemical physics and biophysics to investigate the dynamic properties of complex systems. The method is based on the monitoring of the time-evolution of sample characteristics after optical excitation. When a chromophore is excited the absorbed light is transformed into the energy of an excited electronic state. The system then relaxes to the ground state via various processes, e.g. fluorescence emission from excited singlet states, internal conversion (IC), inter-system crossing (ISC) to a triplet state, transfer to different molecule, chemical reaction etc. (Fig. 2.1, Jablonski diagram). Transient absorption is the most informative technique among the linear regime time-resolved methods since it can measure the population dynamics of every intermediate state which takes part in the relaxation process and has some optically allowed transitions (see **Chapter 1**).

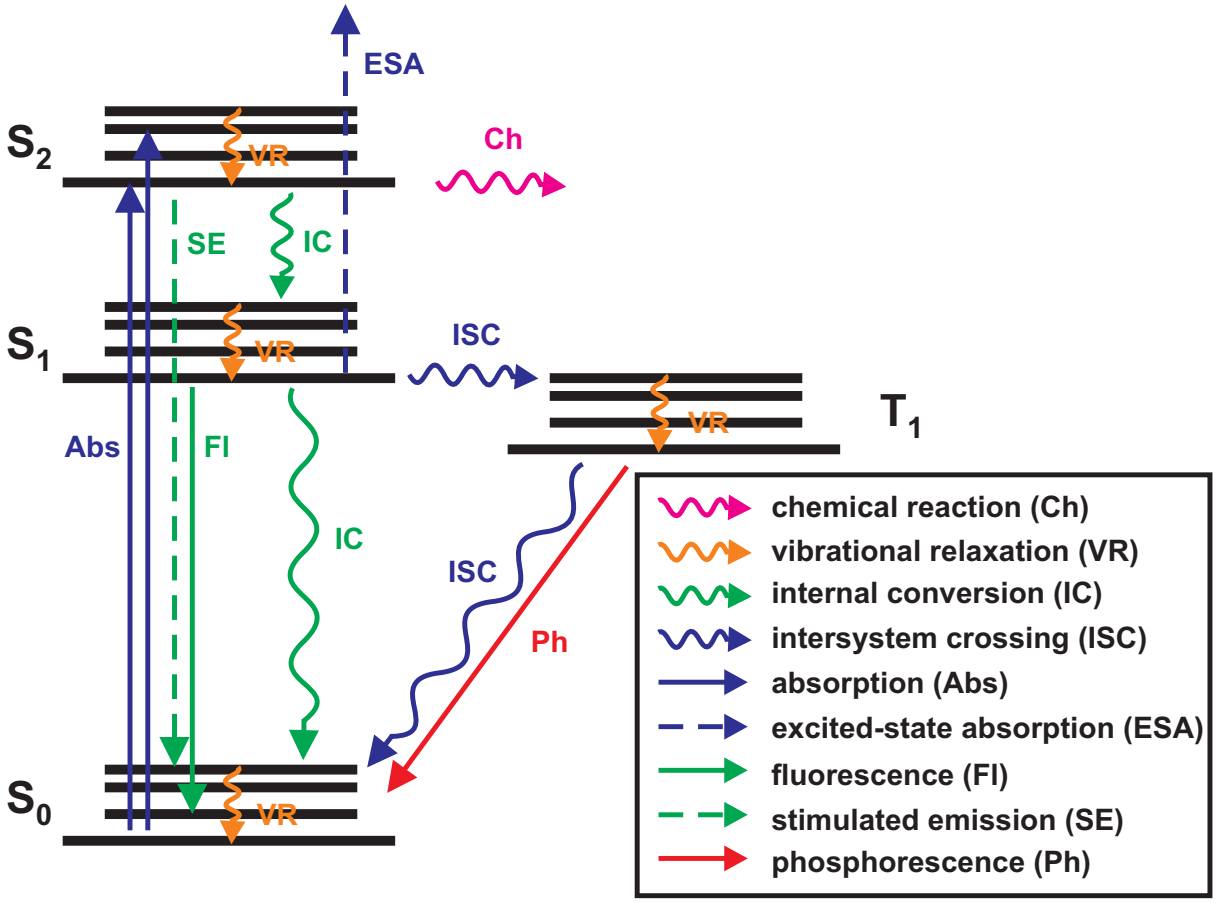

Figure 2.1. Jablonski diagram of possible transitions between electronic states (S_n – singlet, T_n - triplet) of a molecule. Straight arrows – radiative transitions, wavy arrows – radiationless transitions. S_0 – ground state, S_1 and S_2 – excited singlet states, T_1 – triplet state, Abs – absorption of photons (excitation), Fl – fluorescence, SE – stimulated emission, ESA – excited-state absorption, VR – vibrational relaxation, IC – internal conversion, ISC – intersystem crossing, Ph – phosphorescence, Ch – photoinduced chemical reaction.

The transient absorption is a pump-and-probe technique where the change in the absorption of the sample is measured by a probe pulse at a delay Δt after the sample excited by pump pulse at t=0. The absorbance A of the media or optical density (OD) is a function of the wavelength of the light and it is defined by the Lambert-Beer law and is as follows:

$$A(\lambda) = -\log\left(\frac{I(\lambda)}{I_0(\lambda)}\right)$$

Here $I_0(\lambda)$ – is the incident intensity, and the $I(\lambda)$ – is the intensity of the transmitted light. The probe pulse has low energy and is spectrally broad in order to measure all the possible transitions in the $\Delta\lambda$ spectral rage. In contrary, the pump pulse is usually strong and spectrally narrow in order to excite only a specific electronic level. Thus measuring absorbance of the sample after excitation by a pump pulse A_{on} and absorbance without preceding excitation A_{off} one can follow the changes in the sample. The difference absorbance ΔA is:

$$\Delta A(\lambda,t) = A_{on}(\lambda,t) - A_{off}(\lambda,t) = -\log\left(\frac{I_{on}(\lambda)}{I_0(\lambda)}\right) + \log\left(\frac{I_{off}(\lambda)}{I_0(\lambda)}\right) = -\log\left(\frac{I_{on}(\lambda)}{I_{off}(\lambda)}\right)$$

Measuring the spectrum of $\Delta A(\lambda,t_i)$ at each delay time t_i and scanning the delay time the evolution of $\Delta A(\lambda,t)$ can be recorded. Since the absorbance A_{off} probes the population of the ground state and does not change with time, whereas the A_{on} measures the absorbance of the population by the pump pulse excited state, the $\Delta A(\lambda,t)$ describes the relaxation of the excited state(s). It is important to note that interpretation of the transient absorption data is often complicated due to the time and spectral overlap of the different electronic transitions. The ΔA spectra can be both positive (excited state absorption, ESA) and negative (ground state beaching and stimulated emission, GB / SE). In some cases an additional pulse is introduced between the pump and probe pulses in order to measure more selectively a transition of interest or to deplete a particular state (F. Gai et al., 1997; D.S. Larsen et al., 2003; W. Wohlleben et al., 2004).

2.2 Experimental setup

The measurements were performed with the help of an integrated one-box, computer controlled Ti:Sapphire amplified laser system (Libra, Coherent) (Fig. 2.2). This system contains an integrated Vitesse (Coherent, Paio Alto) seed laser, an Evolution (Coherent) pump laser, a regenerative amplifier and a stretcher/compressor unit. The seed laser produces very weak ultrashort pulses (FWHM <50 fs) at 80 MHz repetition rate and is composed of a CW diode-pumped Nd:YVO_4 laser (second harmonic at 532 nm) and a mode-locked Ti:Sapphire oscillator (800 nm). The Evolution pump laser for the regenerative amplifier is a diode-

pumped, second harmonic (527 nm) Q-switched Nd:YLF laser. The integrated stretcher/compressor and the regenerative amplifier are used for chirped pulse amplification of the Ti:Sapphire output to a power of 1.4 W, 3 kHz repetition rate, pulse width of 60-80 fs (transform-limited regime). The amplified pulses are centered at 800nm. From the Libra output, part of the excitation is used for white light continuum generation to produce probe pulses and the main part is directed to the optical parametric amplifier (TOPAS, Light Conversion), where the frequency of the excitation is doubled in the BBO crystal and the output wavelength can be tuned in the 400-510 nm range. The TOPAS output power is ~5 mW. In order to avoid unwanted polarization effects, polarization of the pump and the probe beams was set at 54.7° (magic angle) between the polarization directions.

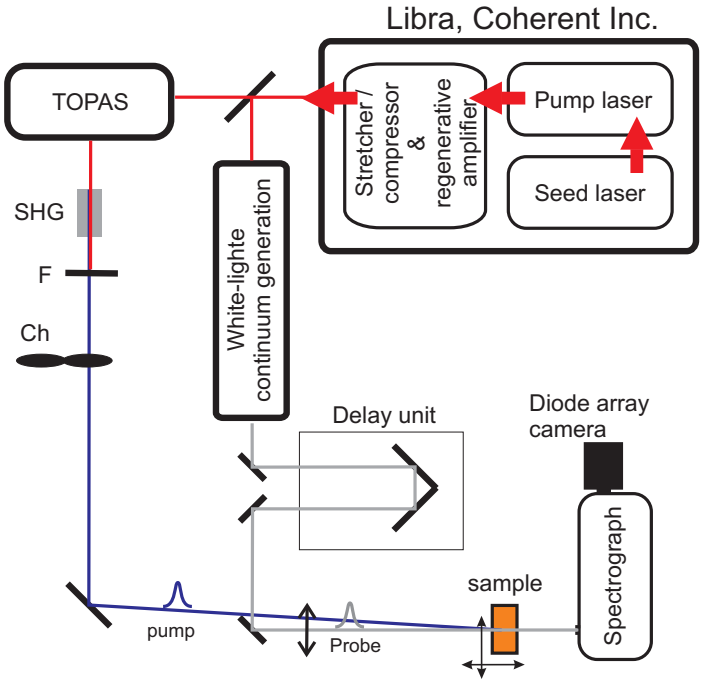

Figure 2.2. Scheme of the experimental setup for transient absorption measurements. SHG – crystal for second harmonic generation, F – filter, Ch – chopper.

Typical excitation parameters were: λ_{exc}=470..510 nm, FWHM ~4 nm, D~120 μm, f=3 kHz, E_{pulse}~1..10 nJ, t_{pulse}=70 fs.

For detection a home-built diode array camera system with 250 channels was used. The system is able to measure 3000 spectra/s at full resolution of 0.5 nm per pixel (wavelength range ~125 nm).

2.3 Sample preparation

The sample (carotenoids in solution) of OD~0.5-1 per mm was placed in a 1 mm quartz cuvette and moved in a Lissajous scanner during the experiment to avoid photodegradation. Before and after every transient absorption measurement the steady-state spectra of the sample were measured in order to control the stability. Purification of the sample was performed the same day as the TA measurement as follows. A HPLC system (Waters Alliance 2695) connected to a 996 diode array detector was used with an YMC-Pack C30 column (YMC, 250x10 mm, 5 μm) (L.C. Sander et al., 1994). The carotenoid solution was dissolved to a high concentration in a solvent (e.g. n-hexane, methanol) and filtrated through a 0.2 μm syringe filter. Under semi-preparative isocratic conditions with a flow of 5 ml/min the sample was fractionated as the main component of the elution profile at the characteristic absorption peak of the desired carotenoid. The collected fractions were dried under vacuum and checked again by analytical HPLC in the same system as above mentioned. The analytical check was made with an YMC-Pack C30 column (YMC, 250x4.6 mm, 5 μm), a flow of 1 ml/min and 11 min isocratic conditions. Specific purification details are described in each chapter separately.

2.4 Analysis of time-resolved data

The simplest case of a time-resolved measurement is a single wavelength decay of a two-level system. The relaxation dynamics is described then by a linear differential equation

$$\frac{dn(t)}{dt} = -k \cdot n(t) \qquad (1),$$

where $n(t)$ is the population of the excited state, k_{ij} – is the relaxation rate from the excited state j to the ground state i. The solution of this equation is an exponential function, and therefore the experimental decay can be fitted by a monoexponential decay: $n(t) = n(0) \cdot exp(-k \cdot t)$. Here the relaxation rate k_{ij} represents the sum of the rates of all deactivation processes of state j, e.g. fluorescence (k_{fl}), non-radiative (thermal) relaxation (k_{nr}), intermolecular energy transfer (k_{ET}), photochemistry (k_{PC}) etc., and the inverse of the rate k is the lifetime of the excited state: $1/\tau = k = k_{fl} + k_{nr} + k_{ET} + k_{PC} + \ldots$

More complex systems (most biological and chemical systems) contain N>1 excited states. In many cases bi-molecular processes are excluded on the short time scales considered here, and the dynamics can be described by a system of first order differential equations. In this case the optical response $I(t)$ depends on the excitation λ_{exc} and detection λ_i wavelengths and within the *single-decay analysis* is described by a sum of N exponentials:

$$I(t,\lambda_{exc},\lambda_i)=\sum_{j=1}^{N}A_j(\lambda_{exc},\lambda_i)\cdot\exp(-k_j(\lambda_{exc},\lambda_i)\cdot t) \quad (2),$$

where $A_j(\lambda_{exc},\lambda_i)$ is a pre-exponential factor (amplitude of the '*j*' component).

2.4.1 Global analysis

As follows from Eq. 2, for a more complete description of the properties of the system one has to measure decays at several excitation/detection wavelengths. Description of a set of M kinetics with single-decay analysis (Eq. 2) will give M*N amplitudes and M*N relaxation rates. However in general the system has only N relaxation rates which are independent of the excitation/detection wavelengths. This means that it is not correct to apply the single-decay analysis to data where certain parameters (relaxation rates in this case) are constant for the individual measurements of the set. For the description of such multi-wavelength experiments the so-called *global analysis* has been developed. In the global analysis the set of N relaxation rates is kept the same for all '*i*' measurements (k_j in this case are called global parameters) and only the amplitudes of the N components are varied from measurement to measurement:

$$I(t,\lambda_{exc},\lambda_i)=\sum_{j=1}^{N}A_j(\lambda_{exc},\lambda_i)\cdot\exp(-k_j\cdot t) \quad (3).$$

The pre-exponential factors $A_j(\lambda_{exc},\lambda_i)$ are associated with the relaxation rate k_j, or lifetime τ_j, and are plotted against wavelength λ_i to form the so-called decay-associated spectrum (DAS) of the lifetime component '*j*'. The representation of the global analysis in form of DAS is informative and gives an immediate view on the lifetimes and the spectral distribution of the rise/decay signals.

In global and single-decay analysis the models (2) and (3) describe an ideal signal assuming the δ-pulse excitation. However in a real experiment, the data contains additional contributions from the instrument, which can be described by the instrument-response function (IRF) and noise. In order to account for the IRF, it is usually either measured or estimated by a function (e.g. Gaussian, Lorentzian) which is convoluted with the model function:

$$I(t,\lambda_{exc},\lambda_i)=\sum_{j=1}^{N}A_j(\lambda_{exc},\lambda_i)\cdot\exp(-k_j\cdot t)\otimes IRF(t) \quad (4),$$

where the sign ⊗ - indicates the convolution integral. After convolution (4) of the theoretical signal described by the fitting parameters with the IRF, the resulting signal is compared with the measured data. The best fit is found via a least-square minimization routine of the model (3) to the experimental data is found. The criterion for the fit is defined by the χ^2-value (A.R. Holzwarth, 1996) as follows:

$$\chi^2 = \frac{1}{N-p-1}\sum_{j=1}^{m}\sum_{i=1}^{n}\left(\frac{Y_{ij}-G_{ij}}{\sigma_{ij}}\right)^2 \quad (5),$$

where Y_{ij} is the measured data at t_i delay and λ_j wavelength, G_{ij} is the modeled signal, σ_{ij} is the standard deviation, n – number of the data points in the individual experiment, m – number of experiments, N – total number of the data points, p – total number of independent fit parameters. The standard deviation function is a measure of the noise in the data and its correct calculation is critical for the good fit. The standard deviation depends on the type of the measurement and has Poissonian distribution ($\sigma_{ij} = \sqrt{Y_{ij}}$) in case of photon counting techniques and is constant (signal-independent) in transient absorption experiments.

2.4.2 Target analysis

The exponential analysis (global or single-decay analysis) is a mathematical description of the experimental data and the obtained DAS (or DADS) and lifetimes do not directly provide the photophysically interesting properties of the system. This method is applied when no additional information on kinetic or other properties of the system is available. However when there is *a priori* knowledge about the kinetic scheme or if particular alternative kinetic schemes should be tested on the data the *target analysis* method is preferable. The target analysis aims to reveal the real physical processes and properties of the system and uses for fitting a specific model with a defined compartmental scheme, rate constants, spectra etc. The relaxation dynamics in the general case is described by a system of homogeneous first order differential equations:

$$\frac{dX(t)}{dt} = T \cdot X(t) + \varepsilon \cdot f(t) \quad (6),$$

$X(t)$ is a vector of populations of N species (compartments), T – kinetic transfer matrix ($N \times N$ matrix of rate constants k_{ij}), ε - vector of species absorbances at t=0, $f(t)$ – temporal excitation function. The transition matrix is defined as follows:

$$T_{ij} = k_{ij} - \delta_{ij} \cdot \sum_{m \neq i} k_{im} \quad (7),$$

Here the off-diagonal elements $k_{i \neq j} > 0$ are the rate constants of energy transfer/relaxation between the i and j compartments/states and the diagonal elements $k_{ii} < 0$ describe the thermal dissipation in a particular compartment i to the ground state. The equation (7) can be solved analytically (I.H.M. van Stokkum et al., 2004): $X(t)=exp(T \cdot t) \otimes \varepsilon f(t)$. Using the eigenvalue decomposition $T=UVU^{-1}$ the exponent takes the form $exp(T \cdot t) = U \cdot exp(V \cdot t) \cdot U^{-1}$, where U and V are the eigenvector and eigenvalue matrixes of the T matrix, respectively. Both matrices

contain important information: while the eigenvalue matrix elements are a measure of the lifetime of each compartment/state (V_{ii}=$-1/\tau_i$), the U matrix elements give the rise (V_{ij}<0) and decay (V_{ij}>0) of the population of a particular compartment i.

The final expression describing the experimental time-resolved data takes the form:

$$I(t,\lambda_{exc},\lambda_i)=\sum_{k=1}^{N} SAS_k(\lambda_i)\cdot(U^{-1}\cdot\varepsilon(\lambda_{exc}))_k\cdot U_{jk}\cdot\sum_{j=1}^{N}\exp(V_j\cdot t)\otimes f(t) \qquad (8).$$

Here SAS_k is the spectrum of species k (species-associated spectra, SAS). The SAS represents the actual spectrum of the species equal to the steady-state spectrum of the compartment/state if it could be measured separately. It follows that the DAS are linear combinations of SAS:

$$DAS_j(\lambda_i)=\sum_{j=1}^{N} c_{jk}\cdot SAS_k(\lambda_i) \qquad (9),$$

with coefficients c_{jk} dependent on all the rate constants, the excitation wavelength, and the absorbances $\varepsilon(\lambda_{exc},t=0)$ of the species.

2.4.3 Lifetime density analysis

When the relaxation is described by linear differential equations, the decay is described by as many exponentials as there are intermediates in the system. Often without a priory knowledge on the object it is difficult to predict the number of lifetimes and their values. Also the lifetime values may vary at different wavelengths and simple global analysis may not be able to resolve them. This problem is solved in the *Lifetime Density Analysis* (LFD) (R. Croce et al., 2001). The method combines the exponential series method, used for describing lifetime distributions (A. Siemiarczuk et al., 1990), with a regularization procedure (G. Landl et al., 1991). The regularization allows to stabilize the solution and obtain the true lifetime distribution. One well known method used for such an analysis is the *Maximum Entropy Method* (MEM) (J.-C. Brochon, 1994; V.A. Lorenz-Fonfria and H. Kandori, 2006) which allows to obtain lifetime distributions with both positive and negative amplitudes. The LFD method used for analysis in this work is based on the Laplace transformation of the experimental decays $S_j(t,\lambda_{exc},\lambda_i)$ to the lifetime distribution $\Phi_j(\tau,\lambda_{exc},\lambda_i)$ convoluted with the instrument-response function $IRF(t)$:

$$S(t,\lambda_{exc},\lambda_i)=\left[\int_0^{\infty}\Phi(\tau,\lambda_{exc},\lambda_i)\cdot\exp(-t/\tau)\cdot d\tau\right]\otimes IRF(t) \qquad (10).$$

The Laplace transformation converts the signal into a distribution of exponential amplitudes versus the exponential time constants, in analogy to the Fourier transformation which converts the signal into a spectrum – distribution of sinusoid amplitudes versus frequencies.

In practice the continuous lifetime distribution function $\Phi_j(\tau)$ is approximated by a large number of fixed lifetimes (>50) equally spaced on the logarithmic scale. Because the Laplace transform is an ill-posed problem a regularization procedure is a necessary part of the analysis. The regularization is based on the introduction of additional information limiting the smoothness and putting bounds on the norm of the solution. One of the most often used regularization methods, the *Tikhonov regularization* is based on the minimization of the solution norm together with the residual norm: $||Ax-b||^2 + \lambda||\Gamma x||^2$ (G.H. Golub et al., 1999) . Here, since in ill-posed problems 'A' may have a non-unique solution, the additional term with the Tikhonov matrix Γ and the weight of the residual norm λ are introduced which gives a preference to a particular solution. Along the regularization, the IRF(t) and the chirp of the white light continuum are included in the procedure and thus the output data is a noise-free deconvoluted true signal, which describes in the best possible way the experimental curve. This procedure is applied to all the decays at every wavelength independently, no assumption of a correlation between different wavelength channels is taken.

The LFD map representation of the data has pronounced advantage. Once such a lifetime distribution is obtained the target analysis can be performed on kinetics calculated from these LFD maps since it represents a condensed transformation of the experimental data. The calculated kinetics are essentially identical to the measured data, except that the noise and chirp contribution are already removed. The target analysis performed in this way appeared to be more efficient if a large number of exponentials is involved and/or it allows to distinguish more reliably between different kinetic models which yield close-lying lifetimes. It is less time-consuming and gives a quick overview of the most important fitting parameters (fit quality, lifetimes and rate constants, evolution of states populations, species-associated spectra, etc.).

2.4.4 Complex target analysis for systems with strong coupling

In some particular cases the relaxation dynamics cannot be described by a sum of exponential functions, i.e. the simple differential equation can not describes the data. One example is a system of coherently coupled states, where the coherent term is a complex quantity calculated from the Hamiltonian of the system (F. Bloch, 1957; T. Plakhotnik, 2006). Another example are high-intensity experiments where the non-linear spectral terms have to be taken into account (e.g. annihilation in a system of aggregated molecules (V. Barzda et al., 2001)). In any of these cases the solution can not be obtained by the single-value decomposition procedure and the differential equation has to be solved numerically (in a few simplified model systems it can be solved analytically (D. Maslov and E. Ostroumov, 2005;

J.L. Perez Lustres et al., 2007)). In the current work for the analysis of the coherent effects a MATLAB code (*MATLAB R2006b*, The *Mathworks*, Natick, MA, USA) was written. The fitting procedure consisted of several steps (Fig. 2.3). On a preliminary stage, the experimental data is read and the starting values and constraints for the parameters of the fitting model are defined. Then the cycle of the iterative optimization is started. Inside the cycle, first the system of differential equations is solved using the classical Runge-Kutta method. The IRF(t) is either convoluted with the obtained solution or incorporated inside the solver. Then the amplitudes of the species (SAS) are calculated via linear fitting of the species populations to the experimental data. On the final stage the amplitudes and the time dependent populations of the species are used in a nonlinear least-square routine. Inside this routine a function whose sum of squares has to be minimized is calculated. The output residuals of the least-square routine are used to vary the fitting parameters in the following cycle. When the fitting conditions are met (i.e. the termination tolerance is reached or the maximum number of iterations is exceeded), the non-linear fitting procedure is stopped and the output parameters and modeled kinetics are saved.

The code allows both single-decay and global multi-wavelength analysis. In addition, a more complicated analysis can be performed when several different sets of measurements are fitted together. In this case a certain number of the fitting parameters are used globally for all sets of data while the rest are free parameters local for each set of data. This complex analysis can give more informative results when the same system is measured at different conditions. One example is the excitation wavelength dependent measurements. In that case the resulting data combine both excitation and detection wavelength dependencies $I(\lambda_{exc},\lambda_{det})$ and give three-dimensional spectra. Such an analysis is also potentially useful for observation of changes taking place in e.g. biological sample exposed to (or being grown under) different conditions. If according to the *a priory* knowledge only some model parameters are changed during this exposure while others are constant they can be defined as local for each treatment parameters while the rest of the parameters are independent on the measurement conditions and are treated globally.

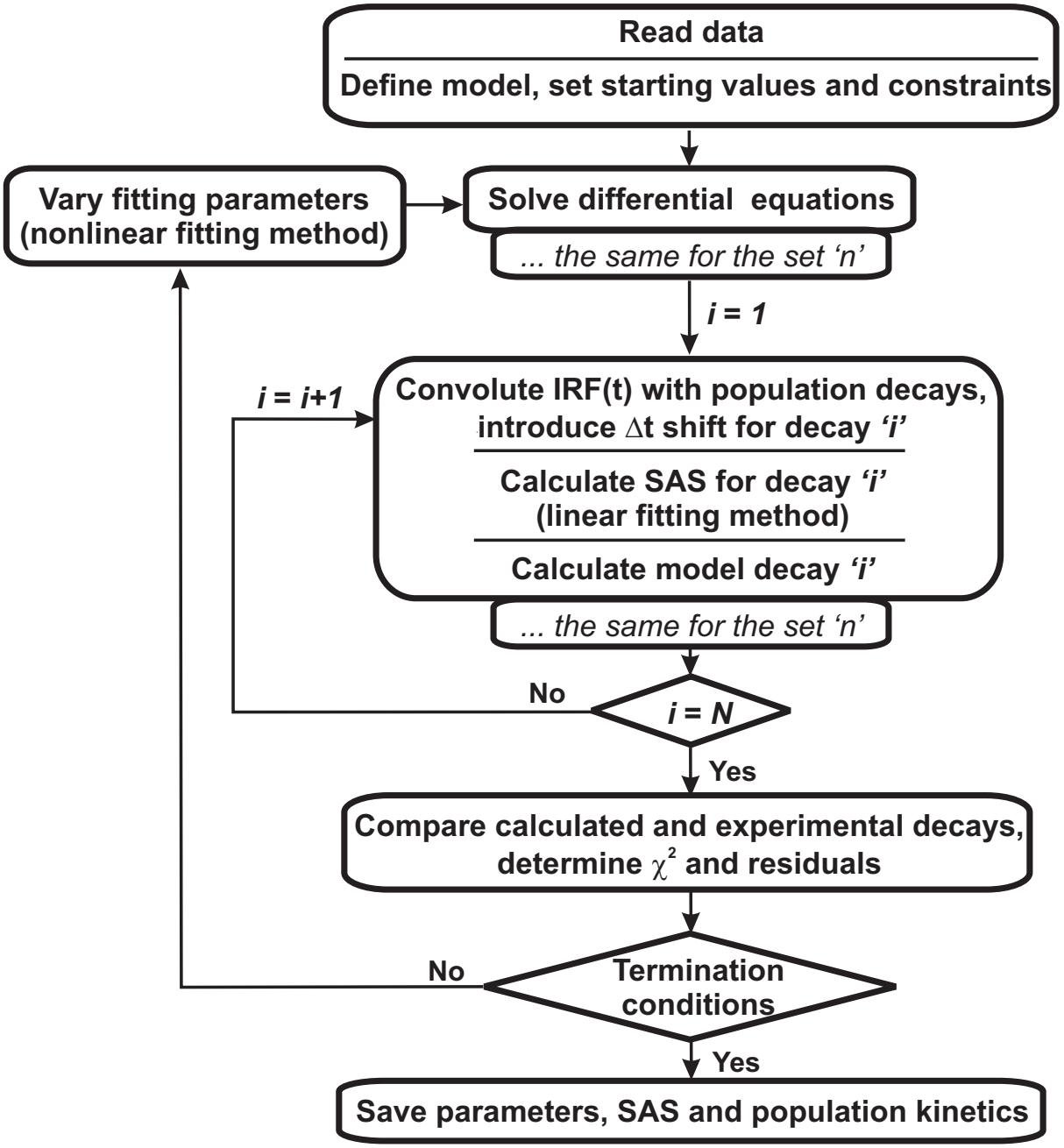

Figure 2.3. Block-diagram of the algorithm of global target fitting procedure of the time-resolved data.

Chapter 3

Electronic Coherence Provides a Direct Proof for Energy-Level Crossing in Photoexcited Lutein and β-Carotene

This chapter is based on the publication Evgeny Ostroumov, Marc G. Müller, Christel M. Marian, Martin Kleinschmidt, and Alfred R. Holzwarth. Phys.Rev.Lett., 103 (2009) 108302

We investigate femtosecond transient absorption dynamics of lutein and β-carotene. Strong oscillations up to about 400 fs are observed, depending on excitation/detection wavelength and solvent. We propose electronic quantum beats as the origin of these oscillations. They provide direct proof for strong coupling of the $1B_u^+$ with another electronic "dark" state predicted by quantum chemical calculations to be the $1B_u^-$ state resulting in a crossing within a dynamic relaxation model. The overall dynamics can be described well by an optical Bloch equation approach.

3.1 Introduction

Carotenoids are a large group of molecules with very diverse biological functions. They act as antioxidants, photoreceptors, energy and electron transfer cofactors and in particular as photoprotectors involved in regulatory mechanisms ((A.J. Young and G. Britton, 1993) Chapt.8). For understanding these diverse functions a detailed knowledge of the electronic level structure and excited state dynamic properties is essential. However, the excited state properties of carotenoids are very complex and not well understood. Thus rather controversial interpretations are found in the literature (for a review see (T. Polivka and V. Sundström, 2004)). The "dark" S_1 ($2A_g^-$) and the strongly allowed S_2 ($1B_u^+$) states are generally accepted as the two lowest excited states. The ground state (GS)→S_2 ($1B_u^+$) transition gives the strong color to carotenoids while the one-photon transition to the S_1 ($2A_g^-$) state is forbidden. This state plays however an important role in many photoprotection processes (T. Polivka and V. Sundström, 2004). Since the lifetime of the S_2 state is very short – in the range of 100-300 fs, the fluorescence yield of carotenoids is generally very low.

Early theoretical considerations led to the suggestion that there may be additional "dark" electronic states located between the above-mentioned S_1 and S_2 states in longer chain carotenoids (P. Tavan and K. Schulten, 1987). These states might play key roles in the relaxation dynamics of the S_2 and S_1 states, in the electronic interaction of carotenoids with other molecules, and in photoprotective and energy/electron transfer processes. Indeed a series of steady state and time-resolved spectroscopic studies by the Koyama group (T. Sashima et al., 1999; M. Ikuta et al., 2006) provided experimental evidence for the existence of these additional "dark" states ($1B_u^-$, $3A_g^-$), which were proposed to be located below the $1B_u^+$ state for carotenoids of $N \geq 9$-10 but were ignored or questioned in the interpretation of most spectroscopic and time-resolved data (T. Polivka and V. Sundström, 2004; T. Buckup et al., 2006; D.M. Niedzwiedzki et al., 2006). Also, some of the experimental observations of Koyama et al. have been reinterpreted in terms of vibrationally hot S_1 and S_0 states (T.

Buckup et al., 2006) or as a two-photon absorption to a higher singlet state (D. Kosumi et al., 2005).

For steady-state fluorescence measurements ((A.J. Young and G. Britton, 1993) Chapt.9, (B. DeCoster et al., 1992)) a mirror image relationship of absorption and fluorescence bands was claimed. However, for a number of carotenoids the fluorescence spectrum deviates quite substantially from a mirror image (M. Mimuro et al., 1992). From all the available data on carotenoids it is clear that both temporal and spectral characteristics of fluorescence are much more complex than is generally assumed. Recently highly damped coherent oscillations in the transient absorption (TA) signals after femtosecond pulse excitation were demonstrated for β-carotene (J.L. Perez Lustres et al., 2007). These oscillations were interpreted as evidence for electronic state coherence and were attributed to the coupling between the S_1 and S_2 states.

We report a study of the ultrafast relaxation dynamics and fluorescence of two carotenoids, lutein (N=10) and β-carotene (N=11), under a range of different conditions. A highly oscillatory behavior is observed in the early relaxation dynamics.

3.2 Materials and Methods

Crystalline β-carotene was received as a gift from Hoffmann-La Roche, Basle, Switzerland. Crystalline lutein was received as a gift from Denk Feinchemie, Munich, Germany. Purification of the substances was performed on a Waters Alliance 2695 with a 996 photodiode array detector used with a YMC-Pack C30 column (YMC, 250x10 mm, 5 μm) (L.C. Sander et al., 1994). The crystalline carotenoid was dissolved at high concentration in DCM (in case of lutein the same volume of MeOH was added) and filtrated with a 0.2 μm syringe filter. Under semi-preparative isocratic conditions with a flow of 5 ml/min and changing polarity of the solution carotenoid was fractionated as the main component of the elution profile at 453 nm for β-carotene and 447 nm for lutein. The collected fractions were dried under vacuum and checked again by analytical HPLC in the same system as described above. The analytical check was made with a YMC-Pack C30 column (YMC, 250x4.6 mm, 5 μm).

Femtosecond transient absorption measurements were performed at room temperature as described earlier (R. Croce et al., 2001). Shortly, the Ti:Sapphire laser system was used to generate 2-5 nJ transform-limited pulses of 60 fs width from a tunable optical parametric amplifier at 3 kHz focused to a 120μm diameter spot. Absorption changes were detected with a spectral resolution of 0.5 nm in a vertically and horizontally shifted quartz cuvette with a

path-length of 1 mm and an OD ca. 0.5–0.8/mm at the excitation wavelength using magic angle polarization between the excitation and probe pulses.

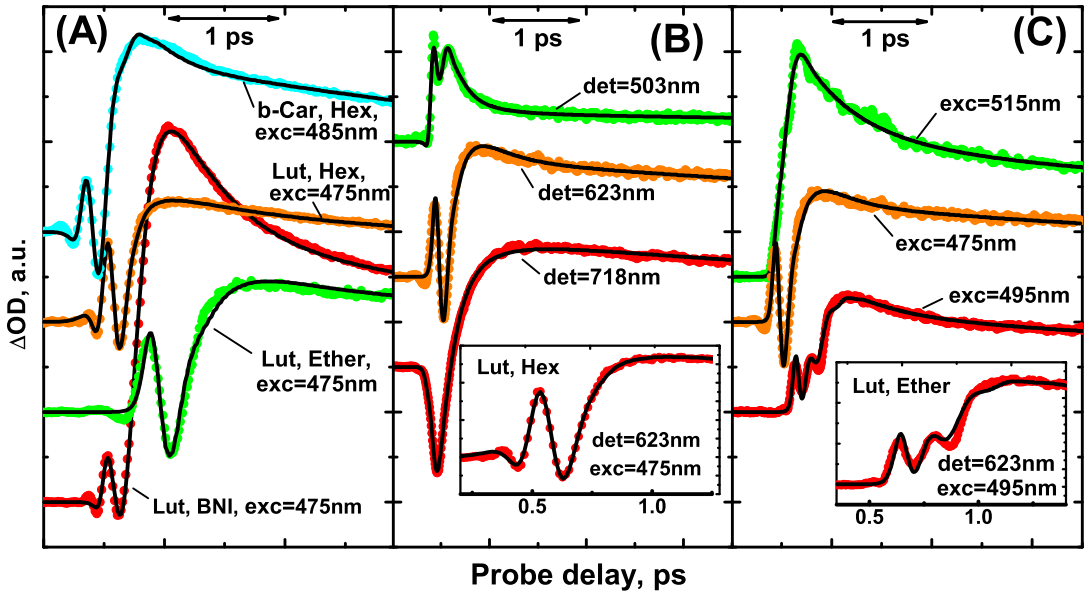

Figure. 3.1. Absorption transients of β-carotene in HEX, and lutein in BNI, DEE and HEX, detection at 623nm (A); lutein in DEE detected at 503 nm, 623 nm, 718 nm (B); lutein in DEE excited at 475 nm, 495 nm, 515 nm, detection at 623nm (C). Insets show time-scaled absorption dynamics of lutein excited at 475 nm (B) and 495 nm (C). The colored curves show the measurements and the black curves the results of global fitting.

3.3 Results and Discussion

3.3.1 Transient absorption

The relative amplitude and characteristics of the oscillations are strongly dependent on the type of carotenoid, the excitation wavelength and the solvent. For lutein in the apolar solvents n-hexane (HEX) and diethyl ether (DEE) we observe oscillations of extremely large amplitude, about 2-3 times higher than for β-carotene in the time range up to 300-400 fs (Fig. 5.1). For benzonitrile (BNI) the shape of the oscillations is generally maintained but the amplitude is reduced by nearly an order of magnitude. The oscillations are only pronounced in the 600-700 nm spectral region – i.e. outside the excitation region and in a range where only excited state absorption (ESA) and stimulated emission (SE) contribute to the signal. They are rather small or absent in the shorter wavelength region where the ESA of the S_1 state is located (Fig. 5.1B). Another important point is their excitation wavelength dependence (Fig. 5.1C). After excitation at 495 nm a well resolved double peak replaces the single oscillation observed for λ_{exc} = 475 nm. It is clear that the observed kinetics can not be

described by a simple combination of exponential kinetics. We rather ascribe the oscillations to electronic quantum beats caused by coherent excitation of strongly coupled excited states. For a theoretical description we thus require a model that includes coherence terms. The simplest possible theory is a solution of the optical Bloch equations (J.L. Perez Lustres et al., 2007) in a density matrix approach with elements ρ_{ij}:

$$\begin{cases} \left(\frac{\partial \rho_{ij}}{\partial t}\right)_{i,j=1,2} = -\frac{i}{\hbar}(H\rho - \rho H)_{ij} - \gamma_{ij}\rho_{ij} \\ \frac{\partial \rho_{33}}{\partial t} = -\gamma_{33}\rho_{33} + \gamma_{11}\rho_{11} + \gamma_{22}\rho_{22} \\ \frac{\partial \rho_{44}}{\partial t} = -\gamma_{44}\rho_{44} + \gamma_{33}\rho_{33} \\ \frac{\partial \rho_{55}}{\partial t} = -\gamma_{55}\rho_{55} + \gamma_{44}\rho_{44} \end{cases}$$

The Hamiltonian consists of the state energies $H_{11}=H_{22}=E$ and the coupling terms $H_{12}=H_{21}=V$. Relaxation is implemented as rate constants of depopulation γ_{ii} and decoherence $\gamma_{12}=\gamma_{21}$. The equations were solved numerically and fitting to the experimental data was performed using home-written Matlab (Mathworks) code. The level scheme and relaxation pathways are shown in the inset of Fig. 5.2A.

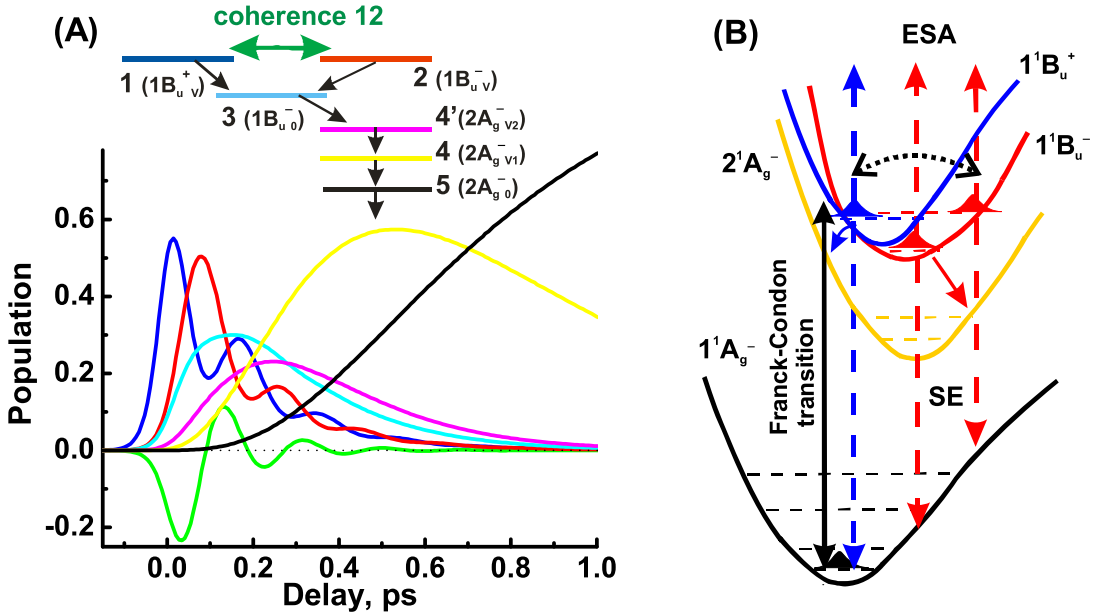

Figure 5.2. Population dynamics of lutein in DEE excited at 495 nm (left) calculated using the Bloch equation approach (see text). The kinetic model scheme with assignment to the electronic states is shown (top). Note the oscillatory populations in states 1 and 2. The coherence term is shown in light green.

The fitted theoretical TA signals (black curves) are overlaid on the experimental TA signals (colored curves) in Fig. 5.1. The calculated population dynamics of the various states of lutein in DEE (λ_{exc}=495 nm) are shown in Figure 5.2A. All fit parameters are summarized in Table 3.1. The pronounced population oscillations of the two coherently excited states are caused by the large electronic coupling V_{12}. The relaxation rates of the three highest energy states form the core of the model and describe the evolution in the first 300-400 fs. The model – despite its rather simple form – describes the kinetics remarkably well. This very good agreement (Fig. 5.1) strongly suggests that the basic features of the excited state level structure and dynamics are described properly. The two highest energy state populations relax with lifetimes in the range of 50-100 fs, in good general agreement with earlier simpler analyses not taking into account coherence terms. The relaxation rates of the two lowest states represent very well the known lifetimes of the vibrationally hot and relaxed S_1 states of lutein and β-carotene (T. Polivka and V. Sundström, 2004). Since coherent coupling was taken into account only for the V_{12} matrix element and the energy gap between the coherently coupled states was assumed to be zero, it is likely that the value for the coupling strength (between 300 and 700 cm^{-1} for lutein in apolar solvents, c.f. Table 3.1) may be somewhat overestimated but is generally considered to be reasonable. Only for relatively strongly coupled excited states we may expect coherent electronic oscillations. The resulting electronic dephasing times of 30-90 fs (Table 3.1) appear to be very reasonable (A.V. Pisliakov et al., 2006) and are fully consistent with our interpretation of the oscillations as manifestations of electronic coherences. Damping is nearly completed already after two oscillation periods (Fig. 5.2A). From the period of the coherent beating (160 fs, corresponding to 210 cm^{-1}, Fig. 5.2A) for lutein in apolar solvent it is clear that these signals are not due to vibrational oscillations (J. Hauer et al., 2008). The fits indicate stronger interaction energies V_{12} for lutein in apolar solvents, which are however strongly dependent on the exact excitation wavelength, substantially weaker coupling for β-carotene in apolar solvents (HEX, DEE), and further strongly reduced coupling in the highly polarizable BNI (P.O. Andersson et al., 1991) for both carotenoids. As compared to our previous study for β-carotene (J.L. Perez Lustres et al., 2007) where excitation occurred at the far red edge of the $S_0 \rightarrow S_2$ absorption, the oscillation amplitudes are much higher under our conditions and the TA-signals differ substantially from the present data where excitation has been chosen near the peak of the S_2 absorption band.

TABLE 3.1. Values of coupling strength V (cm^{-1}) and relaxation rates (ps^{-1}) (see assignment to the electronic states on the Fig. 5.2), resulting from the global fitting for the kinetics under different experimental conditions of solvent and excitation wavelength. The rates γ_{44} and γ_{55} agree with literature data for the relaxation on the longer time scale.

Sample / solvent	lutein / DEE			lutein / BNI	β-Car / HEX
λ_{exc} (nm)	475	495	515	475	485
V	700	560	330	180	530
γ_{12}	29	11	15	20	12
γ_{11}	6.5	6.8	11	9.0	6.8
γ_{22}	12	4.2	12	7.2	5.9
γ_{33}	13.6	9.4	11.5	-	20
γ_{44} (γ_{44}')	3.1	2 (10.4)	1.7	1.9	6.2
γ_{55}	0.062	0.072	0.071	0.061	0.12

The observed large oscillations in lutein can not occur primarily between the traditionally assumed S_2 and S_1 excited states for several reasons. First, the high frequency oscillation requires strong electronic coupling in the order of several hundred cm^{-1} which would not be possible for the large S_2–S_1 electronic energy gap of ~7000 cm^{-1}. Secondly, the quantum beats are damped with decoherence times well below 100 fs while the strong ESA of the S_1 state only rises with lifetimes of ca. 600 fs in the ~530-560 nm region. Thus another electronic state must be located very close to the S_2 state with a crossing near the Frank-Condon (FC) region. If this is the case, the observed oscillations provide the most direct evidence for the existence of the earlier proposed lower lying $1B_u^-$ state (P. Tavan and K. Schulten, 1987; T. Sashima et al., 1999). However, since the observed kinetics is rather unusual we sought for an independent confirmation of the existence of the $1B_u^-$ state nearby the S_2 ($1B_u^+$) state. Thus experimental fluorescence spectra were studied in detail and high level quantum mechanical calculations were performed using a method suitable to tackle the complex excited state structure of carotenoids (S. Grimme and M. Waletzke, 1999; J.-P. Zhang et al., 2001; M. Kleinschmidt et al., 2009). Technical parameters of the calculations were the same as in recent work on carotenoids with phenolic end groups (M. Kleinschmidt et al., 2009).

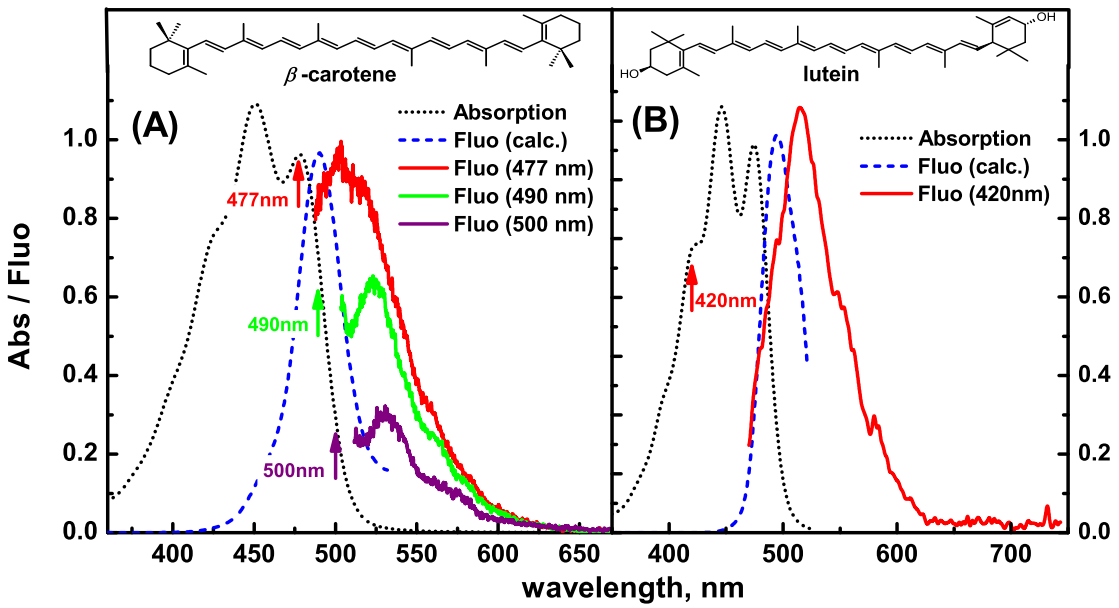

Figure 5.3. Absorption and fluorescence spectra of β-carotene in HEX (A) and lutein in DEE (B) together with the theoretical fluorescence spectra (blue) calculated from the absorption using the Stepanov relationship [18]. Note the large deviations of experimental and calculated spectra. The chemical structures of β-carotene and lutein are shown at the top.

3.3.2 Steady-state spectra

In Fig. 5.3 absorption and fluorescence steady-state spectra of β-carotene and lutein are shown together with the calculated theoretical fluorescence spectra, utilizing the Stepanov relationship (C.M. Marian et al., 2009). In the absence of other electronic states close to the S_2 ($1B_u^+$) state the fluorescence spectra are expected to show good mirror image relationship with the absorption. However Fig. 5.3 reveals that the fluorescence in its largest part does not arise from the strongly absorbing S_2 state, but must arise from a lower-lying state, which at the same time can not be the traditional "dark" S_1 state. This new state which is responsible for most of the fluorescence apparently does not have a strong absorption, but has a broad strongly red shifted fluorescence that extends, in particular for lutein, up to 700 nm. For β-carotene a strong excitation wavelength dependence of the fluorescence maximum is demonstrated (Fig. 5.3A). We consider this fluorescence behavior as clear evidence for the existence of an additional state slightly below the S_2 state. The long tail of the fluorescence band of this state can be explained by a pronounced shift of the excited state potential surface(s) vs. the nuclear coordinates of the electronic GS.

3.3.3 Quantum chemical calculations

Quantum chemical calculations using a parallelized version of the combined DFT/MRCI method (S. Grimme and M. Waletzke, 1999) performed for lutein and β-carotene show that upon geometry relaxation in the $1B_u^+$ potential well the multi-configurational state of $1B_u^-$ symmetry drops below the S_2 state and gains a substantial transition dipole moment as compared to the transition dipole for the GS geometry (see Table 3.2). For lutein in apolar solvent, which comes very close to the *in vacuo* situation assumed for the theoretical calculations, the crossing of the $1B_u^+$ and $1B_u^-$ states is predicted to be close to the potential minimum of the $1B_u^+$ state. For β-carotene the crossing is predicted to occur a bit further away from the potential energy minimum. At the intersection of these potential energy surfaces strong non-adiabatic coupling between the $1B_u^-$ and $1B_u^+$ states is expected. This situation allows coherent excitation and the resulting strong oscillations. Thus all our experimental observations as well as the results of the theoretical calculations support the notion that the relaxed $1B_u^-$ state in lutein is located just below the $1B_u^+$ state, in agreement with earlier suggestions (B.I. Stepanov, 1957). A conical intersection and dynamical level crossing between these states is predicted (Fig. 5.2). The exact energy differences of these two states will be determined by N and by the solvent since the location of the $1B_u^+$ state strongly depends on solvent polarizability (P.O. Andersson et al., 1991). This leads us to the electronic level structure and dynamic relaxation model shown in Fig. 5.2. Excitation pulses with energies corresponding to the FC transition of the $1B_u^+$ state do not excite substantially the $1B_u^-$ state since it is located above the $1B_u^+$ state and has a small transition dipole. For lutein in apolar solvent the most favorable situation is realized for the observation of coherent oscillations since the FC region of $1B_u^+$ and the crossing of the $1B_u^+$ and $1B_u^-$ states are energetically very close. These features explain the pronounced dependence of the oscillations on the excitation wavelength and the solvent. Note that quantum chemical calculations for these carotenoids place the $3A_g^-$ strictly above the $1B_u^+$ state at all nuclear geometries studied in contrast to previous suggestions (T. Sashima et al., 1999).

TABLE 3.2. Calculated energetic positions (cm^{-1}) and oscillator strengths f(r) of the $1B_u^+$ (S_2), $1B_u^-$ and $2A_g^-$ (S_1) states at the S_0 (FC transition) and the $1B_u^+$ state minimum geometries (m.g.).

Compound	$1B_u^+$ / f(r)	$1B_u^-$ / f(r)	$2A_g^-$	$3A_g^-$
Lutein, S_0 m.g.	19875 / 3.70	22238 / 0.17	16651	26987
Lutein, $1B_u^+$ m.g.	18863 / 2.19	17857 / 1.64	12554	23224
β-carotene, S_0 m.g.	19510 / 3.66	21371 / 0.31	16040	25795
β-carotene, $1B_u^+$ m.g.	18324 / 3.15	17096 / 0.83	11922	22019

3.4 Conclusions

We can exclude coherent artifacts or other causes as the origin of the oscillations. The pure solvents did not give such signals under identical conditions and such oscillations were not observed on the same apparatus for a very wide range of other compounds and conditions. Also, the oscillations are only observed strongly if the carotenoids are excited close to the maximum of the first strong absorption band, which corresponds to the crossing region of the two states. Vibrational coherences in the GS are excluded since they have much higher frequencies (above 1000 cm^{-1}) which could not be excited by our pulses, they would not depend critically on the solvent, their dephasing times are more than an order of magnitude larger than those observed here, and they occur in different wavelength regions (J. Hauer et al., 2008).

The complex development of the TA and steady-state fluorescence features as well as the calculations strongly suggest the existence of the $1B_u^-$ state that has been mostly ignored in the interpretation of ultrafast dynamics so far. The predicted large increase of the transition dipole moment of the $1B_u^-$ state in the relaxed conformational state is consistent with the experimental observation that the main part of the fluorescence of lutein and β-carotene do not derive from the $1B_u^+$ state. The model explains the broad red-shifted fluorescence spectrum of these carotenoids as a consequence of the strong excited state potential shifts of the excited states vs. the GS. Thus our results cannot be explained in terms of the often invoked traditional S_2-S_1-S_0 model and a much more sophisticated dynamic relaxation model is necessary (Fig. 5.2). Our conclusions should apply generally for longer chain carotenoids and are highly relevant for the understanding of the photochemical and photoprotection functions of carotenoids. The present work has been performed as a project of the SFB 663 (B2, C1) and is printed at its instigation with financial support provided by the Deutsche Forschungsgemeinschaft.

Chapter 4

Ultrafast relaxation dynamics of lutein: The Redfield theory approach

This chapter is based on the manuscript by Evgeny E. Ostroumov, Marc G. Müller, and Alfred R. Holzwarth. (2010), *to be submitted*

The Redfield theory approach was applied to the analysis of the femtosecond transient absorption data of lutein with the aim to better describe the electronic coherence reported in (E. Ostroumov et al., 2009). A competition between stimulated emission and excited-state absorption (ESA) originating from the $1B_u^+/1B_u^-$ states is observed in the 570-700 nm spectral range. Excitation at the red edge of the absorption spectrum results in a hypsochromic shift and strong increase of the amplitude of the excited state absorption band. The oscillatory future of experimental decays proposed to result from the strong coupling of the coherently excited $1B_u^+$ and $1B_u^-$ states. The fast damping of the oscillations is assigned to the coupling to the phonon bath and the coupling of the $1B_u^-$ state to the vibrationally excited $2A_g^-$ (S_1) state of the carotenoids.

4.1 Introduction

Carotenoids belong to one of the most abundant group of molecules in nature. They play vital functions in many living organisms and are of particular importance in photosynthetic organisms due to their high efficiency in both light harvesting as well as photo-protection. The electronic properties of carotenoids are defined mostly by their polyene conjugated chain and to some extent by various end groups (A.J. Young and G. Britton, 1993). The ambiguity comes from the complex system of carotenoid excited states. Most carotenoids belong to the C_{2h} symmetry group. The first excited state (S_1) has the same A_g^- symmetry as the ground state and is therefore one-photon forbidden ('dark state', see (T. Polivka and V. Sundström, 2004). The second excited state (S_2) is of B_u^+ symmetry and is responsible for the strong absorption of carotenoids in the blue-green region of the spectrum. In a number of works additional 'dark states' have been reported to be located below the S_2 ($1B_u^+$) state for carotenoids with conjugation length $N \geq 9$. However due to the very short lifetime of the initially excited S_2 state the study of the early relaxation dynamics is technically difficult and highly controversial results and interpretations were reported in the literature (T. Polivka and V. Sundström, 2009).

The early theoretical calculations reported by Tavan and Schulten (P. Tavan and K. Schulten, 1987) showed that states of $1B_u^-$ and 3 A_g^- symmetry can be located between the $1B_u^+$ (S_2) and $2A_g^-$ (S_1) states for longer chain polyenes and carotenoids. This result was supported by a series of experimental studies in the Koyama group (for a review see (Y. Koyama et al., 2004)). The $1B_u^-$ state was first experimentally detected by resonance Raman spectroscopy in spheroidene, lycopene and β-carotene (T. Sashima et al., 1999; T. Sashima et al., 2000). In femtosecond time-resolved measurements the excited state dynamics of several open-chain carotenoids on the time-scales of 50-100 fs and 200-300 fs was ascribed to $1B_u^-$

and $3A_g^-$ states, respectively in addition to the $1B_u^+$ relaxation (R. Fujii et al., 2003; M. Ikuta et al., 2006). Further support for the location of these intermediate dark states below the $1B_u^+$ state came from transient absorption measurements of β-carotene using 15 fs excitation pulses (G. Cerullo et al., 2002). The excited-state absorption (ESA) band around 800 nm was assigned to the $1B_u^+$ state which decayed within 10 fs to the S_x (proposed to be the $1B_u^-$) state with an ESA signal in the 900-1000 nm spectral region. However the same signals were reinterpreted by (D. Kosumi et al., 2005) as two-photon absorption to the nA_g^- state (620-800 nm band) and ESA of the $1B_u^+$ state (1000 nm band). Lustres et al. (J.L. Perez Lustres et al., 2007) came to similar conclusions and ascribed the transient absorption signal of β-carotene observed at 800 nm with 35 fs decay time to a coherent contribution from the solvent and 950 nm band to the $1B_u^+$ ESA with 160 fs decay time. Thus the existence of a $1B_u^-$ state below $1B_u^+$ remained doubtful and most authors in the following concluded that $1B_u^-$ state does not contribute to the $1B_u^-$ relaxation dynamics.

Recently we showed however that in lutein and β-carotene depending on the experimental conditions strong oscillations occurred in the femtosecond time range and the relaxation dynamics could not be explained without taking the $1B_u^-$ state into account (E. Ostroumov et al., 2009). Using a relatively simple theoretical model based on the optical Bloch equations this oscillatory signal was attributed to electronic coherence taking place between the coherently excited and strongly coupled $1B_u^+$ and $1B_u^-$ states. This approach, which simulated the crossing of the $1B_u^+$ and $1B_u^-$ potential surfaces, allowed to explain the main spectroscopic and dynamic features of these carotenoids quite well although some problems remained, e.g. overestimated coupling strengths. Using the optical Bloch equations one can describe relaxation dynamics including coherent terms however the method does not allow to determine physical parameters of the system, i.e. coupling to the phonon bath, vibrational modes, absolute values of the electronic states described by the Hamiltonian. In order to solve this problem the Redfield theory approach in its general form is applied in the present work for the analysis of the reported transient absorption data (Fig. 4.1, for description of the measurement procedure and sample preparation see (E. Ostroumov et al., 2009)). In the Redfield theory the dynamics of the system is calculated in eigenstate representation. This allows to calculate the relaxation rates (the Redfield relaxation tensor) directly from the Hamiltonian and the spectral density function, in contrast to the optical Bloch equation approach where elements of the relaxation matrix are free fitting parameters.

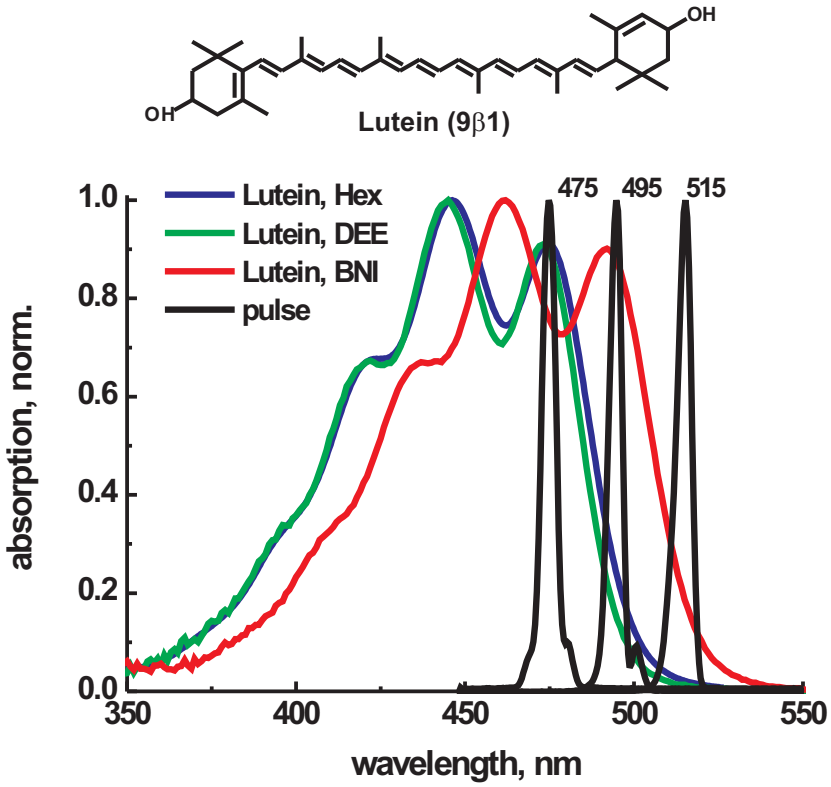

Figure 4.1. Absorption spectra of lutein in n-hexane (HEX, solid green and blue lines), diethyl ether (DEE, dashed green line) and benzonitrile (BNI, dash-dotted green line). The pulse profiles are shown at selected excitation wavelengths by black lines. Molecular structure of lutein is shown in the top.

In present work five-state model is proposed for description of the relaxation dynamics of lutein. Strong coupling is observed between states 1 - 2 and 2 - 3 of the model. The first pair of states (assigned to the $1B_u^+$ and $1B_u^-$ states) provides the system with coherent terms resulting in oscillatory behavior observed during the first 300 fs. The strong coupling between states 2 and 3 ($1B_u^-$ and *hot*-$2A_g^-$) is responsible for the high damping rate of the coherence (typical time constant of <50 fs). States 3-5 of the model show a strong ESA signal in the 500-650 nm spectral region and are assigned to vibrationally excited and relaxed $2A_g^-$ states.

4.2 Redfield theory approach

For description of the dynamics of dissipative systems traditionally the system-bath approach based on the density matrix formalism is used (V. May and O. Kühn, 2000). The equation for the density matrix operator ρ is defined by the time-dependent Schrödinger equation and reads

$$\frac{\partial \rho}{\partial t} = -\frac{i}{\hbar}[H, \rho] \qquad (1),$$

where the Hamiltonian of the system $H=H_S+H_{S-R}+H_R$, is a sum of the Hamiltonians of the relevant system H_S, the reservoir H_R representing the dissipative environment (thermal bath), and their interaction H_{S-R}. Often the reservoir dynamics is excluded from the consideration by introduction of a reduced density matrix σ which depends on the coordinates of the relevant system only. Then Eq.1 takes the shape

$$\frac{\partial \sigma}{\partial t} = -\frac{i}{\hbar}[H_S, \sigma] - \frac{i}{\hbar} tr_R\{[H_{S-R}, \sigma]\} \qquad (2).$$

The next standard step is the application of the Markovian approximation, which means that no substantial change in σ occurs on the time-scale of the system memory time. This then leads to the well-known Redfield equation (A.G. Redfield, 1957):

$$\frac{\partial \sigma_{ij}}{\partial t} = -\frac{i}{\hbar}\omega_{ij}\sigma_{ij} + \sum_{kl} R_{ijkl}\sigma_{kl} \qquad (3),$$

where ω_{ij} is the resonance frequency of the |i>-|j> transition and R_{ijkl} is an element of the Redfield relaxation tensor. Equation (3) is usually written in the eigenstate representation, but often a system is defined by local states (site representation), i.e. diabatically, and time dependence of the populations of these diabatic states is of interest. Since these two representations are related via $\sigma_{\alpha\beta} = \sum_{ij} c'_\alpha(i) c_\beta(j) \sigma_{ij}$ (c_α - are eigenvectors of the Hamiltonian, Latin and Greek letters correspond to site and eigenstate representation, respectively) there exists no intrinsic difference between them. However equation (3) was derived using the Markov and Born approximations referring to the Hamiltonian in the eigenstate representation and, therefore, actual calculations in general yield different results (V. May and O. Kühn, 2000; P. Herman and I. Barvik, 2001). Thus to observe the behavior of the diabatic system one can either (i) solve (3) defined in the site representation (T. Plakhotnik, 2006; J.L. Perez Lustres et al., 2007), or (ii) define initially the system in the site representation, transform it to the eigenstate representation by means of Hamiltonian diagonalization, solve equation (3) and transform the resulting density matrix $\sigma_{\alpha\beta}$ back to the site representation (J.M. Jean and G.R. Fleming, 1995; D. Egorova and W. Domcke, 2004). The first approach is suitable for a number of simple systems. However the latter approach is the exact one and, at the same time, it is more demanding in terms of the required computing resources.

In Eq.3 all the information on the system-bath coupling is contained in the Redfield relaxation tensor. Some of its elements have a simple physical meaning (V. May and O. Kühn, 2000). Let us discuss this in terms of three categories of the density matrix elements:

1) i=j, k=l – population transfer from state |k> to state |i>;

2) i=k, j=l, i≠j – so-called pure dephasing rate of coherence described by σ_{ij};

3) all other elements – i.e. transfer rates between populations and coherences $\sigma_{ii} \leftrightarrow \sigma_{kl}$ and between different coherences $\sigma_{ij} \leftrightarrow \sigma_{kl}$.

In many cases coupling to the bath is weak and only a few elements of the Redfield tensor are significant, whereas all the rest can be neglected. Since the calculation time drastically depends on the R_{ijkl} size choosing the significant tensor elements, which ahs to be taken into account, is essential. In the secular approximation only those elements of R_{ijkl} are taken into account for which the condition $|\omega_{ij}-\omega_{kl}|=0$ holds. Since within the Markovian approximation it is possible that some elements corresponding to the third category defined above satisfy the secular approximation condition, generally the secular approximation has to be used with care in order to avoid distortion of the results. However in most cases one can neglect the population-to-coherence coupling, and only the first two categories of Redfield tensor elements will contribute to the dynamics of the system. In this approximation, known as Bloch limit (O. Kühn and H. Naundorf, 2003), populations and coherences are described separately by diagonal and off-diagonal part of the density matrix, respectively.

In general the Redfield tensor is complex. Its real part describes the irreversible redistribution of the amplitudes contained in the various parts of the reduced density matrix. The imaginary part introduces terms which can be interpreted as a modification of the transition frequencies (Lamb Shift). The Redfield tensor has often a form

$$R_{ijkl} = \Gamma^{+}_{ljik} + \Gamma^{-}_{ljik} - \delta_{jl}\sum_{a}\Gamma^{+}_{iaak} - \delta_{ik}\sum_{a}\Gamma^{-}_{laaj}$$

$$\Gamma^{+}_{ljik} = \int_0^t d\tau \left\langle H_{S-R} H_{S-R}(\tau)\right\rangle e^{-i\omega_{ik}\tau} \qquad (4).$$

$$\Gamma^{-}_{ljik} = \int_0^t d\tau \left\langle H_{S-R}(\tau) H_{S-R}\right\rangle e^{-i\omega_{lj}\tau}$$

Supposing factorization of the system-bath interaction into system and bath, one obtain (A.G. Redfield, 1957)

$$R_{ijkl} = \left\langle c_{lj} c_{ik}\right\rangle (J_{jl} + J_{ik}) - \delta_{jl}\sum_{a}\left\langle c_{ia} c_{ak}\right\rangle J_{ak} - \delta_{ik}\sum_{a}\left\langle c_{la} c_{aj}\right\rangle J_{al}\ , \qquad (5),$$

where the spectral density J_{ik} is a Fourier image of the time correlation function of the bath and c_{ik} are the eigenvectors of the system, resulting from the diagonalization of the Hamiltonian. In general spectral density is defined as $J_{ij}(\omega_{ij}) = \sum_{S} g^2 \delta(\omega_{ij} - \omega_S)$, with dimensionless coupling '*g*' known as the Huang-Rhys factor. The spectral density can be viewed as the bath density of states weighted by the coupling strength between system and reservoir and the Huang-Rhys factor can be directly obtained from fluorescence/absorption

spectra (Stokes shift) and using data from hole-burning spectroscopy (S. Mukamel, 1995; J. Pieper et al., 1999). Another experimental definition of the Huang-Rhys factor is the intensity ratio of the phonon wing relative to the zero-phonon line (E.J.G. Peterman et al., 1997; E.J.G. Peterman et al., 1998; L. O'Neill and H.J. Byrne, 2005).

4.3 Calculation algorithm

In this work a Hamiltonian including five excited states (levels) was used for the description of the relaxation dynamics of carotenoids. However, since the last three states are known to represent vibrational relaxation within the $2A_g^-$ (S_1) manifold and can be well modeled by a sequential relaxation scheme (see **Chapter 5**), the coupling of only the first three states (E_1, E_2, E_3, V_{12}, V_{13}, V_{23}) were taken into account and relaxation rates and coherent contribution for these states ($R_{1111}..R_{3333}$) were calculated according to Eq. 5. The other elements of the Hamiltonian and the relaxation tensor (E_4, E_5, $R_{4433}..R_{5555}$) were introduced as free parameters:

$$H = \begin{vmatrix} E_1 & V_{12} & V_{13} & & \\ V_{12} & E_2 & V_{23} & & \\ V_{13} & V_{23} & E_3 & & \\ & & & E_4 & \\ & & & & E_5 \end{vmatrix}, \qquad R = \begin{vmatrix} R_{1111} & R_{1122} & R_{1133} & & \\ R_{2211} & R_{2222} & R_{2233} & & \\ R_{3311} & R_{3322} & R_{3333} & & \\ & & R_{4433} & R_{4444} & \\ & & & R_{5544} & R_{5555} \end{vmatrix} \qquad (6).$$

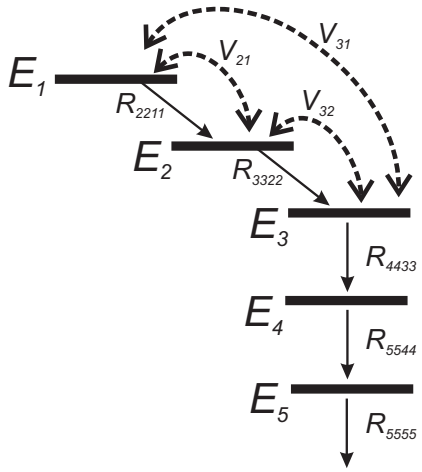

Figure 4.2. Scheme of states (levels) E_i of the model shown in Eq. 6. Solid arrows - relaxation from state i to state j with the rate R_{jjii}, dashed arrows denote couple coupling between states with the coupling strength V_{ji}.

The Hamiltonian in Eq.6 is shown in the site representation, and the initial starting conditions are introduced in this representation. For the iterative fitting procedure the system is transformed to the eigenstate representation however. The Redfield tensor of the first three states R_{ijkl} (i,j,k,l=1..3) is calculated according to Eq.5 and then the full relaxation tensor is

formed by combination with the free relaxation rates of the other states as shown in Eq. 6. Using the full relaxation tensor and the Hamiltonian the time evolution of the density matrix elements is then calculated according to Eq.3. In the last step the amplitudes corresponding to now fixed density matrix elements σ_{ii} are calculated for each wavelength resulting in the species-associated difference spectra (SADS) determined from this global analysis.

For calculation of the R_{ijkl} elements (Eq.5) a spectral density in the form of a multimode Brownian oscillator was used (S. Mukamel, 1995; Y. Zhao and R.S. Knox, 2000):

$$J(\omega) = \sum_j 2\lambda_j \omega_j^2 \frac{\omega\gamma_j}{(\omega_j^2 - \omega^2)^2 + \omega^2\gamma_j^2} \quad (7),$$

where ω_j is the frequency of the mode 'j', γ_j is the damping parameter, $\lambda_j = g_j \cdot \omega_j$ is the coupling strength (reorganization energy), g_j – the Huang-Rhys factor. A system of two modes (one high frequency mode of ~1100 cm^{-1} and one low frequency mode of ~300 cm^{-1}) was used. Data were fitted globally for 40..70 detection wavelengths. The chirp correction for the experimental data was performed by two methods: (i) the chirp was introduced as a free parameter at each wavelength, (ii) the chirp was modeled using the Sellmeier dispersion formula, in which the parameters and optical length were free parameters global for all wavelengths. The second method showed better results, was more efficient and resulted in smoother SADS.

The fitting algorithm was implemented into a MATLAB code (*MATLAB R2010a*, The *Mathworks*, Natick, MA, USA). The elements of Hamiltonian and spectral density were treated as free fitting parameters in the nonlinear least-square routine. The populations (density matrix elements) were calculated using the classical Runge-Kutta method inside the nonlinear least-square function. The excitation function (temporal profile of the excitation pulse) was incorporated inside the differential equation solver. The amplitudes of the populations of different states (i.e. species associated difference spectra, SADS) were calculated via linear fitting algorithm. In order to avoid local minima in the solution space, the fitting procedure was repeated several times (N~50) with starting values of the system parameters varied using a random factor (<30%).

4.4 Results

Transient absorption signals in the form of 3D-maps of lutein measured at various conditions are shown in Figs. 4.3 (short time-scale) and 4.4 (long time-scale). These are the same data that were used in (E. Ostroumov et al., 2009), however here the full range of detection wavelength is shown, rather than few decays at selected wavelengths. The strong positive yellow-red peak in the 500-600 nm region observed in all the subfigures corresponds

to the $2A_g^-$-S_N ESA band and shows a rise ~300 fs after the excitation pulse. On the long and sometimes on the short wavelength sides of the maximum of this ESA band several satellite vibrational bands of the $2A_g^-$-S_N transition are located. These bands are more pronounced in lutein dissolved in hexane and benzonitrile, whereas in diethyl ether solution these vibrational bands are essentially absent. The dynamics in the first 300 fs consists of several mixed positive and negative signals resulting in a very complicated profile. On the blue side of the spectrum the SE and GB signal are observed as negative dark-blue bands. At longer wavelengths at the same delays as the GB signal a positive peak(s) is located and its amplitude increases with increase of the detection wavelength. In every subfigure of Fig. 4.3 the profile of this peak is different having a unique 'finger print' shape characteristic for the carotenoid in a certain solvent at the specified excitation wavelength. At 475 nm excitation wavelength (Figs. 4.3 A,D,E) this signal is present already at 550 nm, it evolves homogeneously along the wavelength scale and rises at the 700 nm to the value comparable to the amplitude of the S_1-S_N signal at this wavelength. In hexane and benzonitrile solutions (Figs. 4.3D,E and 4.4D,E) this ultrafast signal has two vibrational bands at positions similar to the satellite vibrational bands of the $2A_g^-$-S_N transition. However they are red-shifted in comparison to the $2A_g^-$-S_N satellite bands and their intensity rises at long wavelengths, whereas $2A_g^-$-S_N signal decreases. In Figs. 4.3C and 4.4C lutein excited to the very red edge of the absorption band shows strong increase in the amplitude of the ultrafast positive signal with maximum amplitude at 700 nm. This ultrafast signal can not come from the S_1 state since it is not populated at these early delay times and is assigned to the initially excited $1B_u^+$ (S_2) state. Similar increase of the ultrafast ESA signal was observed in other carotenoids (β-carotene, neurosporene) excited to the red edge of the absorption band (not shown). In hexane and diethyl ether solutions with excitation at 475 nm (Fig. 4.4A,D) the amplitude of this ultrafast ESA signal at 700 nm is comparable to the amplitude of the following it $2A_g^-$ (S_1) ESA signal and these two positive signals are separated by gap or even by a negative contribution (SE). This ordering and interchange of positive/negative signals is clearer visible in the transient spectra in Fig. 4.5A,D.

Table 4.1. Values of frequencies 'ω_i', Huang-Rhys factors 'g_i' and damping factors 'γ_i' for two modes obtained during analysis of the experimental transient absorption data .

	ω_1 (cm^{-1})	ω_2 (cm^{-1})	g_1	g_2	γ_1 (cm^{-1})	γ_2 (cm^{-1})
Lut / DET / 475	1197	316	0.4	1.1	35.9	8.1
Lut / DET / 495	1181	339	0.4	1.6	31.2	6.2
Lut / DET / 515	1249	355	0.4	0.7	23.8	2.4
Lut / Hex / 475	1116	311	0.5	0.9	36.4	4.1
Lut / BNI / 475	1032	383	0.2	0.7	31.2	2.7

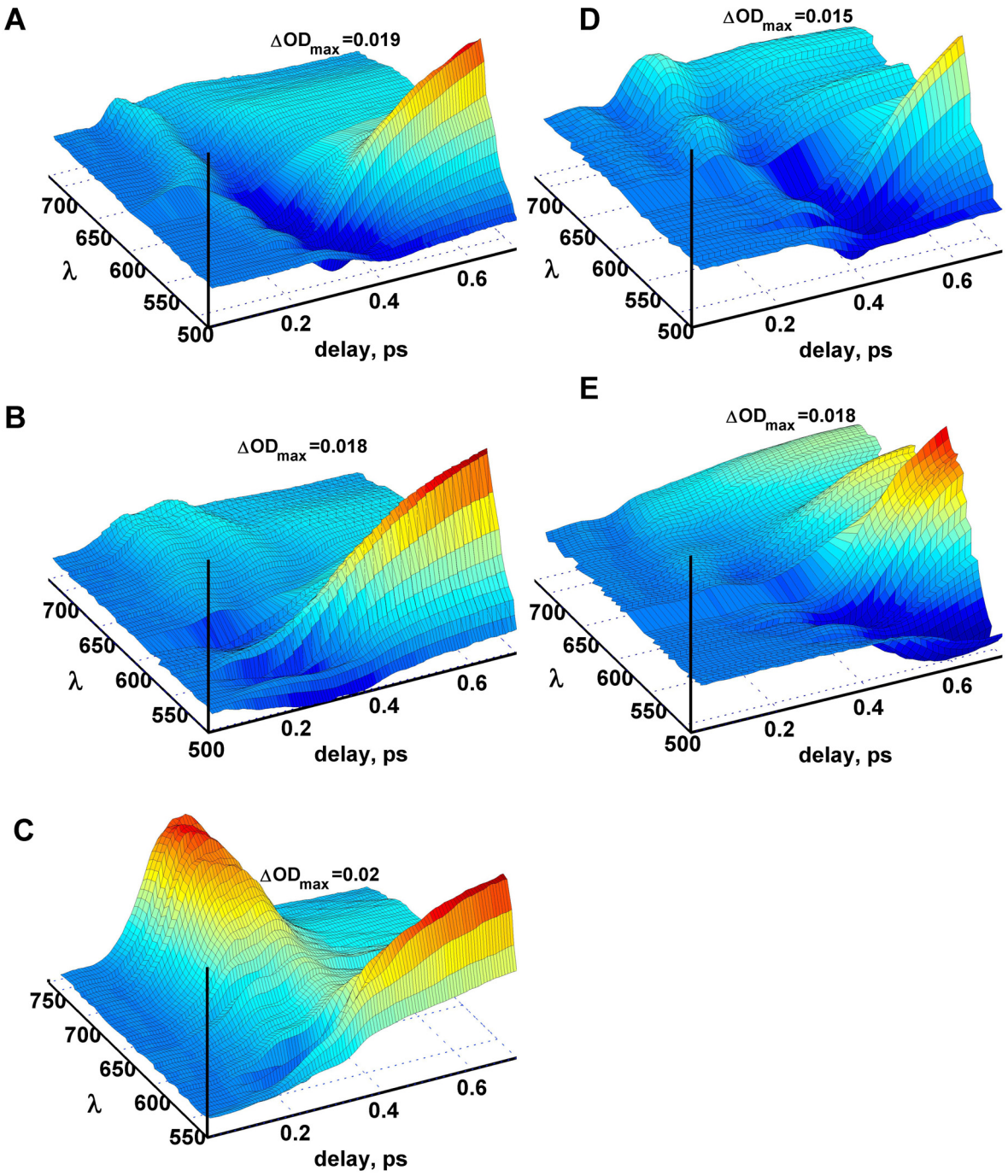

Figure 4.3. 3D maps of transient absorption decays (on the short time scale 0..0.7 ps) of lutein in diethyl ether at λ_{exc}=475 nm (A), at λ_{exc}=495 nm (B), and at λ_{exc}=515 nm (C) and in benzonitrile at λ_{exc}=475 nm (D), in hexane at λ_{exc}=475 nm (E). For convenience of presentation transient data are normalized to the maximum, the maximal optical density is shown for each measurement.

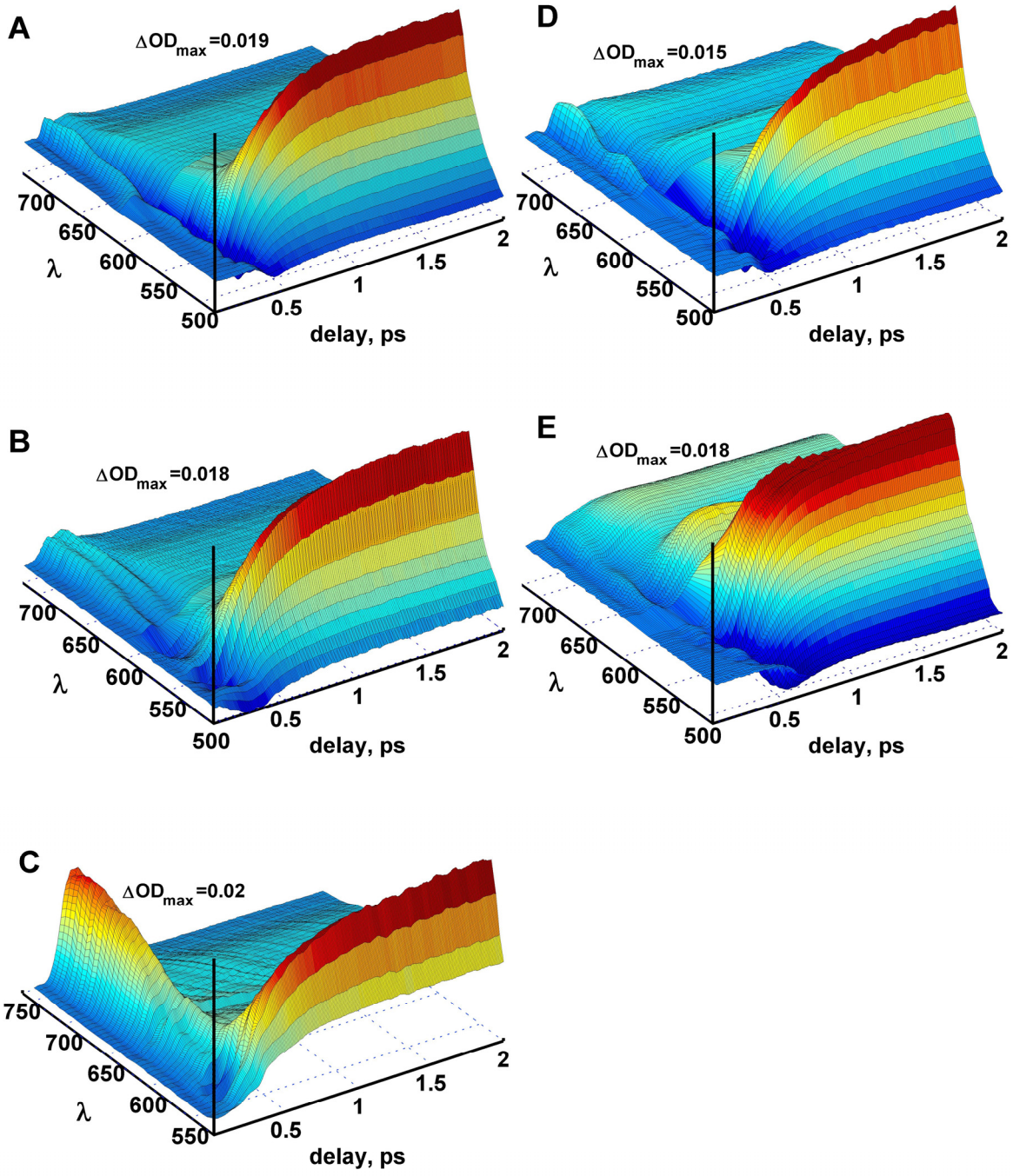

Figure 4.4. 3D maps of transient absorption decays of lutein on the long time scale (for detailed description see Fig. 4.3).

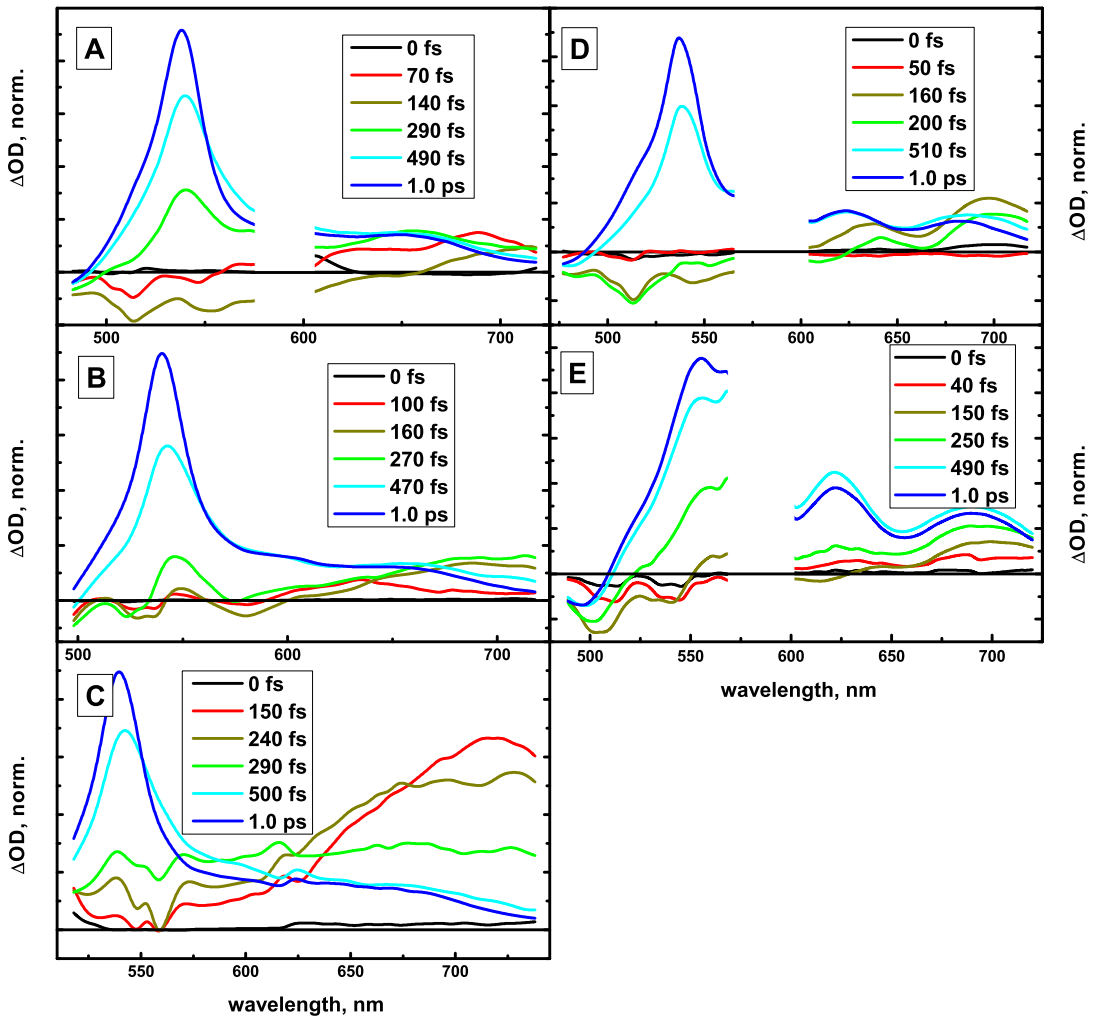

Figure 4.5. Transient spectra at selected delays of lutein in diethyl ether at λ_{exc}=475 nm (A), at λ_{exc}=495 nm (B), and at λ_{exc}=515 nm (C) and in benzonitrile at λ_{exc}=475 nm (D), in hexane at λ_{exc}=475 nm (E).

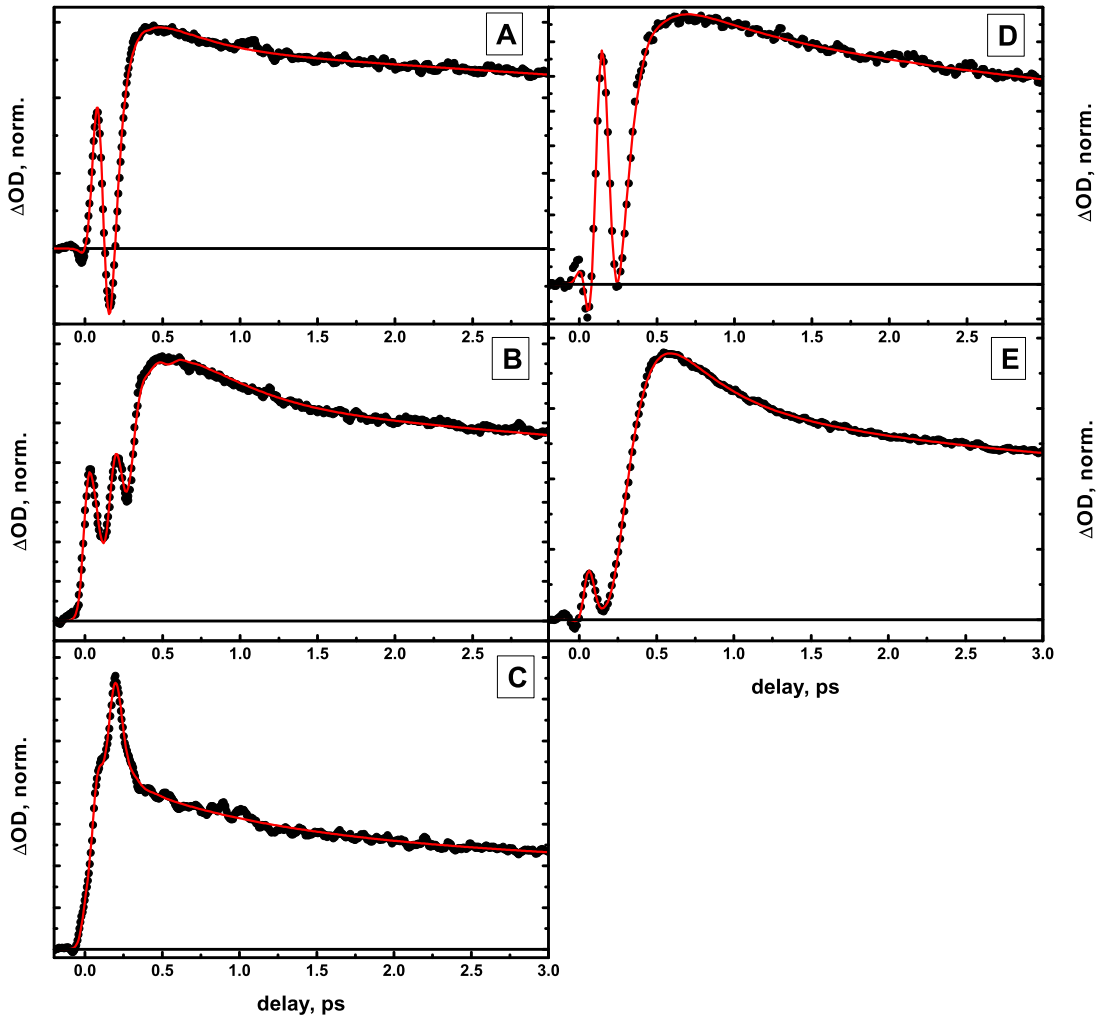

Figure 4.6. Selected decay kinetics of lutein in diethyl ether at λ_{exc}=475 nm (A), at λ_{exc}=495 nm (B), and at λ_{exc}=515 nm (C) and in benzonitrile at λ_{exc}=475 nm (D), in hexane at λ_{exc}=475 nm (E). Detection wavelength λ_{det}=633 nm. Black dots – experimental data, red lines – calculated data resulted from the model shown in Fig. 4.2.

Table 4.2. Values of transfer rates and depopulation rates selected from the Redfield tensor obtained from the experimental TA data according to the model shown in Fig. 4.2.

Rates, ps^{-1}	R_{1122}	R_{1133}	R_{2233}	R_{3344}	R_{4455}	R_{5555}
Lut / DEE / 475	42	0.02	15	3.5	0.35	0.073
Lut / DEE / 495	36	0.00	7.7	1.9	0.35	0.073
Lut / DEE / 515	22	0.00	21	2.5	0.35	0.073
Lut / Hex / 475	14	0.01	10	3.5	0.35	0.073
Lut / BNI / 475	7.2	0.01	7.0	3.5	0.45	0.073

Table 4.3. Values of Hamiltonian elements (energies of states E_i and coupling strengths V_{ij}) obtained from the experimental TA data according to the model shown in Fig. 4.2.

	E_1 (cm^{-1})	E_2 (cm^{-1})	E_3 (cm^{-1})	E_4 (cm^{-1})	E_5 (cm^{-1})	V_{12} (cm^{-1})	V_{13} (cm^{-1})	V_{23} (cm^{-1})
Lut / DEE / 475	20308	19259	18281	15622	14336	194	8	183
Lut / DEE / 495	20011	18758	17891	15622	13836	140	8	177
Lut / DEE / 515	19291	18112	17075	14916	14036	150	5	222
Lut / Hex / 475	20212	19196	18415	15862	14236	101	10	172
Lut / BNI / 475	19172	18712	17609	15120	14136	132	8	119

At longer excitation wavelengths (red tail of the S_2 absorption) the spectroscopic features during the first 300 fs differ substantially. In diethyl ether lutein excited at 495 nm shows almost no red-shifted SE. In its place an additional positive peak is observed (Fig. 4.3B). When excited at 515 nm, these two peaks come very close to each other but still can be resolved in the 560-670 nm region (Fig. 4.3C). The amplitude of this ultrafast ESA band shows a gradual rise when the excitation wavelength is increased.

The positive and negative or two positive signals following each other indicate that at least two states are responsible for dynamics in the first 300 fs prior to the population of the $2A_g^-$ (S_1) state. However lifetime kinetic analysis fails to describe the observed "oscillatory" behavior even if an infinitive number of lifetime components is used (LFD maps based on the Laplace transform (R. Croce et al., 2001)). Therefore a more advanced analysis scheme has to be used for description of this early relaxation dynamics. In (E. Ostroumov et al., 2009) we applied a simplified system of optical Bloch equations with two coherently coupled states. In current work a more general density matrix approach with the Redfield dissipation tensor (Eq.6) is introduced for more complete description of the coupling and coherent dynamics of carotenoid excited states. The selected experimental curves with detection at 633 nm are shown in Fig. 4.6 together with curves calculated according to the model Eq.6. Corresponding values of the fitting parameters are shown in Table 4.1. The frequency values and the damping rates of the two modes show typical for carotenoids values. The high frequency mode (~1100 cm^{-1}) is known to be responsible for the C-C stretching mode and the low

frequency mode (~330 cm^{-1}) corresponds to the torsion or bending vibrations. The Huang-Rhys factors show values in the expected range with ~0.4 and ~1.0 for the high and the low frequency modes, respectively (Table 4.1). The higher Huang-Rhys value for the low frequency mode indicates its stronger coupling to the bath and therefore stronger dissipation. Thus the reorganization energy for both modes is in the range of 300-400 cm^{-1} what is in agreement with characteristic values reported in the literature (N. Christensson et al., 2009). The state energies and coupling strengths are shown in Table 4.3. They were determined from the analysis by fitting of the data using model shown in Eq.6, and are also in agreement with literature. The energies follow the excitation wavelength and depend on the solvent. The dependence on the λ_{exc} can obviously be explained by excitation to the different state manifolds or, in other words, by excitation into different regions of the non-homogeneously broadened excited state. The solvent effect is also clear – in highly polar benzonitrile the energy of the S_2 state is shifted to the lower energies (shift of the absorption spectrum by ~700 cm^{-1}, see Fig. 4.1), whereas both hexane and diethyl ether are non-polar solvents and the state energy determined for experiments on lutein in these two solvents is almost the same. The relaxation rates (selected elements of the Redfield tensor) are shown in Table 4.2. The relaxation rates R_{2211} and R_{3322} correspond to the relaxation rates of states 1 and 2 and show in average very high values (>10 ps^{-1}), meaning that the coherence between these two states has a short lifetime. Indeed, the relaxation from state 2 to state 3 occurs with the time-constant 50..150 fs, which explains why the oscillations observed in the experimental data (see Figs. 4.3 and 4.4) disappear within 300-400 fs. The relaxation rate from state 1 to state 3 is R_{3311}=0 which is explained by the very weak coupling strength V_{13} (see Table 4.3). The rates R_{4433}, R_{5544} and R_{5555} have typical values for lutein and the last two rates were fixed in the analysis in order to avoid uncertainty when the fitting was performed on a short time-scale (<1.5 ps).

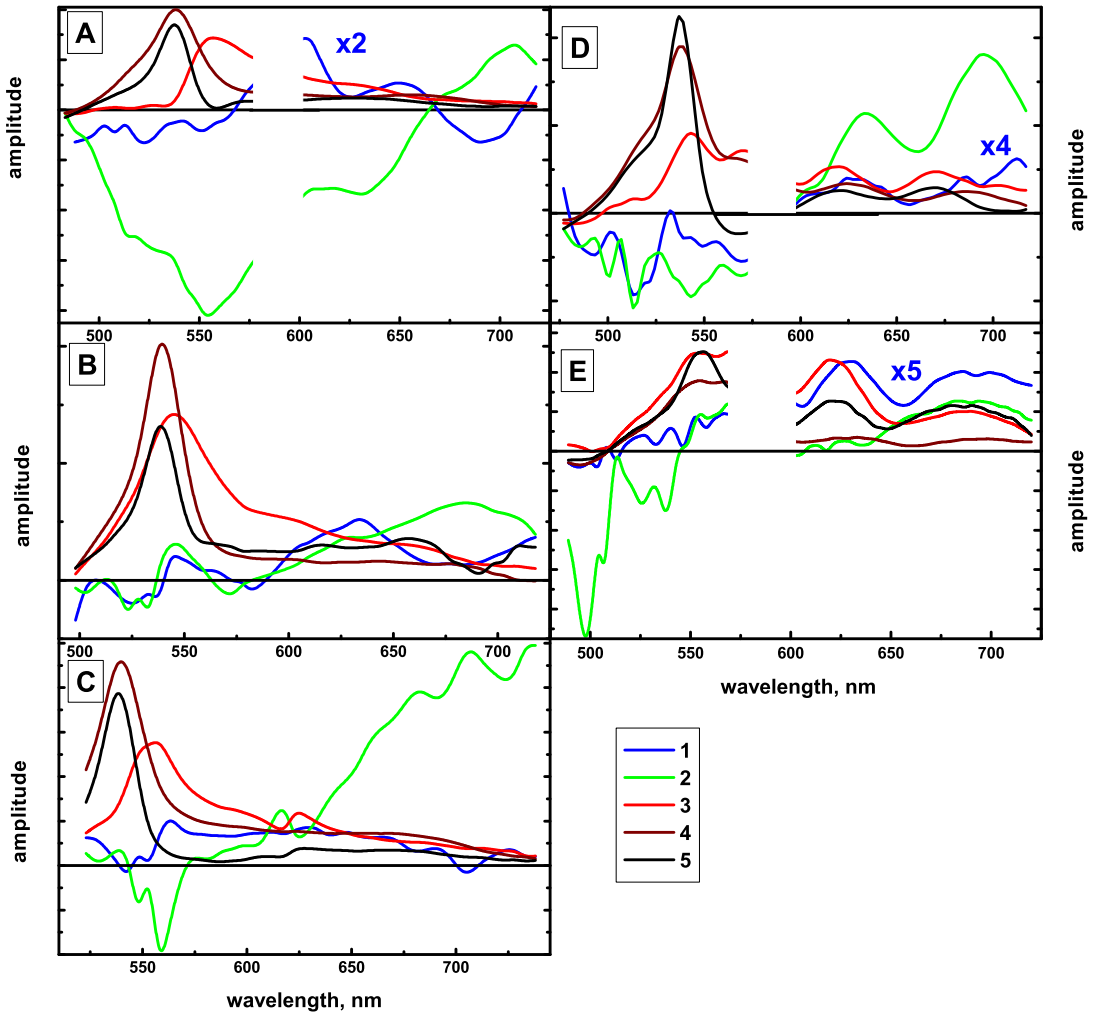

Figure 4.7. Species-associated difference spectra (SADS) in the site representation of lutein in diethyl ether at λ_{exc}=475 nm (A), at λ_{exc}=495 nm (B), and at λ_{exc}=515 nm (C) and in benzonitrile at λ_{exc}=475 nm (D), in hexane at λ_{exc}=475 nm (E). The same state notations are used for all subfigures A-E.

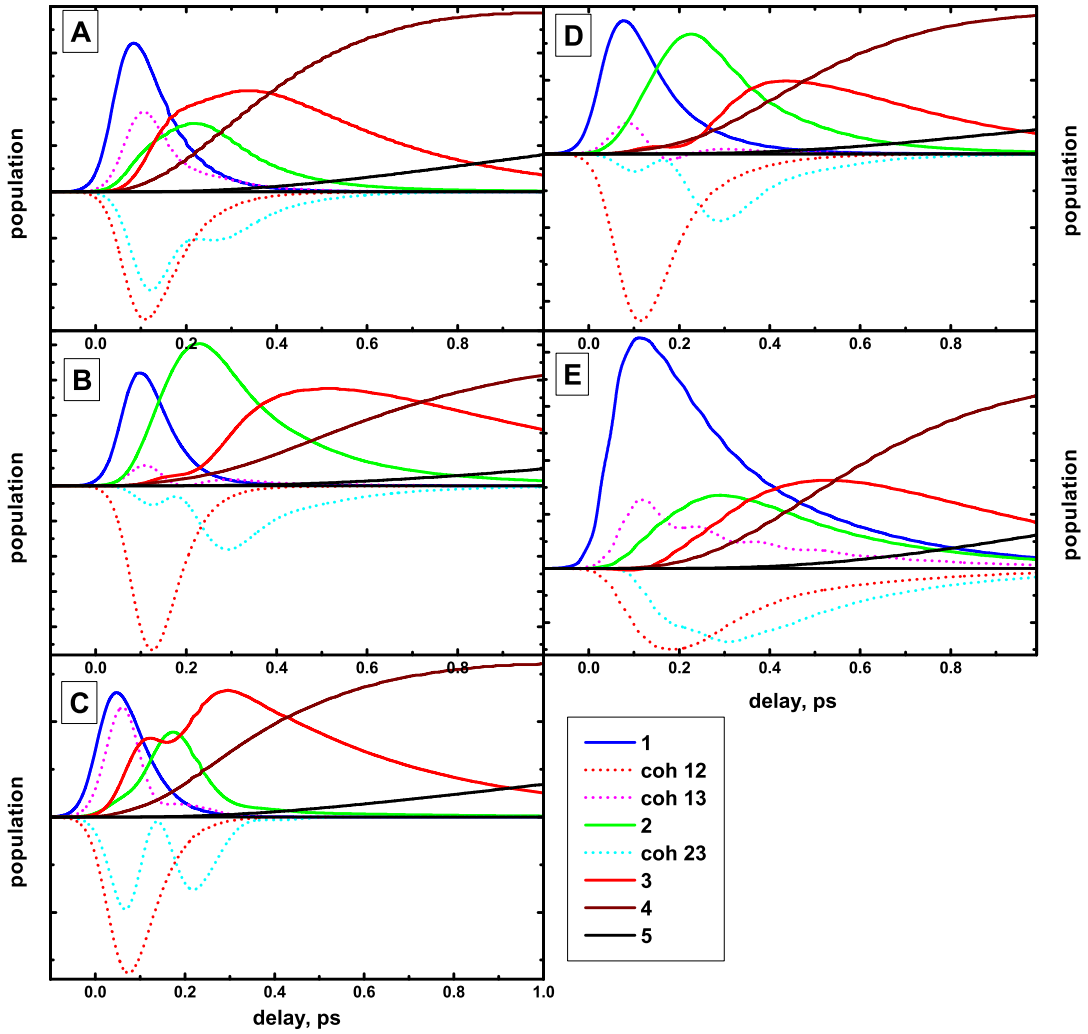

Figure 4.8. Population dynamics and dynamics of coherences in the site representation of lutein in diethyl ether at λ_{exc}=475 nm (B), at λ_{exc}=495 nm B), and at λ_{exc}=515 nm (C) and in benzonitrile at λ_{exc}=475 nm (D), in hexane at λ_{exc}=475 nm (E). The same state notations are used for all subfigures A-E.

The species-associated difference spectra (SADS) and population dynamics of lutein in diethyl ether excited at 475 nm, 495 nm and 515 nm and in benzonitrile and hexane excited at 475 nm are shown in Fig. 4.7 and 4.8, respectively. The populations of coherent terms are shown together with the state populations and are marked by dashed lines. Coherent terms represent contributions of special 'coherent states', states that are formed by the coupling V_{ij} of states i and j. Thus the coherence 1-2 correspond to a new state, produced by the coupling V_{12} of the initially excited state 1 and state 2. It is important to note here that although in general a coherence between states can be formed only if two (or several) states are excited by the pump pulse, in a system of strongly coupled states the coherence can be formed even if in the site representation (Eq.6) all excitation energy is absorbed by state 1 only. Indeed in the eigenstate representation the excitation vector will have non-zero values for those states (e.g. state 2 in Fig. 4.2) that are strongly coupled to the initially excited state. In that case the system will show coherent behavior.

In this work the density matrix elements were calculated in the eigenstate representation but the fitting to the experimental data was performed in the site representation. The fitting can also be performed in the eigenstate representation without transformation of the density matrix into the site representation. In that case the coherent contributions have to be included directly in the fitting and the results (SADS and populations) would correspond to the diabatic states. This procedure can give additional advantages in cases of systems with strong coupling where the Born-Oppenheimer approximation can not be applied. This approach will be applied in carotenoid studies in the next work.

The spectra of 'coherent states' (SADS) can be interpreted in terms of SE and ESA in the similar way as the state spectra. However the origin of the signals is not quite clear for us. For this reason the fit was performed in site representation where coherences do not contribute directly to the fitting and therefore do not have SADS in Fig. 4.7 and we will consider only spectroscopic features of states 1-5. The first two SADS (blue and green) correspond to the initially excited states. The negative contribution at short wavelengths and the positive contribution at longer wavelengths of these states correlate with the dynamics of peaks observed in the first 300 fs (Fig. 4.3). State 2 (green) reveal more red-shifted negative SE signal (<650 nm), whereas state 1 has a positive feature starting already at ~570 nm. The interchange of the positive ESA and negative SE signals is obviously responsible for the 'oscillatory' behavior observed in the experimental decays at early relaxation times. Although general tendency of the SADS of states 1 and 2 is obvious, their profile is strongly indented especially in the short wavelength region. The reason of such behavior is low amplitude of the

signal in the 500-600 nm spectral range and strong mixture of contributions from different transitions (including rising $2A_g^-$-S_N transition). Under such conditions the chirp correction plays a decisive role in the fitting and has a strong influence on the rate constants and SADS of states 1 and 2 of the model Eq.6. In the spectral regions where the features of the decays are not pronounced the SADS and kinetic parameters can not be explicitly determined and large errors and variations are observed (Fig. 4.7). To resolve this problem a more elaborate analysis (e.g. global fit of several experiments with different excitation wavelengths) and/or additional information (e.g. low temperature measurements, ultrafast fluorescence data) is necessary.

The last three SADS in Fig. 4.7 have ESA band in the 500-650 nm region characteristic for the $2A_g^-$ (S_1) state. State 3 shows a red-shift of the maximum of the signal and increased amplitude of the long wavelength shoulder. SADS of states 4 and 5 are very similar to each other having higher amplitude at short wavelengths but state 4 reveals slightly higher amplitude of the red shoulder. We assign states 3 and 4 to vibrationally excited and state 5 to vibrationally relaxed S_1 state. Several alternative schemes of relaxation pathways between states 3-5 are proposed in the literature however this problem is out of scope of the current work. Here we only note that the rate constants of states 3-5 (Table 4.2) agree well with the literature data on lutein and β-carotene (T. Polivka and V. Sundström, 2004). The detailed discussion of assignment of these states and of their arrangement in different electronic level models can be found elsewhere (see **Chapter 5**).

4.5 Discussion

The positive signal above 650 nm observed on the early times of relaxation (<50 fs) was assigned by Cerullo et al. (G. Cerullo et al., 2002) to the $1B_u^+$-S_N ESA transition. However later the same signal was reinterpreted as two-photon absorption process and coherent contribution from the solvent (D. Kosumi et al., 2005; J.L. Perez Lustres et al., 2007). The ultrafast signal shown in this work can not be due to a coherent contribution from the solvent or any high order nonlinear process since overall duration of the signal is 150-200 fs, what is 2-3 times longer than the FWHM of the pulse (<80 fs). The signal shows vibrational structure characteristic for carotenoid electronic transitions (Fig. 4.7D-E) what also disagrees with the hypothesis of coherent effect. It is important to emphasize, that low intensity pump pulses were used in the experiments (<10 nJ) and therefore no nonlinear effects are expected (see **Chapter 5** for description of the intensity dependent measurements). The two-photon absorption of the sample via the $1B_u^+$ (S_2) state can not account for this signal as well, since the signal is located above 600 nm, whereas the excitation pulse is located at 515 nm for Fig.

4.7C and <500 nm for Figs. 4.7A-B and 4.7D-E. Thus the positive ultrafast signal occurring at wavelengths >600 nm corresponds to the ESA from initially excited $1B_u^+$ (S_2) state of the carotenoids. In Fig. 4.7 initially excited state 1 has positive amplitude above 600 nm and therefore we assign state 1 of the model Eq.6 to the $1B_u^+$ (S_2) state.

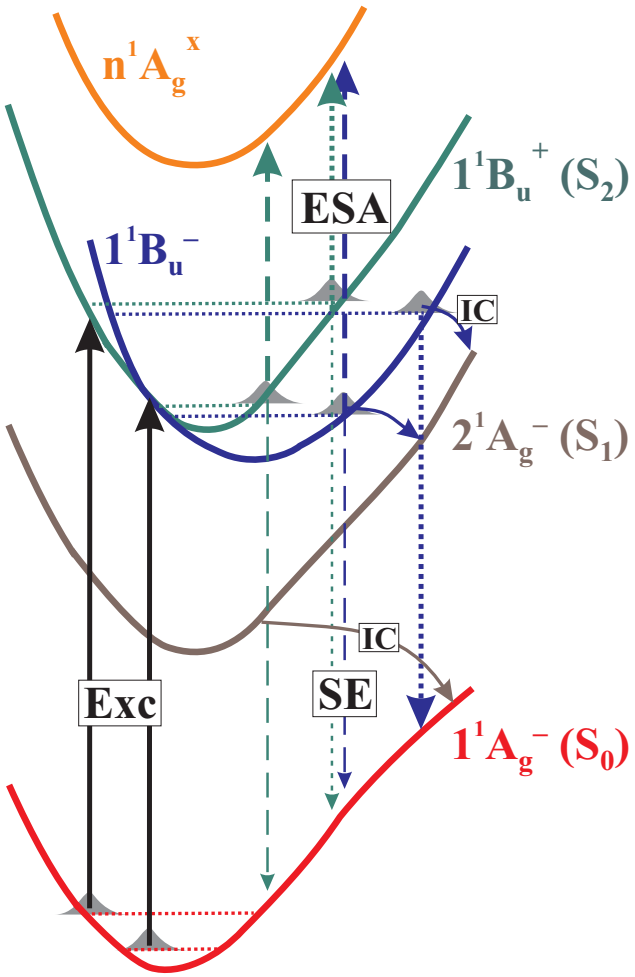

Figure 4.9. Schematic potential energy surface model of lutein. Black up-ward directed arrows – excitation (Exc), green up-ward/down-ward directed arrows – ESA/SE from the $1B_u^+$ state, blue up-ward/down-ward directed arrows – ESA/SE from the $1B_u^-$ state, curved lines – internal conversion (IC). Dotted and dashed lines – excitation to high and low energy states respectively.

In (E. Ostroumov et al., 2009) the $1B_u^-$ state was proposed to be strongly coupled to the $1B_u^+$ (S_2) state in carotenoids with N>9 and to be responsible for the broad (500-650 nm) negative SE band observed in the transient spectra. The contribution of the $1B_u^-$ state to the SE signal was additionally confirmed by the bathochromic shift and distortion of the steady-state fluorescence spectrum of lutein and β-carotene (E. Ostroumov et al., 2009). In Fig. 4.7A the SADS of state 2 show negative signal covering the whole wavelength scale from 500 nm to 700 nm. This SE signal correlates with the negative transient spectra observed at 150-200

fs delays in Fig. 4.3. Therefore we assign state 2 to the $1B_u^-$ state. However the SADS of state 2 changes when carotenoid is excited at longer wavelengths: it becomes similar to the SADS of state 1 showing strong positive ESA signal above 600 nm. This change in the SADS (Fig. 4.7B-C) corresponds to the double peak-profile of the ultrafast ESA band observed in experimental decays in Fig. 4.3B-C. The change from the negative SE to the positive ESA in the SADS of state 2 may be caused by excitation to a lower vibrational band of the $1B_u^-$ state where the competition between dipole moments of $1B_u^-$-S_0 and $1B_u^-$-S_N transitions is favored towards the latter. Indeed, although the $1B_u^+$ and $1B_u^-$ states have different Pariser indexes, when their energy levels come close to each other the symmetry rules do not hold exactly and the two states are expected to show similar spectral features, i.e. at longer excitation wavelengths the $1B_u^-$ state is no longer a 'dark state'.

The results and conclusions can be summarized in the model shown in Fig. 4.9. First we consider dynamics during first 300 fs under excitation of the 0-0 or 0-1 transition (thick black solid arrow). In this case a system of coherently excited eigenstates is formed. In the short wavelength spectral region (<570 nm for lutein) the signal corresponds to the GB and SE from the initially excited $1B_u$ state(-s) (shown as thin green and thick blue dotted downwards directed arrows). At longer wavelengths spectrum of the $1B_u^+$ state reveal positive ESA band (thick green dotted upwards directed arrow) whereas the $1B_u^-$ state still shows negative SE due to the shift along nuclear coordinates of its potential energy surface (E. Ostroumov et al., 2009). The resulting decay has oscillatory-like shape with interchanging positive and negative signals. However when the molecule is excited to the very red edge of the absorption band (low energy side of the 0-0 transition, thin black solid arrow) the picture changes. Because the lower vibrational levels of the $1B_u$ states are excited the energy of the $1B_u$-nA_g^x transition increases and a hypsochromic shift (to the shorter wavelengths) of the corresponding ESA band is observed (thick green and blue dashed upwards directed arrows). As the result the amplitude of the ESA band of the $1B_u^+$ state below 700 nm increases and the competition between negative SE and positive ESA (blue dashed arrows directed upwards and downwards, respectively) takes place in the spectrum of the $1B_u^-$ state. The lower excitation frequency is used the stronger is the positive contribution in the spectrum of the $1B_u^-$ state. This is very well seen in the series of excitation wavelength dependent measurements of lutein in diethyl ether (see Fig. 4.3A-C). At 475 nm excitation the signal following the positive peak in the 600-700 nm detection range has negative amplitude. At 495 nm excitation it becomes positive, forming second peak after the first one and the amplitude of both of them is higher than at 475 nm excitation. At 515 nm these two positive peaks come very close to

each other and their amplitude is comparable to the maximum of the $2A_g^-$-S_N transition meaning that at 515 nm excitation the $1B_u$-nA_g^x transition has maximum dipole moment. This model implies that no vibrational relaxation takes place in the $1B_u$ states and excitation energy is transferred (most probably from the lower lying $1B_u^-$ state) directly to the vibrationally excited $2A_g^-$ (S_1) state (short curved blue arrows). This observation is in agreement with the study of longer time-scale dynamics of β-carotene (see **Chapter 5**).

4.6 Conclusions

The transient absorption study of the relaxation dynamics of lutein in different solvents has shown that complex behavior of the decays in the first 300 fs is a true signal originating from the initially excited electronic states of the carotenoids and not a coherent contribution from the solvent or a two-photon absorption process. The complexity of the decays in the 570-720 nm spectral range exclude any possibility to model the signal with a system of exponential functions (lifetime analysis). Implementation of coherent terms and Redfield tensor in the master equation allowed successful global fitting of the data and determination of the parameters of the model: frequencies, Huang-Rhys factors and damping factors for two frequency modes, and Hamiltonian of the system. More elaborate analysis (e.g. global for several excitation wavelengths analysis) and/or additional information (low temperature measurements, ultrafast fluorescence data, a priory values on the spectral density function) can increase efficiency and precision of the method. The ultrafast dynamics can be described by a system of three coupled states and coherence has to be taken into account. The initially excited state showed positive ESA at λ>570 nm corresponding to the $1B_u^+$-nA_g^x transition. The $1B_u^-$ state revealed strong coupling to the $1B_u^+$ state and showed strongly red-shifted SE signals when excited to the maximum of the 0-0 transition. Under low energy excitation conditions the SE signal is dominated by the ESA coming from the $1B_u^-$-nA_g^x transition and the amplitude of the $1B_u^x$-nA_g^x transition strongly increased. No vibrational relaxation in the $1B_u^+$/$1B_u^-$ states takes place and the excitation wave-packet is transferred from the initially excited states to the $2A_g^-$ (S_1) vibrationally excited state.

Acknowledgements

The present work has been performed as project B2 within the DFG Sonder-forschungsbereich SFB 663, Heinrich-Heine-Universität Düsseldorf and Max-Planck-Institut für Bioanorganische Chemie, Mülheim a.d. Ruhr, Germany

Chapter 5

On the nature of the “dark S*” excited state of β-carotene

This chapter is based on the publication Evgeny E. Ostroumov, Marc G. Müller, Michael Reus, and Alfred R. Holzwarth. (2010), s*ubmitted*

Femtosecond transient absorption spectroscopy has been applied to the isolated carotenoid β-carotene under a large variety of experimental conditions regarding solvent, temperature, excitation wavelength, and intensity to study the excited state relaxation dynamics in order to elucidate the origin of the so-called "dark S* state" that has been discussed very controversially in the literature. The results are analyzed in terms of lifetime density maps and various kinetic models are tested on the data. The sample purification was found to be critical. The appearance of a long-lived lifetime component (τ>10ps) which has been associated in many previous studies with the S* state is due to the presence of an impurity. For pure samples four lifetimes are typically observed (all ≤10 ps at room temperature). Consideration of all the experimental data leads us to exclude relaxation schemes implying a separate electronic S* state formed in parallel to the normal $S_2 \rightarrow S_1$ relaxation scheme. We show that a sequential relaxation scheme involving only vibrationally excited S_1 states and vibrational cooling on the ps time scale fully describes all the data. Thus the assignments of the previously reported "S* state" as a separate electronic state as well as an assignment to a vibrationally excited ground state species is excluded. We also exclude a major conformational change occurring in the exited state(s). The high intensity excitation is proposed to lead in part to a two-photon excitation process that in turn gives rise to a population of a different vibrational state in the S_1 manifold. This population produces spectral changes in the initially created S_1 state (created with ca. 150 fs lifetime and decaying with ca. 500 fs lifetime) which can be explained by a modified vibrational excitation pattern. A similar effect is caused by short-wave excitation. Vibrational cooling in the S_1 state can explain fully all the features of the transient spectra on the picosecond time-scale within the traditional $S_2 \rightarrow S_1 \rightarrow S_0$ relaxation scheme without invoking any additional states.

5.1 Introduction

Carotenoids belong to the parent molecular group of polyenes, linear π-conjugated systems with very special electronic properties (K. Schulten et al., 1976; P. Tavan and K. Schulten, 1987; B.E. Kohler and I.D.W. Samuel, 1995; R.L. Christensen et al., 2008). They form a wide spread class of molecules which perform crucial functions in all biological systems ranging from protection against highly reactive oxygen species, triplets etc. In photosynthetic organisms carotenoids in addition perform light-harvesting and (photo)protective functions (A.J. Young and G. Britton, 1993; H.A. Frank and R.J. Cogdell, 1996; R.L. Christensen, 1999; R.J. Cogdell et al., 2000; A.R. Holzwarth, 2004; T. Renger and A.R. Holzwarth, 2008). Many of these functions are intimately related to the very complex excited state structure and excited state relaxation dynamics of carotenoids (H.A. Frank and R.J. Cogdell, 1996; R.L. Christensen, 1999; T. Polivka and V. Sundström, 2009). Despite a large number of experimental and theoretical studies carried out over the last two decades many questions regarding the photophysical properties of carotenoids are still unclear. It is generally accepted that the strong transition in carotenoids belongs to the $S_0 \rightarrow S_2$ transition – as originally proposed based on quantum chemical calculations (P. Tavan and K. Schulten, 1987) - leading to the $1B_u^+$ state, which rapidly relaxes (within 100-200 fs) to the optically forbidden (from the ground state) S_1 ($2A_g^-$) state (B. Hudson and B. Kohler, 1974; B.S. Hudson et al., 1982) which has a lifetime in the order of ps. However many additional so-called "dark" excited states ($1B_u^-$, $3A_g^-$, S*, $S^‡$, S_x) have been proposed to be located between the S_1 and the S_2 states based on various experimental findings and reported in several ultrafast spectroscopy studies (for reviews see (R.L. Christensen, 1999; T. Polivka and V. Sundström, 2004; H. Hashimoto et al., 2004; R.L. Christensen et al., 2008; T. Polivka and V. Sundström, 2009)). The experimental data leading to the proposal of these additional "dark" states have been discussed very controversially in the literature. Despite the considerable problems that carotenoid excited states pose to linear quantum mechanical computational

methods due to the very high electron correlation in polyene type molecules, it is important to note that, with the exception of the $1B_u^-$ and the $3A_g^-$ states, no clear evidence for the existence of the other experimentally proposed "dark" states has been found in quantum mechanical calculations so far (K. Schulten et al., 1976; P. Tavan and K. Schulten, 1987; C.M. Marian and N. Gilka, 2008; M. Kleinschmidt et al., 2009; E. Ostroumov et al., 2009; J.P. Cerón-Carrasco et al., 2010).

One of the most controversially discussed "dark" states, the so-called S* state, was first proposed on the basis of femtosecond transient absorption of spirilloxanthin and the spirilloxanthin-containing light-harvesting I (LH1) protein complex from *Rhodospirillum rubrum* (P.O. Andersson and T. Gillbro, 1995; C.C. Gradinaru et al., 2001). Spectrally this state was suggested to be responsible for the positive signal on the blue side of the well-known excited state absorption (ESA) band of the S_1 state (P.O. Andersson and T. Gillbro, 1995) and was observed to decay on the long picosecond time-scale, typically slower than the S_1 state. Its dynamics was later explained by parallel population of the S_1 and S* states (C.C. Gradinaru et al., 2001). It was also reported that the S* state of the protein-bound spirilloxanthin in LH complexes acts as precursor of the carotenoid triplet state formed via singlet-triplet homo-fission (E. Papagiannakis et al., 2002; E. Papagiannakis et al., 2003). In (D.S. Larsen et al., 2003) a blue-shifted signal in isolated β-carotene was identified (in this case discussed as a new $S^{\ddagger}$ state, although the features are essentially those of the S* state discussed in other cases, see e.g. (A.E. Jailaubekov et al., 2010)). The ESA signal decayed with a lifetime >50 ps (τ_{S1}~10 ps) and the component was observed to be enhanced upon excitation at 400 nm as compared to the 0-0 excitation (~490 nm). Additional support on the excited electronic state nature of the proposed "dark" S* state came from excitation intensity dependence (E. Papagiannakis et al., 2006). In that work the inhomogeneous saturation of the TA signal at high excitation intensities was explained by the independent relaxation of the S* and S_1 states populated in parallel from the high energy S_{2N} state. The nonlinear dependence

in this case was explained by the second-order process - the two-photon excitation of the S_{2N} state via the S_2 state (see e.g. (T. Polivka and V. Sundström, 2009) for a further discussion of this "two-photon model"). Later on similar spectroscopic features assigned to the S* state have been found in a wide range of other carotenoids, including the most-studied β-carotene (D.S. Larsen et al., 2003; H.H. Billsten et al., 2005; D.M. Niedzwiedzki et al., 2006; E. Papagiannakis et al., 2006; D. Niedzwiedzki et al., 2007; H. Cong et al., 2008; A.E. Jailaubekov et al., 2010). In all of these papers the S* state was assigned to an electronic excited state created from the S_2 state in parallel to the S_1 state.

In (H.H. Billsten et al., 2005) a short-wavelength shoulder in the S_1 ESA band in TA data of isolated zeaxanthin was suggested to originate from the S* state. The lifetime of this state was <5 ps (τ_{S1}~9 ps) and it was enhanced in high energy (short wave) excitation conditions. The model of the excited state electronic nature of the S* state in isolated carotenoids was challenged however by Wohlleben et al. (W. Wohlleben et al., 2004; T. Buckup et al., 2006). These authors interpreted the blue-shifted positive TA signal in carotenoids with conjugation length N≥11 and lifetimes generally longer or comparable to the lifetime of the S_1 state as a vibrationally excited ground state populated via impulsive stimulated Raman scattering (ISRS). The main argument was the absence of an effect of a depletion pulse on the S* signal in contrast to the observed decrease of the S_1 ESA signal. In contrast to that a recent 2D-electronic spectroscopy study excluded the vibrationally hot ground state hypothesis as a possible explanation for the S* state (N. Christensson et al., 2009). Based on the respective Feynman diagrams and simulated spectra it was argued that in the observed 2D spectra of β-carotene only a separate electronic excited state can explain the positive signal in the pump-probe experiment (negative in 2D-spectroscopy). Finally, also a hypothesis of different carotenoid ground state conformers as the origin of the S* state was proposed by the group of H. Frank. The S_1 excited state of a geometric isomer of the parent all-trans molecule was suggested to be responsible for the blue-shifted signal (τ_{S*} ~ 2-3 ps,

τ_{S1}=10-40 ps) in the TA spectrum of several xanthophylls (D.M. Niedzwiedzki et al., 2006). In several longer carotenoids a similar signal but with typical lifetimes longer than the S_1 lifetime (e.g. τ_{S*}=9.7 ps, τ_{S1}=7.2 ps for spheroidene) was explained by the same geometric isomer hypothesis (D. Niedzwiedzki et al., 2007). The geometric isomer in this case was formed, as in the other models, from the S_2 excited state and would return to the all-trans configuration either in the excited S_1 state or upon its relaxation to the ground state. Additional support for this hypothesis came from low temperature experiments where the S*-reminiscent signal showed either lower amplitude or even disappeared, as may be expected for a component arising from major conformational changes (D. Niedzwiedzki et al., 2007; H. Cong et al., 2008).

Here we address in particular the experimental signals obtained in femtosecond TA spectroscopy related to the S* problem in isolated β-carotene. Because of the existing controversies on the origin of the S* state we study in detail the effects of purification of the sample, solvent effects, excitation energy and excitation intensity, as well as temperature effects. Finally, various kinetic schemes are discussed and compared in order to arrive at an interpretation of the origin of the S* state that is compatible with the whole body of observations.

5.2 Materials and Methods

Crystalline (nominally all-trans) β-carotene was received as a gift from Hoffmann-La Roche, Basle, Switzerland. All-trans-β-carotene isolation and purification was performed on a Waters Alliance 2695 system equipped with a 996 photodiode array detector and a YMC-Pack C30 column (YMC, 250x10 mm, 5 μm) (L.C. Sander et al., 1994). β-carotene was dissolved at high concentration in dichloromethane and filtrated through a 0.2 μm syringe filter. Under semi-preparative isocratic conditions with a flow of 5ml/min and 75:20:5 (ethanol:methanol:tetrahydrofurane) all-trans-β-carotene was fractionated as the main peak of

the elution profile detected at 453 nm absorption. As is shown in Fig. 5.1 the original sample contained a large number of impurities. Some of them absorb in the vicinity of the absorption of all-trans-β-carotene and at least one or more peaks (indicated in Fig. 5.1 by an arrow) absorbs maximally around 400 nm (Fig5.1B), For comparison β-carotene obtained from Aldrich was studied. It showed a similar pattern of impurities. The collected fractions were dried under vacuum and checked again by analytical HPLC in the same system as described above. The analytical check was made using a YMC-Pack C30 column (YMC, 250x4.6 mm, 5 µm), a flow of 1 ml/min and 11 min isocratic conditions with 50:50 (methanol:ethyl acetate) and a final washing step to 60:40 (n-hexane:ethyl acetate). Initial femtosecond measurements were performed both on purified and also on non-purified β-carotene samples. For final measurements only the purified samples were used.

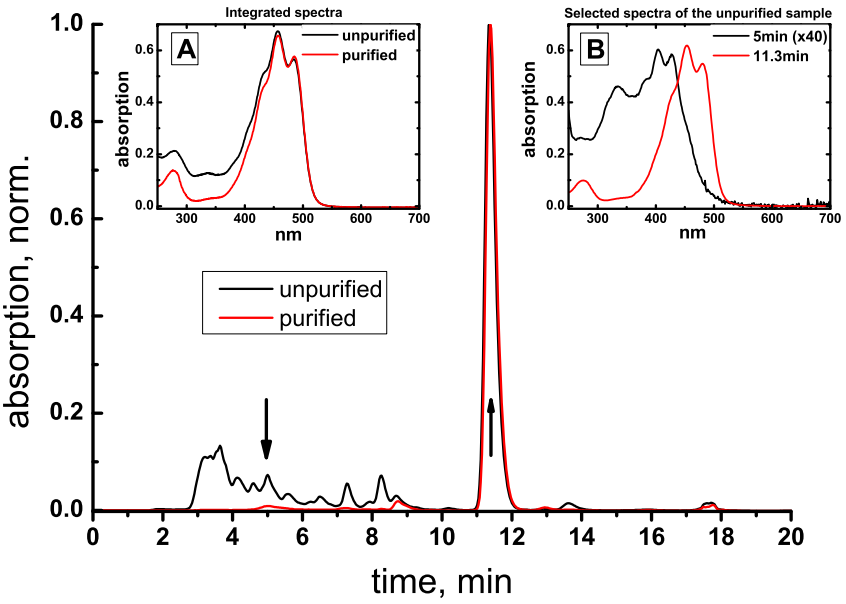

Figure 5.1 HPLC profiles of β-carotene in MTHF before and after purification. Integrated absorption spectra are shown in the inset A. Absorption spectra of unpurified sample taken after 5 and 11.3 minutes (as indicated by arrows) are shown in the inset B.

Femtosecond transient absorption measurements were performed at room temperature in CH_2Cl_2 and n-hexane as described earlier (R. Croce et al., 2001). The Ti:Sapphire laser

system together with regenerative amplifier generated transform-limited pulses at 3 kHz repetition rate. The pulses were focused into a 130 μm diameter spot. In the 470-510 nm spectral range excitation pulses had $\delta\lambda$=4 nm spectral width and τ_p=60-70 fs FWHM length. At 400 nm excitation $\delta\lambda$ was 2-3 nm and τ_p~80 fs. For intensity dependent measurements in MTHF three pulse energies were used. At λ_{exc}=485 nm - 1.4 nJ, 7.0 nJ and 84.0 nJ; at λ_{exc}=485 nm - 20 nJ, 86 nJ and 1 uJ. Where not specified separately the excitation pulses were attenuated to <20 nJ (~$3x10^{14}$ photons /cm^2 /pulse). Pump and probe pulses were polarized at magic angle to each other. All measurements were performed in a 1 mm path length cuvette (OD = 2 - 7 /cm in the maximum of the absorption), which was moved in a Lissajous scanner during experiments in order to keep the average irradiation per sample volume low. Sample stability was controlled by the absorption spectrum and by the HPLC profile before and after the measurements. No substantial degradation was observe during the measurement.

Data were analyzed by the lifetime distribution analysis and are shown as lifetime density maps (LFD maps) (R. Croce et al., 2001). The LFD maps are calculated by an inverse Laplace transformation from the original transient absorption surfaces vs. time and wavelength and represent the amplitudes of the lifetime components in a quasi-continuous lifetime range (analogous to decay-associated difference spectra) (A.R. Holzwarth, 1996). Global target analysis testing various kinetic models was subsequently performed on the LFD maps. White-yellow regions correspond to positive amplitudes and reflect either absorption decay or rise of a bleaching signal. Blue-black regions correspond to negative amplitudes and reflect either absorption rise or decay of the bleaching (R. Croce et al., 2001).

5.3 Results

5.3.1 Signal dependence on purification

The lifetime density maps of MTHF solution of β-carotene (λ_{exc}= 400 nm) before and after purification are shown in Figure 5.2. In unpurified samples the ~50-100 ps component is

well resolved in the 480-540 nm spectral range (Fig. 5.2A). This component is missing after purification (Fig. 5.2B) under the same measuring conditions. The HPLC profiles corresponding to purified and unpurified samples are shown in Figure 5.1 together with the integrated absorption spectra in the inset A. One can see that the original, unpurified, sample has a pronounced absorption shoulder and increased absorption below 400 nm in comparison to pure all-trans β-carotene. As follows from the elution profile of Fig. 5.1 the unpurified batch sample contains a wide range of impurities. One of the main impurities elutes in the time range of 5 min., i.e. before the main β-carotene band. Absorption spectra taken from the HPLC trace at 5 and 11.3 minutes (shown by arrows in Fig. 5.1) are shown in the inset B. The impurity has a blue-shifted absorption profile in comparison to all-trans β-carotene but in general looks like a carotenoid spectrum. It may be due to a shorter chain carotenoid or some other chemical product deriving from β-carotene. The concentration of this impurity as well as the general elution profile measured at various detection wavelengths (not shown) depends somewhat on the batch of β-carotene sample used (β-carotene samples obtained from Aldrich and Sigma showed similar patterns and impurity contents but with somewhat varying relative amounts). Although the impurity concentration is always smaller than that of all-trans β-carotene as judged from the HPLC signal, its relative absorption at 400 nm is much stronger than for β-carotene (Fig. 5.1, inset B). Thus at short excitation wavelengths (in many studies excitation around 400 nm has been used) the contribution of the impurity to the measured signals will be substantially enhanced. In contrary it will be lower for excitation at the red-edge of the β-carotene absorption and the signal from this impurity may disappear when excited at >470 nm. We note however that if unpurified β-carotene is used other impurities absorbing at longer wavelengths may contribute to the signal.

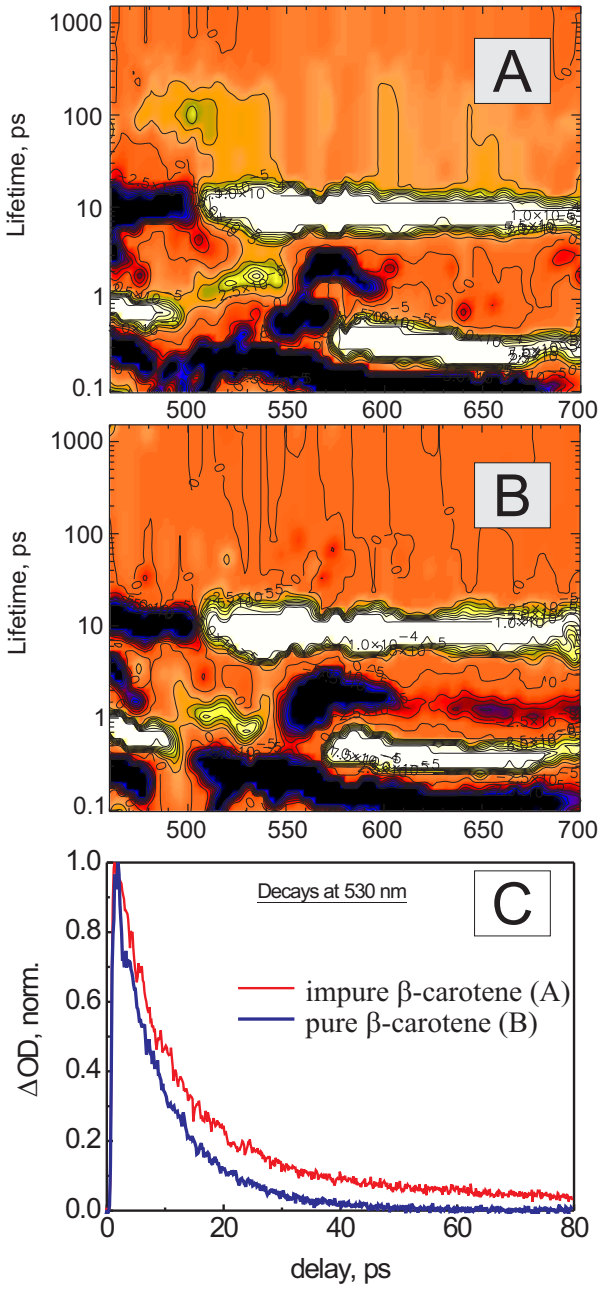

Figure 5.2. Lifetime density maps of β-carotene in MTHF before (A) and after (B) purification (correspond to the HPLC profiles shown in Fig. 5.1A and B). Experimental decays measured at 530 nm in impure and pure samples (C). Excitation wavelength - 400 nm.

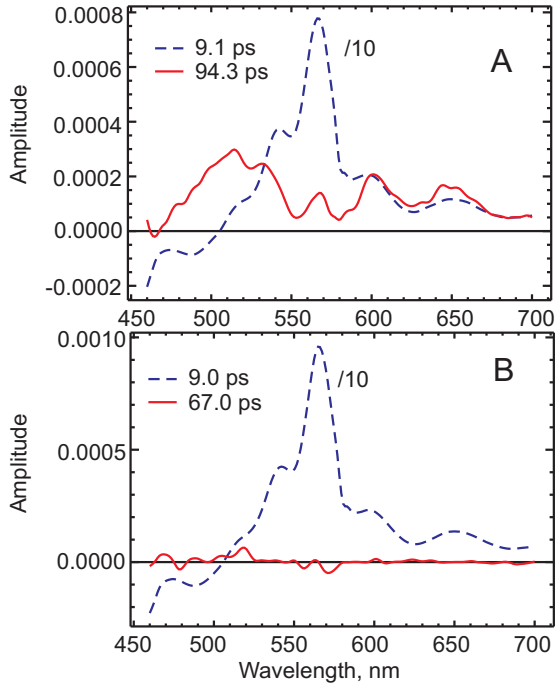

Figure 5.3. Global exponential analysis of data shown in Fig. 5.2A and B. Analysis performed on the timescale >3 ps.

The global lifetime analysis of the TA data from Fig. 5.2 on the timescale >3 ps is shown in Figure 5.3 (A – unpurified, B – HPLC purified). The ca. 9 ps component in both cases shows the well-known shape of the β-carotene S_1 ESA band. The other component (see long-decay contribution at 530 nm in Figs. 5.2 and 5.3) has a much longer lifetime and pronounced amplitude in the unpurified sample, while upon purification this component is absent. Note the main contribution in the range 500-550 nm for this signal (Fig. 5.3), but also contributions around 600 and 650 nm. The additional bands may be due to other impurities that are present in the unpurified β-carotene sample (see Fig. 5.1). We have not isolated and studied separately the various impurities but suspect, based on the absorption spectra of several impurities taken in the HPLC elution profiles, that the impurity with the ca. 5 min retention time will contribute most to absorption in particular for 400 nm excitation and thus gives a pronounced signal with a lifetime longer than the relaxed S_1 state (as measured from the pronounced ESA around 550 nm) exactly in the range where the TA ESA signal due to the "S* state" is generally observed.

5.3.2 Excitation wavelength and solvent dependence at low excitation intensity

To study the dependence of the relaxation dynamics on the excitation wavelength highly HPLC-purified β-carotene was measured. Measurements were performed in MTHF solution with excitation at both 400 nm and 485 nm, and in n-hexane solution with excitation at 400 nm, 475 nm, 485 nm and 509 nm, all at low pulse intensity of <20 nJ. At such intensities the multiple excitation is excluded since probability of excitation is less than 20% for 20 nJ pulse excitation near the peak absorption and correspondingly less at 400 and 509 nm excitation. The corresponding LFD maps, which are essentially decay-associated difference spectra (DADS) on a continuous lifetime scale and result from an inverse Laplace transform of the original data, are shown in Fig. 5.4 (A-B for MTHF and C-F for n-hexane). They reveal directly the involved lifetimes (on a semilogarithmic lifetime scale) as well as the relevant spectral properties associated with these lifetimes. Typically the kinetics of purified β-carotene shows four well-resolved lifetime components on the time scale ≤10 ps and no lifetime contributions above 10 ps. The lifetimes are in the range of ca. 150 fs (S_2 relaxation) and generally three components of 300-600 fs, 1.5-3 ps, and ca. 10 ps which all show strong excited state absorption in the range of ≥550 nm extending till the end of the spectral range. The longest-lived component in particular shows a positive signal down to about 510 nm. Some variations of the spectral shape, position and relative intensity of the bands are observed in the LFD maps over the lifetime and wavelength scale (τ<10 ps, λ=470..700 nm) depending on the solvent and excitation conditions. The most striking changes are observed for hexane as solvent and long excitation wavelengths of 485 nm (Fig. 5.4E) and 509 nm (extreme red-edge excitation, Fig. 5.4F) where the ca. 2 ps component has very small amplitude (Fig. 5.4E) or is essentially absent (Fig. 5.4F).

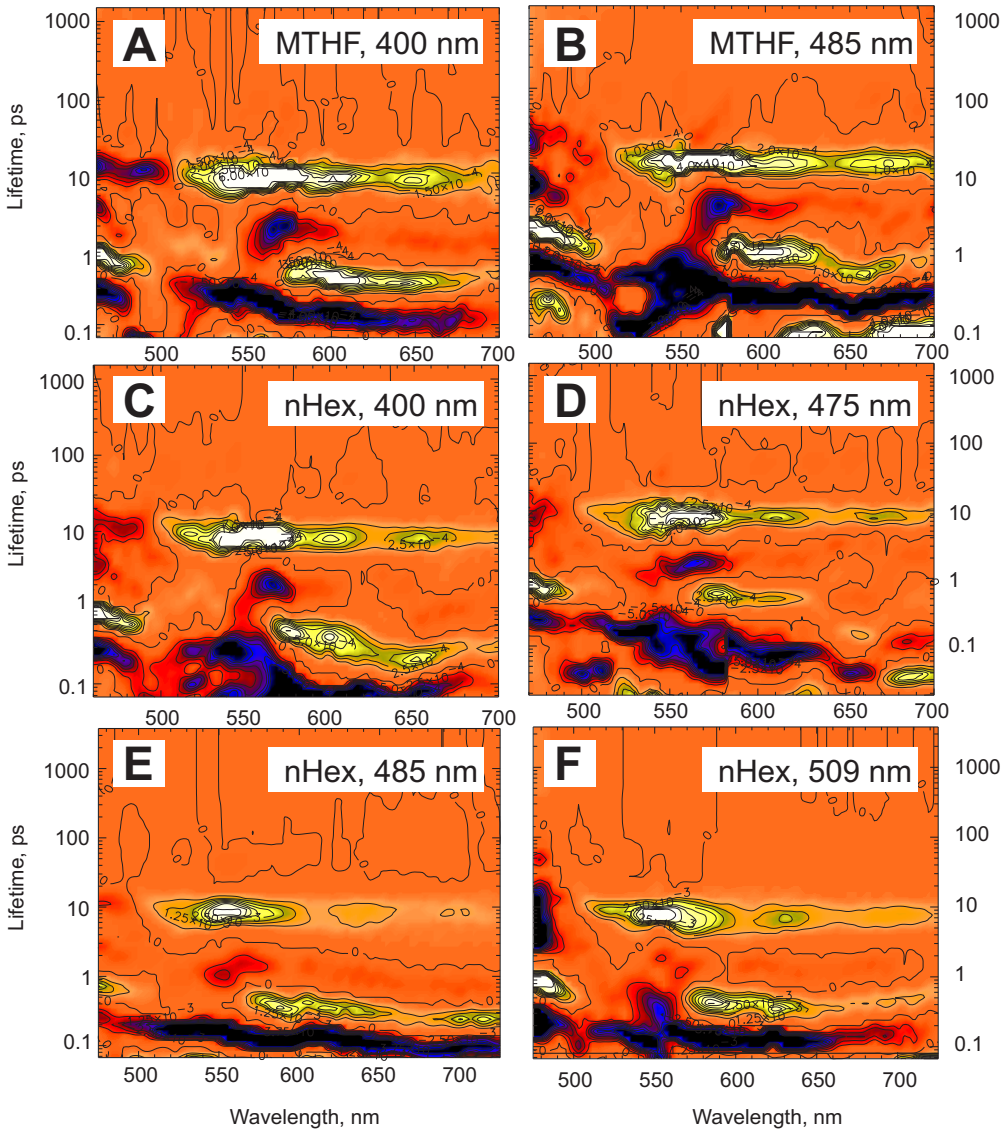

Figure 5.4. Lifetime density maps of β-carotene in MTHF excited at 400 nm and 485 nm (A-B), and in n-hexane excited at 400 nm, 475 nm, 485 nm and 509 nm (C-F).

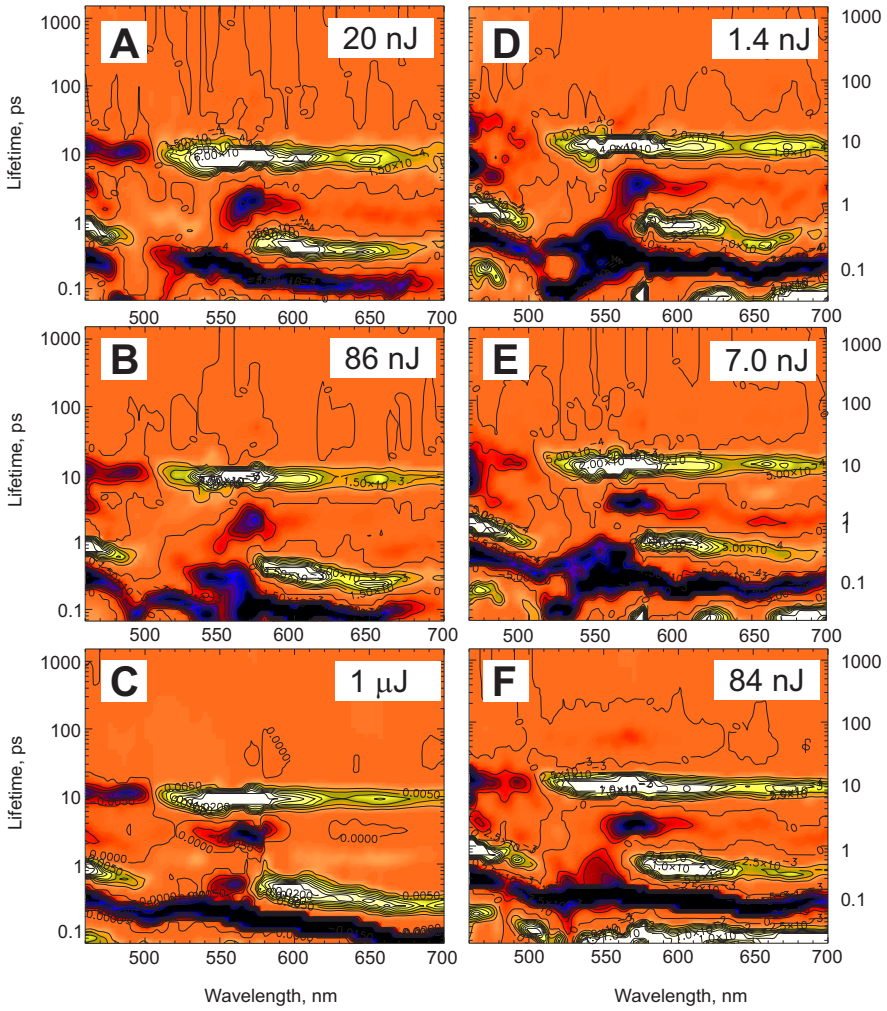

Figure 5.5. Lifetime density maps of β-carotene in MTHF excited at 400 nm (A-C, high excitation intensities) and 485 nm (D-F, low excitation intensities). Values of excitation intensities are shown in the figure.

5.3.3 Intensity dependence

To study the saturation of the transient spectra as well as to reveal any possible pathways or changes in kinetics upon saturation, the intensity dependence of β-carotene kinetics was measured in n-hexane and MTHF (at excitation wavelengths 485 nm and 400 nm) over intensities of 3 orders of magnitude in the energy range from 1 nJ – 1 µJ per pulse. The corresponding LFD maps (Fig. 5.5) again provide a general view on the resulting kinetics. When excited near the first absorption band (0-0-transition) around 485 nm 1 nJ pulse corresponds to an excitation probability of < 1% per carotenoid molecule under our conditions going up to ca. 20% for the 20 nJ pulses. Up to 20 nJ/pulse excitation energy no significant changes were observed in the transient spectra. Pronounced effects on the transient

spectra were observed starting from 60-80 nJ/pulse (corresponding to 60-80% excitation probability per carotenoid). A 1 μJ/pulse excitation energy formally leads to more than 7 absorbed photons per carotenoid. Of course non-linear effects are initiated already at substantially lower excitation probability. But this estimate shows that a large variety of non-linear effects can be potentially initiated under such conditions, starting with two-photon absorption via the S_2 to higher excited states ((E. Papagiannakis et al., 2006), stimulated Raman scattering, and possibly many others. We note that such and even substantially higher excitation intensities have by no means been unusual for experiments in the literature where S* state has been reported (see e.g. (C.C. Gradinaru et al., 2001; D.S. Larsen et al., 2003; E. Papagiannakis et al., 2006). In studies by other groups similarly high excitation intensities have been used, as can be judged from the absorption difference signals reported and from comparison of the difference spectra with our data, although unfortunately the precise excitation energies used can often not be calculated due to insufficient data provided, in particular due to lack of beam diameter data). It is important to note that we observed the same lifetime components at high intensities (Fig. 5.5) as at low intensity (Fig. 5.4) despite the spectral changes observed in the LFD maps (see kinetic analysis for further details below). In particular we did not observe any appearance or enhancement of long-lived lifetime components above 10 ps. Quite generally the spectral and kinetic features remained independent from pulse energy up to about 20 nJ/pulse (in a 130 μm diameter spot). For higher intensities significant changes are observed in the spectra. When the excitation intensity reaches 80-100 nJ/pulse a relative increase of amplitudes of vibrational side band of the 2^{nd} and 4^{th} lifetime components (numbering in the order of increasing lifetime) and a decrease in the positive amplitude of the 3^{rd} lifetime component takes place in the LFD maps (Fig. 5.5). This effect is most pronounced in MTHF solution and less in n-hexane solution.

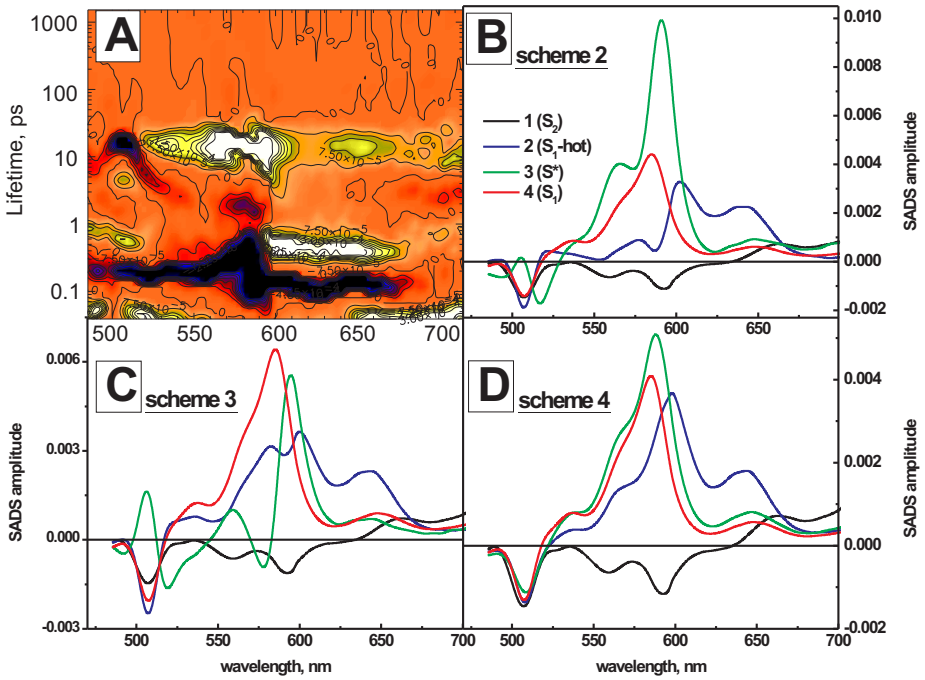

Figure 5.6. Lifetime density map (A) and SADS (B-D) of β-carotene measured at 77K in MTHF with excitation at 400 nm. For explanation of kinetic schemes used in the analysis see Fig. 5.7.

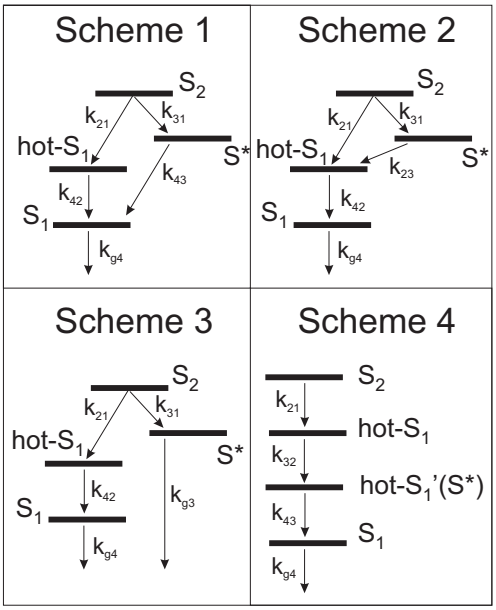

Figure 5.7. Target schemes used for analysis of the data: branching scheme with parallel population of the hot-S_1 and S* states (1-3) and sequential scheme (4).

5.3.4 Low temperature kinetics

Experiments were also performed at 77K with the sample in a MTHF glass in (Oxford Instruments cryostat, model 101). In order to avoid hole-burning during the femtosecond TA

measurements the cryostat was slowly moved (about 0.3 cm/sec) by a Lissajous scanner in the x and y directions perpendicular to the laser beam over an area of ca. 0.5x0.5 cm^2. No signal modification during the time of measurement was observed, indicating the absence of hole burning and other damaging reactions. The LFD map of such an experiment is shown in Fig. 5.6 along with the results of various kinetic analyses (see below). It is important to note that again the same four-lifetime pattern is observed as at room temperature and all lifetimes observed are very close to those found at r.t. except for the longest-lived one assigned to the S_1 state to GS decay which was increased from ca. 10 ps to ca. 15 ps.

5.4 Discussion

In order to elucidate the origin and fate of the signal(s) assigned to the "dark S* state(s)" in carotenoids in general and β-carotene in particular, we will in the following analyze the overall kinetics in terms of various kinetic model schemes which have been discussed in the literature for the relaxation of carotenoids excited from the ground state to the S_2 state and giving rise to S* state(s) (see e.g. (C.C. Gradinaru et al., 2001; D.M. Niedzwiedzki et al., 2006; D. Niedzwiedzki et al., 2007; H. Cong et al., 2008; T. Polivka and V. Sundström, 2009). This kind of analysis gives as the result the so-called SADS for the intermediate states in the models, as well as the connecting rate constants (A.R. Holzwarth, 1995; A.R. Holzwarth, 1996). The various kinetic schemes used here are shown in Fig. 5.7. They include several branching schemes tested previously (see references above) where a vibrationally excited S_1 state and the S* state are formed in parallel (branched models) from the S_2 state (Schemes 1-3 in Fig. 5.7) and a purely sequential scheme, where all lifetime components other than the S_2 relaxation can be described by a sequential vibrational cooling process within the S_1 state and eventual return to GS from the vibrationally relaxed S_1 state. The three branched schemes only differ in the fate of the S* state, relaxing either directly to GS or back to the S_1 state. As can be expected from these schemes, number 1 and 2 hardly differ from each other and give essentially the same results in the SADS and kinetic data. We

do not test here the "trivial" model represented by an unconnected parallel decay of each of the species belonging to the 4 lifetimes since such a scheme would clearly not be in agreement with the vast amount of reliable existing knowledge about carotenoid excited state relaxation and has thus already been excluded by previous work.

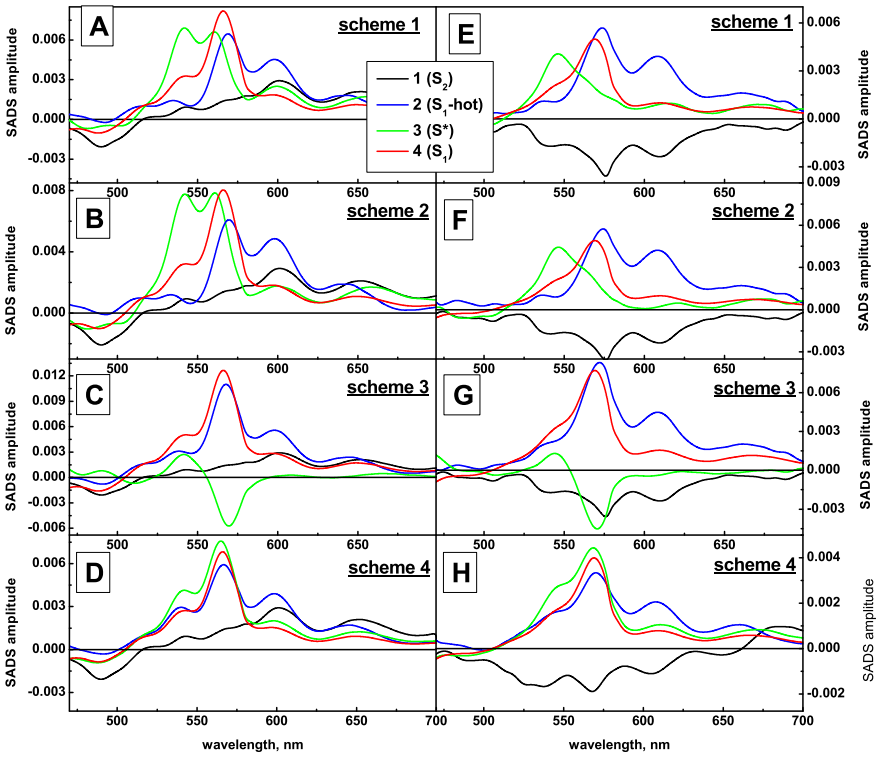

Figure 5.8. SADS of β-carotene in MTHF excited at 400 nm (A-D) and 485 nm (E-H). SADS correspond to schemes shown in Fig. 5.7: scheme 1 (A,E), scheme 2 (B,F), scheme 3 (C,G), scheme 4 (D,H).

Under all conditions studied here pure all-trans β-carotene shows a component of ca. 150-200 fs lifetime and a component of 10 ps lifetime (r.t.) which lengthens to 15 ps at low temperature. On the basis of their lifetimes and DADS (LFD maps Figs. 5.4 and 5.5) as well as their SADS (Figs. 5.8 and 5.9) - which are essentially the same for all model kinetic schemes shown in Fig. 5.7 - these two lifetime components (150 fs and 10-15 ps) can be assigned unequivocally to the decay of the initially excited S_2 state (150-200 fs component) and to the decay to GS of the vibrationally relaxed S_1 state, respectively. This interpretation is

in full agreement with all other relevant results reported in the literature (see (T. Polivka and V. Sundström, 2004; T. Polivka and V. Sundström, 2009) as reviews). We are not going to discuss here any further the exact kinetic and spectral details of the fastest component formally reflecting the S_2 state relaxation. This has been done in a recent extensive work where we showed that the S_2 relaxation kinetics is actually quite complex and involves, at least for lutein and β-carotene, the population of an intermediate $1B_u^-$ state and an oscillatory term due to electronic coherence (E. Ostroumov et al., 2009). We will neglect here those details of the S_2 relaxation and in general assume a combined $1B_u^+/1B_u^-$ state as the initial state from which both vibrationally excited S_1 as well as S* (if relevant) are formed. This simplification is justified for the present analysis since the S* state is generally supposed to have much longer lifetime than the two $1B_u$ states. We will thus concentrate in the following on the SADS and their dependence on the various experimental parameters of the two intermediate lifetime components which are in the range of ca. 0.5 ps and 2 ps. Note that these components have been observed as well in many previous experiments by other groups. The ca. 0.5 ps component has been assigned to vibrationally unrelaxed (hot) S_1 states (H.H. Billsten et al., 2002; H.H. Billsten et al., 2005). In a few cases (c.f. Table 5.1) the ca. 2-5 ps component – depending on the particular carotenoid studied - was however assigned to the S* state (H.H. Billsten et al., 2005; D.M. Niedzwiedzki et al., 2006; D. Niedzwiedzki et al., 2007). The origin of this component will be discussed in detail below.

Table 1. Lifetimes of the S_1 and S* (or S*-reminiscent) states reported in literature for various carotenoids of conjugation length N. Unless indicated otherwise the measurements were carried out at r.t

Molecule	**N**	**Solvent / Medium**	**λ_{exc} (nm)**	**τ [ps], hot-S_0**	**τ [ps], S*/$S^‡$/ S_1-trans**	**τ [ps], S_1**	**Ref.**
M15	15	CS_2, toluene	590	6-13	n.d.	1-1.3	[1]
M19	19	hexane/ether/CS_2		3-10		0.4-0.6	
Spirilloxanthin	13	hexane	540	n.d.	6	1.4	[2]
Spheroidene	10	LH2	475	n.d.	5	1.5	[3]
Spirilloxanthin	13	hexane	520	n.d.	n.d.	1.35	[4]

Spheroidene	10	reconstituted B850-complex	500	n.d.	7	1.5	[5]
β-Carotene	11	hexane	400, 500, 530	n.d.	65	10	[6]
β-Carotene	11	hexane	490	10.1	n.d.	9.3	[7]
Zeaxanthin	11	methanol					
Lycopene	11	hexane	505	5.8		4.2	
Zeaxanthin	11	methanol	485	n.d.	n.d.	9.2	[8]
			400		2.8	9	
			266		4.9	9.8	
Neoxanthin	8	pyridine	481	n.d.	2.7	37.6	[9]
Violaxanthin	9		485		5	26.1	
Lutein	10		491		2.9	15.6	
Zeaxanthin	11		497		2.8	10.2	
β-Carotene	11				3.4	9.5	
Rhodopin glucosid	11	LH2	525	n.d.	30	3	[10]
m9	9	benzene	450	39.1	n.d.	41.5	[11]
β-Carotene	11		495	10.2		9.5	
M13	13		525	6.7		2.52	
M15	15		555	7.7		1.02	
Neurosporene	9	acetone + CS_2 (room T)	0-0 transition	n.d.	n.d.	23	[12]
Spheroidene	10				9.7	7.2	
Rhodopin glucosid	11				5.2, 19	4.2	
Rhodovibrin	12				3.1	2.2	
Spirilloxanthin	13				3.8, 20	1.3	
Neurosporene	9	77K			n.d.	35	
Spheroidene	10				n.d.	11.6	
Rhodopin glucosid	11				7.4	5.9	
Rhodovibrin	12				8	2.7	
Spirilloxanthin	13				3.8	1.7	
Violaxanthin	9	EPA, 77K	484	n.d.	n.d.	33.5	[13]
Lutein	10		491		10.2	19.7	
Zeaxanthin	11		500		8.2	14.7	
Neurosporene	9	EPA	0-0 transition	n.d.	32 (trans)	n.d.	[14]
Spheroidene	10				12 (trans)		
Spirilloxanthin	13	2-MTHF			4.9 (trans)		
Neurosporene	9	EPA	0-0 transition		n.d.	22 (cis)	
Spheroidene	10					8.2 (cis)	
Spirilloxanthin	13	2-MTHF				5.1 (cis)	
β-Carotene	11	benzonitrile	545	n.d.	10	9	[15]
β-Carotene	11	3-methyl-pentane	400	No detailed analysis provided			[16]
Rhodopin glucosid	11	LH2	525				

References for the table:

[1] P.O.Andersson, T.Gillbro, J. Chem. Phys. 103 (1995) 2509.
[2] C.C.Gradinaru, J.T.M.Kennis, E.Papagiannakis, I.H.M.van Stokkum, R.J.Cogdell, G.R.Fleming, R.A.Niederman, R.van Grondelle, Proc. Natl. Acad. Sci. USA 98 (2001) 2364.
[3] E.Papagiannakis, J.T.M.Kennis, I.H.M.van Stokkum, R.J.Cogdell, R.van Grondelle, Proc. Natl. Acad. Sci. USA 99 (2002) 6017.
[4] E.Papagiannakis, I.H.M.van Stokkum, R.van Grondelle, R.A.Niederman, D.Zigmantas, V.Sundström, T.Polivka, J. Phys. Chem. B 107 (2003) 11216.
[5] E.Papagiannakis, S.K.Das, A.Gall, I.H.M.van Stokkum, B.Robert, R.van Grondelle, H.A.Frank, J.T.M.Kennis, J. Phys. Chem. B 107 (2003) 5642.
[6] D.S.Larsen, E.Papagiannakis, I.H.M.van Stokkum, M.Vengris, J.T.M.Kennis, R.van Grondelle, Chem. Phys. Lett. 381 (2003) 733.
[7] W.Wohlleben, T.Buckup, H.Hashimoto, R.J.Cogdell, J.L.Herek, M.Motzkus, J. Phys. Chem. B 108 (2004) 3320.
[8] H.H.Billsten, J.Pan, S.Sinha, T.Pascher, V.Sundström, T.Polivka, J. Phys. Chem. A 109 (2005) 6852.
[9] D.M.Niedzwiedzki, J.O.Sullivan, T.Polivka, R.R.Birge, H.A.Frank, J. Phys. Chem. B 110 (2006) 22872.
[10] E.Papagiannakis, I.H.M.van Stokkum, M.Vengris, R.J.Cogdell, R.van Grondelle, D.S.Larsen, J. Phys. Chem. B 110 (2006) 5727.
[11] T.Buckup, J.Savolainen, W.Wohlleben, J.L.Herek, H.Hashimoto, R.R.B.Correia, M.Motzkus, J. Chem. Phys. 125 (2006) 194505-194505-7.
[12] D.Niedzwiedzki, J.F.Koscielecki, H.Cong, J.O.Sullivan, G.N.Gibson, R.R.Birge, H.A.Frank, J. Phys. Chem. B 111 (2007) 5984.
[13] H.Cong, D.M.Niedzwiedzki, G.N.Gibson, H.A.Frank, J. Phys. Chem. B 112 (2008) 3558.
[14] D.M.Niedzwiedzki, D.J.Sandberg, H.Cong, M.N.Sandberg, G.N.Gibson, R.R.Birge, H.A.Frank, Chemical Physics 357 (2009) 4.
[15] N.Christensson, F.Milota, A.Nemeth, J.Sperling, H.F.Kauffmann, T.Pullerits, J.Hauer, J. Phys. Chem. B 113 (2009) 16409.
[16] A.E.Jailaubekov, S.H.Song, M.Vengris, R.J.Cogdell, D.S.Larsen, Chem. Phys. Lett. 487 (2010) 101.

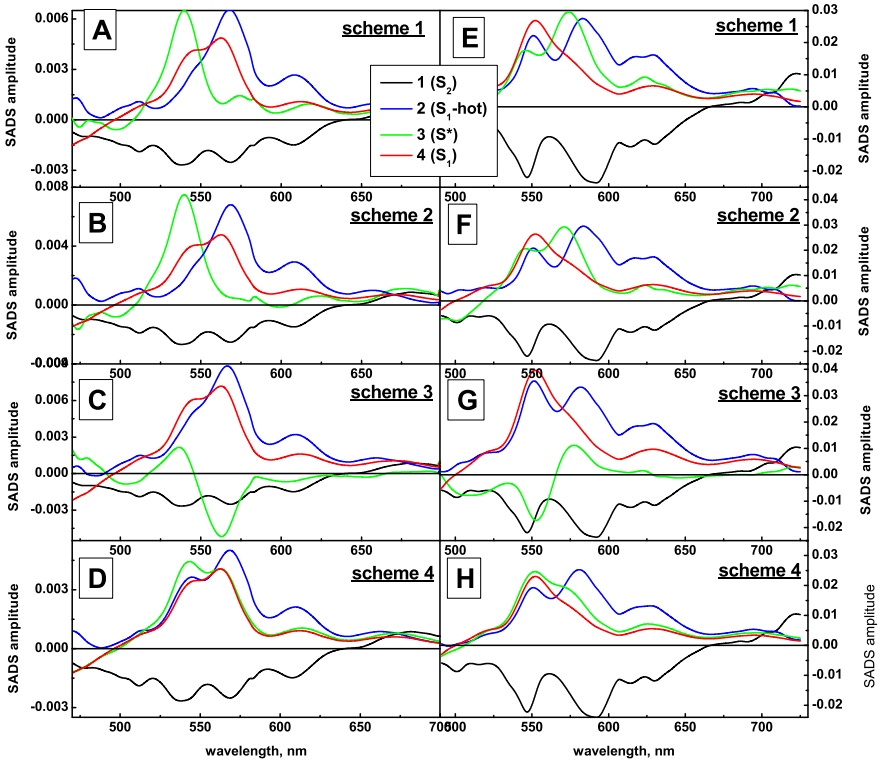

I

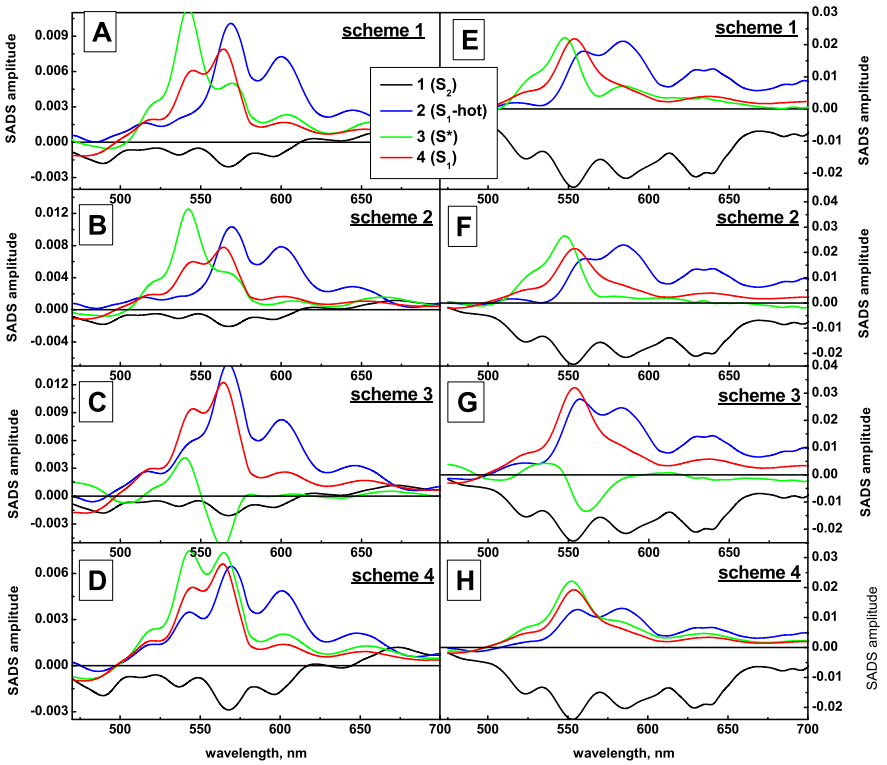

II

Figure 5.9. SADS of β-carotene in hexane excited at I: 475 nm (A-D) and 509 nm (E-H); II: 400 nm (A-D) and 485 nm (E-H). SADS correspond to schemes shown in Fig. 5.7: scheme 1 (A,E), scheme 2 (B,F), scheme 3 (C,G), scheme 4 (D,H).

5.4.1 Purification effects

Careful HPLC purification and oxygen-free preparation/handling of the samples led to the complete loss of the TA signal peaking around 530 nm, i.e. at the short-wave side of the main S_1 ESA signal, with 20-100 ps lifetime observed at r.t. in both solvents (Fig. 5.1). For β-carotene this signal (or accordingly in other carotenoids an ESA signal with lifetime also considerably longer than the S_1 relaxation lifetime) had been taken in early work as evidence for the existence of a special S* state (P.O. Andersson and T. Gillbro, 1995; C.C. Gradinaru et al., 2001; E. Papagiannakis et al., 2002; D.S. Larsen et al., 2003; E. Papagiannakis et al., 2003; E. Papagiannakis et al., 2003; E. Papagiannakis et al., 2006). Neither high excitation intensity, short wavelength excitation, nor solvent change did bring back that long-lived signal during the time course of an experiment when a HPLC purified all-trans β-carotene sample was used. This characterizes the 20-100 ps lifetime component reported by other authors, which is observed by us only in non-purified samples, as an impurity. Notably this long-lived component is also not formed again under the conditions of our measurement over several hours. Thus for example a medium to high yield photoreaction from β-carotene producing this product can also be excluded. The absorption spectrum of this impurity (Fig. 5.2B) suggests that it might also be a carotenoid, possibly with shorter conjugation length than β-carotene or some isomer or other chemical product derived from it. Quite independent of the exact nature of this impurity it is clear that the presence of this impurity is tightly related to the signals originally reported in the literature for carotenoid TA experiments which were interpreted as indicating the presence of the S* state. In Table 5.1 an overview of the literature reporting on S* states in carotenoids, including β-carotene is provided. In most cases the lifetime of the S* state was reported to be substantially longer than the lifetime of the relaxed S_1 state (ca. 10 ps for β-carotene at r.t.). Note also from that table that different groups did find very different lifetimes for the S* state of the same compound in cases where the assumed S* state had a longer lifetime than the relaxed S_1 state. Without going into

further detail we can conclude that TA signals reported in the literature with lifetimes longer than 10 ps for β-carotene at r.t. (see Table 5.1) constitute no indication for the existence of a S* state - of whatever electronic nature - in β-carotene. These long-lived components rather derive from impurities contained in the samples. The chemical nature of these impurities may well be of carotenoid type, but the exact origin is irrelevant for the following discussion of the potential S* state origin/properties. We note here that quite similar observations, i.e. disappearance upon careful HPLC purification of longer-lived TA components, which were originally assigned to S* state origin in the literature, have been made by us for quite a range of carotenoids other than β-carotene (data not shown). Absence of a state with longer lifetime than the relaxed S_1 state in β-carotene has also been reported previously (H.H. Billsten et al., 2005). We conclude that if a "S* state" or similar exists at all in β-carotene then its SADS and kinetics could only be related to one or both of the intermediate lifetime components observed in our data. This will be the focus of the following discussion. Note however that such an assignment would constitute a drastic deviation from the interpretation chosen in those papers which originally postulated the existence of an S* state (c.f. Table 5.1).

Table 5.2. Spectral positions of maxima of the third and forth SADS in scheme 1.

solvent	**MTHF**	**n-hexane**		
λ_{exc}	**485 nm**	**475 nm**	**485 nm**	**509 nm**
SADS 3 (S*)	547 nm	539 nm	547 nm	571 nm
SADS 4 (S_1)	568 nm	560 nm	555 nm	551 nm

Table 5.3. Kinetic rates (ps^{-1}) obtained by analysis of measurements on β-carotene in hexane and MTHF at different excitation wavelengths applying kinetic schemes from Fig. 5.7.

Solvent/ λ_{exc} / kinetic	k_{21}	k_{31}	k_{24}	k_{23}	k_{32}	k_{42}	k_{43}	k_{g4}	k_{g3}
MTHF / 400 / scheme 1	2	4.5	–	–	–	2.7	0.5	0.11	–
MTHF / 400 / scheme 2	2	4.5	–	0.5	–	2.7	–	0.11	–
MTHF / 400 / scheme 3	2	4.5	–	–	–	2.7	–	0.11	0.5
MTHF / 400 / scheme 4	8	–	–	–	2.1	–	0.45	0.11	–
MTHF / 485 / scheme 1	2	4.5	–	–	–	2.7	0.5	0.11	–
MTHF / 485 / scheme 2	2	4.5	–	0.5	–	2.7	–	0.11	–
MTHF / 485 / scheme 3	2	4.5	–	–	–	2.7	–	0.11	0.5
MTHF / 485 / scheme 4	8	–	–	–	2.1	–	0.45	0.11	–
Hexane / 400 / scheme 1	2	4.5	–	–	–	2.7	0.5	0.11	–
Hexane / 400 / scheme 2	2	4.5	–	0.5	–	2.7	–	0.11	–
Hexane / 400 / scheme 3	2	4.5	–	–	–	2.7	–	0.11	0.5
Hexane / 400 / scheme 4	11.5	–	–	–	2.7	–	0.5	0.11	–
Hexane / 475 / scheme 1	2	5	–	–	–	2	0.55	0.115	–
Hexane / 475 / scheme 2	2	5	–	0.55	–	2	–	0.115	–
Hexane / 475 / scheme 3	2	5	–	–	–	2	–	0.115	0.55
Hexane / 475 / scheme 4	12	–	–	–	1.5	–	0.8	0.12	–
Hexane / 485 / scheme 1	2	5	–	–	–	2.7	0.65	0.115	–
Hexane / 485 / scheme 2	2	5	–	0.65	–	2.7	–	0.115	–
Hexane / 485 / scheme 3	2	5	–	–	–	2.7	–	0.115	0.65
Hexane / 485 / scheme 4	8	–	–	–	2.8	–	0.9	0.11	–
Hexane / 509 / scheme 1	2	5	–	–	–	2.7	0.65	0.13	–
Hexane / 509 / scheme 2	2	5	–	0.65	–	2.7	–	0.13	–
Hexane / 509 / scheme 3	2	5	–	–	–	2.7	–	0.13	0.65
Hexane / 509 / scheme 4	7.5	–	–	–	2.7	–	0.7	0.13	–

5.4.2 Kinetic modeling

We will now discuss the results of the kinetic modeling in terms of the different kinetic schemes (Fig. 5.7). We will address first the low intensity experiments using different excitation wavelengths and solvents. All relevant results of this modeling are shown in Figs. 5.8 and 5.9. The rate constants resulting from the modeling are summarized in Table 5.2. Table 5.3 summarizes the spectral maxima of the third and fourth SADS for model scheme 1.

At this point it is helpful to first evaluate shortly the reasons why we do not present and discuss the observed kinetics in terms of DADS or of so-called evolution-associated

difference spectra (EADS), as has often been used in the literature to discuss the results of TA measurements on carotenoids. The DADS present general lifetime analysis of the data, however they do not provide information on the real physical model. They are rather a phenomenological way of description than an exact model. As a matter of fact in some cases the states can disappear from DADS having at the same time substantial population. Indeed, as shown in Fig. 5.10 if two states have identical or very similar spectra (SADS) independently on their arrangement (sequential population in Fig. 5.10B or parallel in Fig. 5.10C) the amplitude of one of the state in DADS (LFD map) will be zero. Therefore DADS are entirely unsuitable to discuss any of the important spectral signatures and differences of the various lifetime components since they represent linear combinations of the SADS of the real intermediates. EADS on the other hand only provide relevant new information in the case that a true sequential kinetic scheme applies (or should be tested). Apart from that EADS also represent linear combinations of the SADS and are thus also not helpful to gain any insights into a complex kinetics behavior. For these reasons we only discuss and compare here the SADS resulting from global target analysis of different kinetic models. Note that all four kinetic schemes have the same number of intermediates. They thus have the same number of (identical) lifetimes and from a formal fit quality criterion can thus not be distinguished. They all result in the identical purely mathematical fit quality. What will be different however are the rate constants involved and more importantly the resulting SADS of the different states. The latter thus provide the most important criteria for accepting or rejecting one of the kinetic schemes in Fig. 5.7.

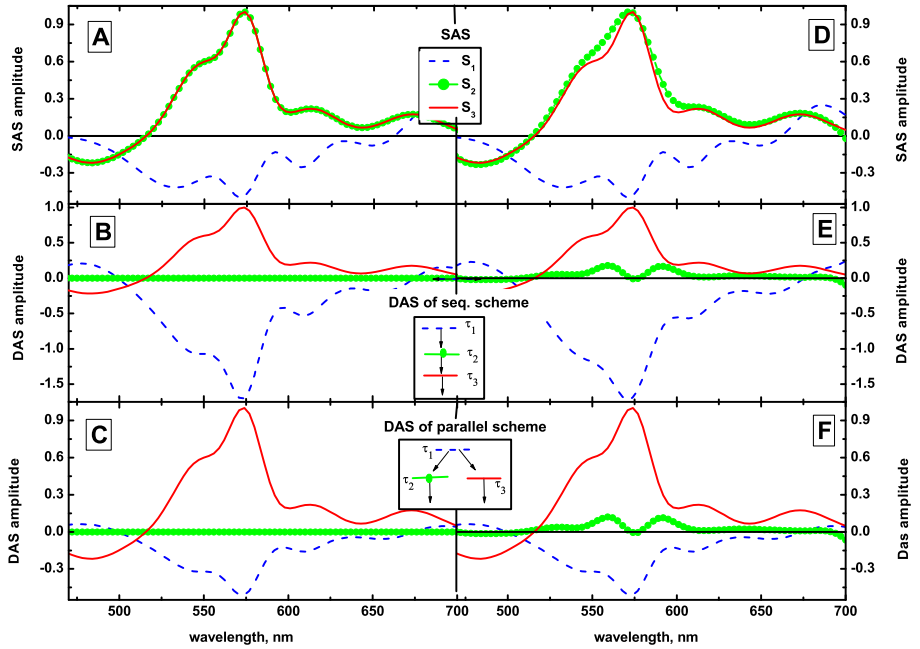

Figure 5.10. DAS (B-C and E-F) calculated from the SAS (A and D) in case of sequential (B and E) and parallel (C and F) kinetic schemes. In panels A-C the 2nd and 3rd SAS are identical, in panels D-F the 2nd and 3rd SAS differ.

The first SADS (in the figures always the same numbering and color scheme is used) has for all kinetic model schemes a negative amplitude characteristic for the initially excited S_2 state and corresponds to the GB, SE, and possible ESA signals of the S_2 state that decays with a lifetime of 150-200 fs. Independent of the kinetic model tested the second and the last SADS show weak GB at wavelengths <500 nm and strong positive (ESA) bands above ca. 500 nm. The ESA bands for these two components are quite typical for the S_1-S_{1N} ESA transition. We therefore assign these two components to vibrationally hot-S_1 (SADS 2) and the vibrationally relaxed S_1 (SADS 4) states, respectively. This is again in full agreement with the generally accepted interpretation of β-carotene TA experiments. The most notable feature in these SADS is however that the second and the fourth SADS show also an ESA vibrational band or band origin (as observed in all kinetic models) located around 520 nm, i.e. the wavelength where typically the ESA of the "S* state" has been observed.

A striking and important difference in those SADS as compared to previously published works (see e.g. (H. Cong et al., 2008; D.M. Niedzwiedzki et al., 2009); comparison with other work is not directly possible since in most cases no SADS were calculated, but the comparison at the DADS level fully supports our statement) where the data is analyzed in terms of kinetic models, is the pronounced resolved vibrational band structure. In all SADS assigned to the S_1 state two to three vibrational satellites are observed on the long-wave side of the maximum, and an additional one on the short-wave side (around 520 nm). In many cases the vibrational band structure of the second and fourth (as well as the first) SADS in our r.t. experiments is even better than for some previous low temperature experiments. This difference can not only be explained by better wavelength resolution in the detection system of our experiment (0.5 nm resolution per channel), since some of the bands are still fairly broad. We observe a vibrational progression in all cases involving several frequencies between 900 cm^{-1} and 1300 cm^{-1}. This is very helpful for the analysis and later assignment since the inspection of all the SADS data shows that this vibrational progression and in many cases a similar intensity pattern – including the short-wave band around 520 nm - is not only observed in the second and fourth SADS but also in the SADS of component 3 (previously assigned to S*). We will return to that important feature below. Notably these pronounced vibrational structures and frequencies observed in the SADS are for all the kinetic models essentially the same and are also independent of the excitation wavelength. For the different kinetic models the second and fourth SADS do show a relatively minor dependence of the relative (vibronic) band intensities. A more pronounced dependence of the relative vibronic band intensities is observed however for different excitation wavelengths and also some dependence on the solvent (Figs. 5.8 and 5.9).

In contrast to the other SADS the third SADS in the kinetic modeling depends very strongly on the applied kinetic model and shows very strong variations in the shape of the spectrum, depending also on the excitation wavelength and partially also on the solvent. In

models where the S* state relaxes back to the S_1/hot-S_1 states (schemes 1 and 2, Fig. 5.7) the third SADS shows an ESA band shifted to short wavelengths in comparison to the relaxed S_1 ESA band, and shows properties of the "S* state" ESA as discussed in the literature at least for some of our experimental conditions, although not for all of them. If the assumed S* state relaxes directly to the GS (scheme 3, Fig. 5.7) – a model that has been favored in the literature - this component shows a very untypical and unexpected positive/negative amplitude band pattern. In most cases (Figs. 5.8C,G and 5.9C) the longer wave part is negative, which could only indicate a stimulated emission, but for long excitation wavelength (Fig. 5.9G) the signs of these two bands are even reversed. Taking into account all the previous suggestions for the nature of the "dark S* state" it is not physically reasonable that the SADS of this state shows a strong negative component reflecting SE. Thus this model must be excluded since it results in physically unreasonable and unrealistic SADS. Such a clear exclusion is apparently not immediately possible however for the kinetic schemes 1 and 2. Nevertheless it is not evident why the ESA spectrum (SADS) of the putative S* state formed directly from the initially excited S_2 should show the large variations upon excitation wavelength (sometimes one band only, sometimes a double band structure is observed). In some cases (Fig. 5.4) the major ESA bands in the third SADS are even located at 550 nm and sometimes even well above 550 nm (Fig. 5.4A,B,E) or look entirely odd (Fig. 5.4F) (c.f. Table 5.3 for the pronounced excitation wavelength dependence of the SADS maxima of component 3 in kinetic scheme 1; note that very similar data are obtained for kinetic scheme 2). Such ESA bands in SADS as are obtained here for a variety of conditions for component 3 are not in agreement with the previously proposed nature of the S* state and its spectral features in the literature, i.e. a twisted conformation showing a generally single maximum ESA band located well on the short-wave side of the vibrationally relaxed S_1 ESA band. Thus the presented data (additional doubts come from the intensity dependence and the low temperature data discussed below) constitute substantial doubt if the kinetic schemes 1 and 2 can explain the available data

consistently. In our view these unspecific and non-systematic variations across the various experimental conditions in the SADS of component 3 for schemes 1 and 2 can not be explained reasonably within these branching kinetic models.

We are thus left with kinetic scheme 4. Inspection of all relevant data (Figs. 5.8 and 5.9) shows that the three SADS for components 2-4 show all very similar SADS, i.e. identical well resolved vibronic structures – although the relative vibronic band intensities vary to some extent depending on the excitation wavelength and solvent. In particular all three SADS under all experimental conditions show a satellite band at 535 nm, i.e. the wavelength where the putative S* state was reported to have its single ESA band maximum. The most notable feature is that these spectra are actually so similar and that they all show the 535 nm band. This strongly suggests that also state 3 likely belongs to the same electronic state, i.e. the S_1 state, as the other two states, and just represents a state of different vibrational excitation degree. We will discuss below whether all the observed features of these SADS can be explained in a consistent model, but here we conclude that only kinetic scheme 4 (purely sequential model) does not constitute any obvious contradictions or inconsistencies with regard to the resulting SADS.

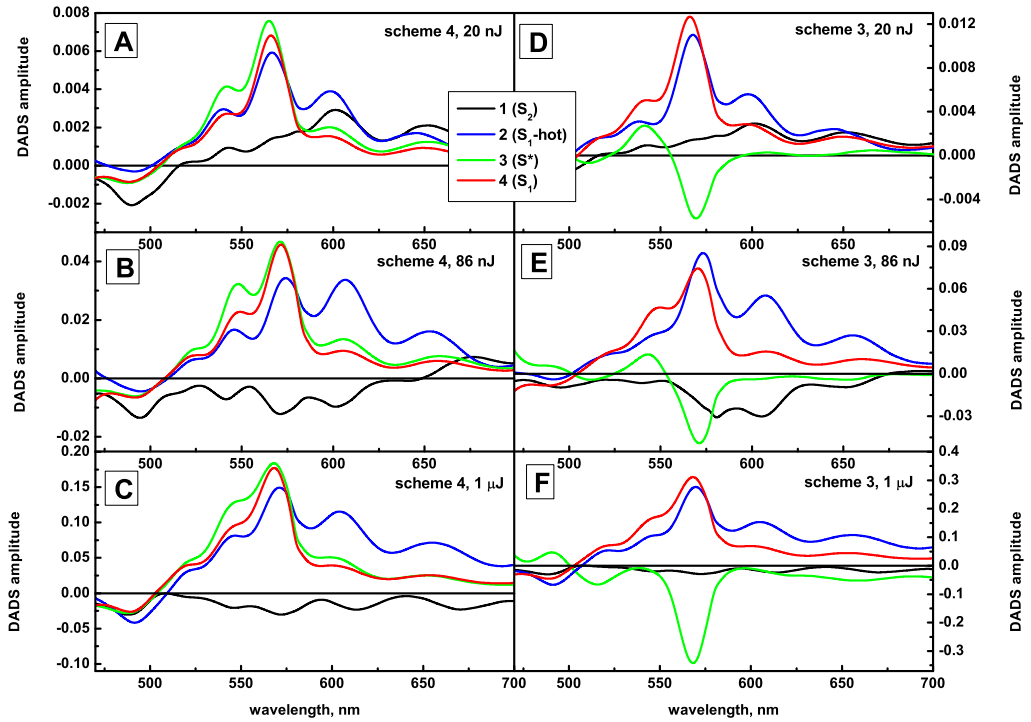

Figure 5.11. SADS of β-carotene in MTHF excited at 400 nm with 20 nJ pulses (A,D), 86 nJ pulses (B,E) and 1 μJ pulses (C,F). SADS in (A-C) correspond to sequential scheme (scheme 4 in Fig. 5.7), SADS in (D-F) correspond to branching scheme (scheme 3 in Fig. 5.7).

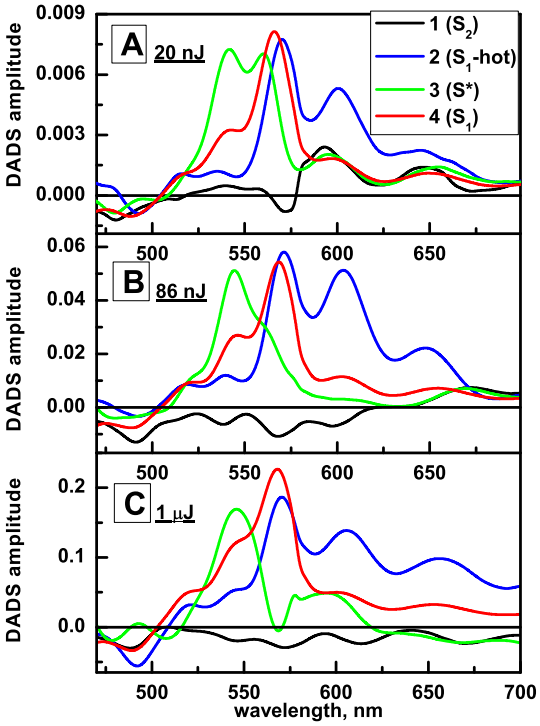

Figure 5.12. SADS of β-carotene in MTHF excited at 400 nm with 20 nJ pulses (A), 86 nJ pulses (B) and 1 μJ pulses (C). SADS correspond to scheme 2 in Fig. 5.7.

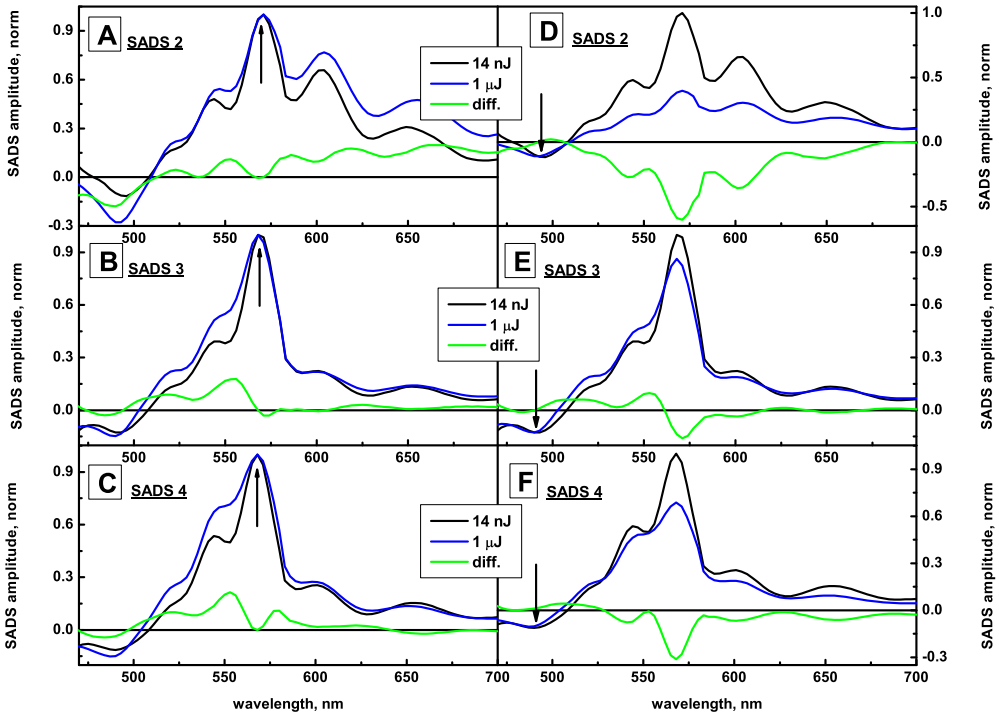

Figure 5.13. Comparison of 2nd (A and D), 3rd (B and E) and 4th (C and F) SADS from low intensity (14 nJ, black line) and high intensity (1 µJ, blue line) measurements of β-carotene in hexane. Difference spectrum is shown by green line. For analysis sequential scheme was used. SADS are normalized to the maximum (A-C) or to the GB signal (D-F) (see arrow).

5.4.3 Excitation intensity dependence of SADS

Fig. 5.11 as well as Figs. 5.12 and 5.13 present the results of the target analysis on the experiments using increased excitation intensity. As seen in Fig. 5.11 kinetic scheme 4 results in SADS for the states 2-4 that for high intensities (Fig. 5.11B and C) only show somewhat varying vibronic band intensity, in particular for the ca. 600 nm ESA band of the SADS for state 2. We note again that all 2-4 SADS show the vibronic band at ca. 530 nm, i.e. again the wavelength where previously the ESA of the S* state has been located. Kinetic scheme 3 in contrast shows again physically very unreasonable SADS for state 3 – a large negative SADS band is observed for high intensity. For low intensity the SADS also shows a positive/negative spectrum (c.f. above) (D.M. Niedzwiedzki et al., 2006; D. Niedzwiedzki et al., 2007). If S* would be a true state its SADS should be more or less independent from the excitation intensity. Fig. 5.12 shows the intensity dependence for 400 nm excitation

wavelength in MTHF for the kinetic scheme 2 (very similar data are obtained for kinetic scheme 1). Again, the SADS of state 3 are strongly intensity dependent, changing from all positive double maximum spectrum with two additional red-shifted satellite bands at low intensity, to a two band spectrum and even a negative sign component at long wavelength for high intensity. Again these features exclude kinetic scheme 2 (and similarly scheme 1) as reasonable descriptions of the relaxation kinetics of β-carotene since a more or less intensity independent SADS for component 3 parts should be expected if it were a separate excited state or a conformational intermediate. A further important feature is the fact that the vibronic structure are less resolved and blurred at high excitation intensity. In our view the major part of this effect can be explained in terms of the model shown in Fig. 5.14.

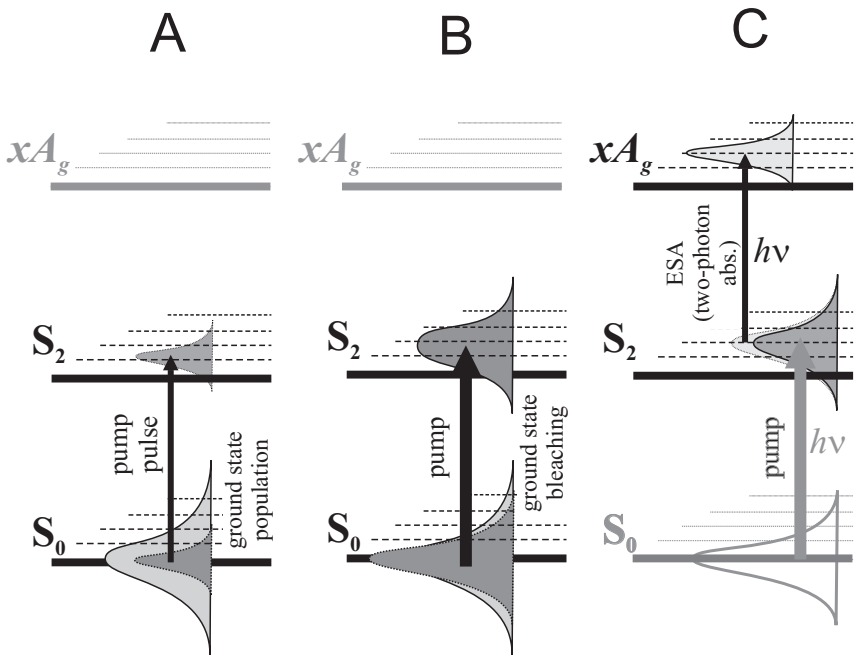

Figure 5.14. Energy level schemes of a carotenoid molecule depicting excitation in linear regime (A) and two mechanisms of the saturation, observed in SADS at high excitation intensities: – the ground state bleaching mechanism (B) and the two-photon absorption mechanism (C).

The spectral width of the laser excitation pulse is narrower than the inhomogeneous broadening of the system. Thus at low excitation intensity a transient hole will be burnt within the inhomogeneous width of the absorption band and a replica of the excitation pulse will be created in the excited S_2 state. This leads to a fairly good vibronic resolution and narrow

bands in all SADS. At high intensity the absorption transition is saturated and the full inhomogeneous width of the system will be excited and a corresponding spectrally broad replica will be created in the excited state, leading to broader band signals and less well resolved vibronic structure (c.f. Fig. 5.13). In addition other effects can take place at high excitation intensities. At ca. 60-80 nJ/pulse the two-photon excitation via the S_2 state becomes important. The relaxation pathways from the S_{2N} state are not known. One possibility is that relaxation occurs back to the S_2 state. However on the short time scale there would be high vibrational excitation (possibly in both optical and thermal modes). In view of the known slow vibrational relaxation of at least some vibrational modes this would lead to a different vibrational population pattern in the initially created hot S_1 state after the ultrafast (ca. 150-200 fs) internal conversion from the S_2 state. Alternatively, or in addition, direct S_1 population by IC could occur directly from the S_{2N}. In that case again a different non-Boltzmann type vibrational excitation pattern in the initially created S_1 state would be created. Within any of these S_{2N} relaxation models the two-photon excitation of the S_{2N} state can explain well the modified relative amplitudes of vibronic bands in SADS 2-4 observed at high excitation intensity (Fig. 5.13). It is thus clear that for high excitation intensity many additional features in the SADS may appear which can not be resolved or assigned unequivocally but can be principally understood from modified vibrational pattern in the S_1 state. Thus low intensity excitation (excitation probability well below 20%) should be the best conditions for clarifying the origin of the S* state and comparing the various kinetic models. This puts a question, does the relaxation kinetics require a separate “dark S* state”?

5.4.4 Low temperature effects

Fig. 5.6 shows the target analysis of low temperature (77K) data for the different kinetic schemes. Scheme 1 is not included since it shows results very similar as scheme 2. The most notable feature in Fig. 5.6 is the fact that the ca. 2 ps component is not absent as would be expected if the “S* state” would be due to a conformationally twisted conformation

formed by relaxation from the S_2 state. Such a relaxation would certainly be slowed down substantially in a frozen glass. The lifetime of formation and decay of this component are however the same at r.t. and at 77K. This essentially excludes a conformational change as an origin of the ca. 2 ps component. For kinetic scheme 2 a very unusual SADS for component 3 is obtained. The negative (GS) bleaching band is not located at the wavelength where it is observed for the other components. This component is rather positive at that wavelength (505 nm) and a negative (bleach) signal is observed instead around 515 nm. Furthermore the maximum of the SADS is not at 530 nm nor at the second positive band at 560 nm but appears at 580 nm, i.e. very uncharacteristic and unexpected for an S* state. We thus exclude kinetic scheme 2 as a reasonable model description of the kinetics also on the basis of the low temperature measurements. Scheme 3 can be excluded on similar grounds. The SADS of component 3 shows similar unexpected but even more pronounced spectral features as for scheme 2 (positive band at the expected GS bleach position and a negative band around 515) but in addition shows a further negative band at 575 nm. For both schemes also the SADS for component 3 looks rather distorted. We conclude that only kinetic scheme 4 gives physically reasonable SADS. For all observed states the GS bleach band is of the same intensity and at the same position, and the SADS of components 2-4 show very similar band structure, although with different intensity distributions, in the various SADS. All three SADS show a pronounced ESA band at the wavelength where typically the S* band ESA absorption has been located. There are two notable features: (i) SADS 2 and 4 are very similar and (ii) SADS 3 shows the highest intensity not at 575 nm (as is the case at r.t.) but at 600 nm, which is only the second strongest band at r.t. Taken together, the data strongly suggest that only kinetic scheme 4 provides a physically reasonable and consistent description of the low temperature data. This scheme is identical to the best fitting scheme for the r.t. data. Even the lifetimes remain essentially the same, except for the last (vibrationally relaxed S_1) state whose lifetime increases somewhat at low temperature. This essentially exclude a major conformational

change in the excited state which has been proposed as one interpretation of the putative "S* state".

5.4.5 Interpretation of the S1 ESA signals

We will now discuss in detail the assignment of the various states in scheme 4 and the details of their SADS upon the various experimental parameters. The implication of scheme 4 is that after the decay of the initially excited S_2 state with a lifetime of 150-200 fs the entire subsequent relaxation kinetics can be interpreted as vibrational cooling/relaxation within the S_1 manifold. Can the resulting SADS and also their dependence on the various experimental parameters be understood within such a scheme? Upon internal conversion (IC) from the S_2 manifold to the S_1 manifold primarily non-totally symmetric vibrational modes will be excited (so-called "inducing modes"). Although it is not known exactly which vibrational modes relax slowly, it may be expected that it is primarily the relaxation of these "inducing modes" that will lead to the observed relatively slow vibrational relaxation pattern. The scheme in Fig. 5.15 explains why it should be expected that the observed vibrational frequencies should be the same or very similar in the SADS of the different vibrationally excited (hot) S_1 states. This would be the case for example if there occurs primarily a shift in the potential energy minimum of the S_1 and the S_{1N} states. Then the SADS (providing that only ESA contributes to the signal) of the different S_1 states would look very similar independent of the exact vibrational excitation pattern. In reality some non-harmonic distortion will however be present as well. This will lead to larger differences in the relative vibrational band amplitudes, and also in some frequencies, observed in the ESA signals of the differently excited hot S_1 states. In the experiments we do indeed observe very similar frequencies, including the vibrational band around 540 nm in all the three S_1 states. Excitation wavelength, excitation intensity, solvent, and even low temperature, have only minor effects on the relative intensity pattern of the SADS for states 3 (partially relaxed S_1) and state 4 (fully vibrationally relaxed S_1). This is quite understandable in terms of Fig. 5.15 since relatively low quantum numbers

of the vibrationally hot states and thus little deviation from the harmonic behavior can be expected. The high similarity of SADS 3 and 4 observed under all conditions clearly suggests that they belong to the same chemical species and also to the same excited state, thus implicitly excluding also an S* origin of SADS 3. Under these conditions it is also clear why for long excitation wavelengths the signal for state 3 (ca. 500 fs component) shows a small or in some cases an almost negligible amplitude in the DADS (or LFD maps). As follows from the simulations shown in the Fig. 5.10 this does not imply that state 3 becomes less populated, but it simply implies that the SADS of states 3 and 4 become almost identical.

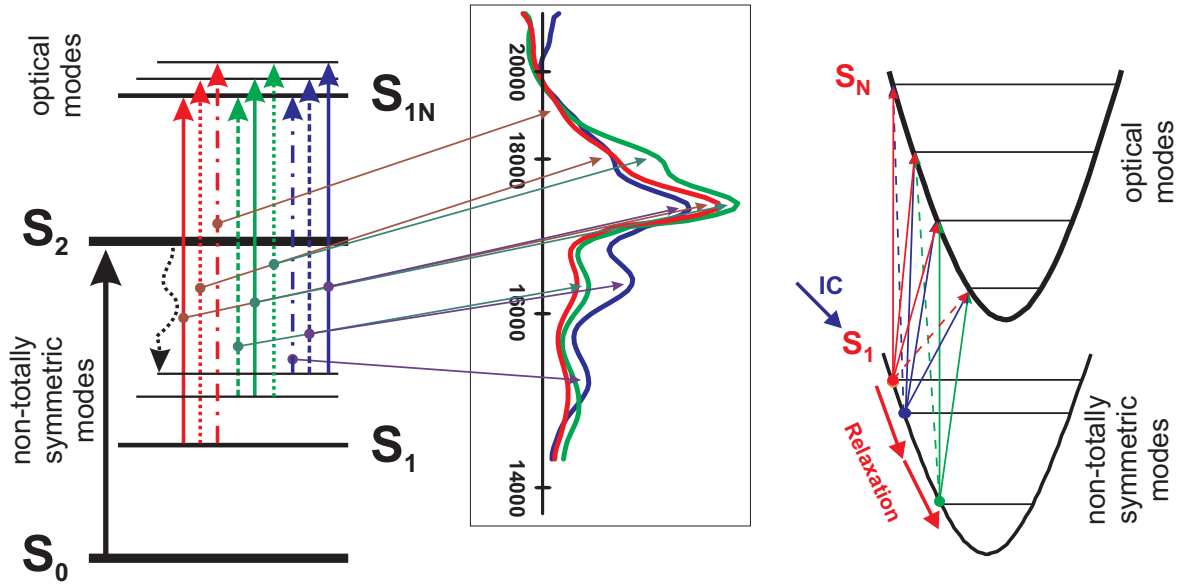

Figure 5.15. Electronic level scheme (on the left) and typical SADS observed in current this work (in the center). The bands in the SADS are assigned to the transitions from the S_1 state to the S_N state by arrows with respective color (red – from relaxed S_1, green – from first vibrationally excited S_1 state, blue –from second vibrationally excited S_1 state). On the right side a potential energy surface model is shown for explanation of different dipole transition moments (Franck-Condon factors).

In contrast to the SADS of states 3 and 4 the relative vibrational intensity pattern for the SADS of state 2 depend in particular on the excitation wavelength and the excitation intensity. This is again understandable in our view on the basis of the schemes in Fig. 5.15. Excitation at short wavelengths will lead to higher vibrational levels of the S_1 state and probably also to different excited modes in the vibrationally excited S_1 state after the initial ultrafast IC from the S_2 state. A similar effect is expected for high intensity excitation at

longer wavelengths, since molecules excited to the S_{2N} state by two-photon absorption will create a different vibrational population in the initially created hot S_1 state. Thus the observed effects on the SADS of state 2 appear generally quite reasonable, even though it may be hard to fully analyze and assign the spectral observations in detail. Thus scheme 4 allows a consistent interpretation of the observed SADS and their dependence on the various experimental parameters without invoking the S* state.

5.5 Conclusions

Consideration of a large set of femtosecond transient absorption data recorded under a large variety of experimental conditions does not provide any evidence for the existence of a separate electronic or conformational state referred as the "S* state" in the literature. Quite in contrast our data show that the postulate of such a state, which is populated in parallel to the hot S_1 state from the initially excited S_2 state, leads to severe inconsistencies with the data and physically unreasonable SADS.

We conclude that:

i) The long-lifetime signal ($\tau_{S*}>\tau_{S1}$) with a transient spectrum in the short-wavelength region reported for isolated β-carotene is caused by a contamination of the sample. In a highly purified sample no such long-lived component is present.

ii) The transient absorption signals in the femtosecond to picosecond range of β-carotene are best described in terms of a sequential relaxation model where the previously proposed "S* state" actually represents a vibrationally hot S_1 state. In contrary branching models, which involve the "dark S* state" (C.C. Gradinaru et al., 2001; D.S. Larsen et al., 2003; W. Wohlleben et al., 2003; E. Papagiannakis et al., 2006; H. Cong et al., 2008) do lead to inconsistencies in the resulting SADS across the wide range of experimental conditions used in this work.

iii) The TA signal of β-carotene shows a dependence on the intensity of the pump pulse and on the excitation wavelength confirming previous observations (H.H. Billsten et al., 2005; E. Papagiannakis et al., 2006; A.E. Jailaubekov et al., 2010). Nevertheless, the sequential model provides internally consistent SADS in contrast to the parallel models with branching to the S* state. The effects of short-wave excitation can be explained consistently within our model. Presented in this work results on the excitation wavelength dependence are very similar as those found for zeaxanthin, another carotenoid with the same conjugation length as β-carotene (H.H. Billsten et al., 2005).

iv) We specifically exclude a large conformational change in the excited state and/or a trans-cis-isomerization as the possible explanation for the TA signals previously assigned to a "dark S* state" (D. Niedzwiedzki et al., 2007; H. Cong et al., 2008; D.M. Niedzwiedzki et al., 2009).

We finally note that quantum mechanical calculations of the excited states of a range of carotenoids did not provide any hint for the existence of a separate additional excited state below the $1B_u^+$ / $1B_u^-$ states that could be related in any way to a hypothetical "S* state" (C.M. Marian and N. Gilka, 2008; M. Kleinschmidt et al., 2009; E. Ostroumov et al., 2009; J.P. Cerón-Carrasco et al., 2010). It would indeed be surprising that such a state would not appear in such calculations if it did exist. The existence of slowly relaxing vibrational hot states in carotenoids, which fully explains our data, in contrast is a well-accepted concept for carotenoid excited state relaxation and fully explains all our data

Acknowledgments

The present work has been performed as project B2 within the DFG Sonder-forschungsbereich SFB 663, Heinrich-Heine-Universität Düsseldorf and Max-Planck-Institut für Bioanorganische Chemie, Mülheim a.d. Ruhr, Germany.

Chapter 6

Excited state relaxation dynamics and electronic properties of a quinoid carotenoid

This chapter is based on the publication Evgeny E. Ostroumov, Marc G. Müller, Claas Hundsdörfer, Wilhelm Stahl, Christel M. Marian, and Alfred R. Holzwarth. Chemical Physics (2010), doi:10.1016/j.chemphys.2010.04.030

A combined study of the quinoid carotenoid DHIRQ by femtosecond transient absorption spectroscopy and quantum chemical calculations revealed its very complex electronic structure and ultrafast relaxation dynamics. The two quinoid end-rings are found to cause a strong bathochromic shift of the absorption spectrum and to decrease the main relaxation time of the S_1 state to 400 fs. Transient absorption data of DHIRQ show a substantial difference of its spectroscopic features to other carbonyl carotenoids. Various alternative kinetic models including an intramolecular charge transfer (ICT) state are discussed in order to assign the electronic structure and the relaxation dynamics.

6.1 Introduction

Despite intense research, the electronic excited-state level structure and the excited-state relaxation processes in carotenoids are not well understood (for a recent review see e.g. Polivka et al.(T. Polivka and V. Sundström, 2009)). While for all carotenoids the first excited state is characterized as the $2A_g^-$ (S_1) state, and the strongly absorbing state as the $1B_u^+$ (S_2) state, there exists a substantial controversy about the location of other states that should be present in carotenoids, e.g. the $1B_u^-$ state and higher-lying A_g states. A particularly controversial point of fundamental relevance for the understanding of the excited state relaxation dynamics is the question whether additional electronic states are located between the $2A_g^-$ state and the $1B_u^+$ state (T. Polivka and V. Sundström, 2009). We have recently shown that indeed the $1B_u^+$ and the $1B_u^-$ state are close to each other in carotenoids of conjugation lengths n=10 (lutein) and n=11 (β-carotene) (E. Ostroumov et al., 2009) and that these states actually cross dynamically after electronic excitation upon conformational and electronic relaxation from the initially excited Franck-Condon (FC) region. Further poorly understood problems arise with carotenoids that contain hetero-atoms in the conjugated system. Here carotenoids carrying carbonyl groups are of special interest since they form intramolecular charge transfer (ICT) states. The spectroscopic features and relaxation dynamics of these carotenoids show a strong dependence on the solvent polarity. In polar solvents their absorption spectra are essentially unstructured and the lifetime of the ICT state decreases by a factor of 3-10 in comparison to non-polar solvents (D. Zigmantas et al., 2001; D. Zigmantas et al., 2002; D. Zigmantas et al., 2004). These carotenoids play special roles in a number of photosynthetic antenna systems from marine organisms (H.A. Frank, 1999; E. Papagiannakis et al., 2005; G. Guglielmi et al., 2005; T. Polivka et al., 2007). Among the carotenoids with a carbonyl group incorporated in the conjugated electronic system there are compounds which are substituted with a quinoid end groups. An example of such a carotenoid is 3,4-dihydro-4,3′-retro-Φ-Φ-carotene-3,3′-dione (DHIRQ) - a planar molecule with a

system of fully conjugated double bonds (C.M. Marian et al., 2009) (Fig. 6.1). It is an oxidation product of the phenolic carotenoid 3,3'-dihydroxyisorenieratene (DHIR) which occurs in bacteria such as *Brevibacterium linens* and has been shown to be a very efficient multifunctional antioxidant (H.D. Martin et al., 2009). In contrast to the yellow-red DHIR, the oxidized molecule is a blue compound with an absorption maximum of ca. 580 nm in chloroform (G. Nybraaten and S. Liaaen-Jensen, 1971).

We present here the results of a spectroscopic and theoretical investigation of the excited-state energies and relaxation dynamics of the DHIRQ molecule. This molecule, in particular in more polar solvents, shows longer-wave absorption bands and lower excited-state energies than any naturally occurring carotenoid and belongs to a class of blue carotenoids which can be synthesized from natural starting compounds (S. Liaaen-Jensen and G. Kildahl-Andersen, 2008).

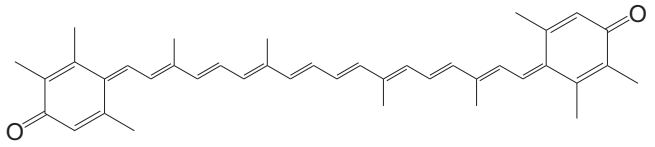

Φ,Φ-carotene-3,3'-dione (DHIRQ, isorenieratene-3,3'-dione)

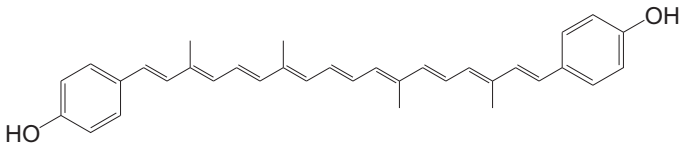

3,3'-dihydroxy-16,17,18,16',17',18'-hexanor-Φ,Φ-carotene (DHHC)

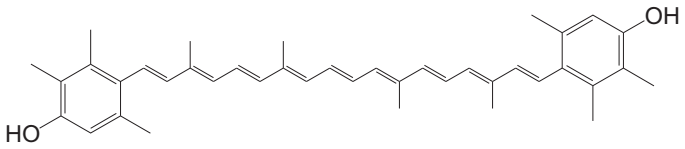

3,3'-dihydroxyisorenieratene (DHIR)

Figure 6.1. Molecular structure of DHIRQ, DHIR and DHHC carotenoids.

6.2 Experimental procedures and computational details

6.2.1 Experimental

Φ,Φ-carotene-3,3'-dione (DHIRQ, isorenieratene-3,3'-dione) was synthesized and purified as described elsewhere (H.D. Martin et al., 2009). Steady-state absorption spectra were measured on a Cary 100 (Varian) spectrometer in HPLC-quality dichloromethane (CH_2Cl_2), n-hexane (first dissolved in a very small amount of CH_2Cl_2) and carbon disulfide (CS_2). Before use solvents were dried on an aluminium oxide column and degassed and bubbled with argon.

Femtosecond transient absorption measurements were performed at room temperature in CH_2Cl_2 and n-hexane as described earlier (R. Croce et al., 2001). The excitation pulse width was ~80 fs, FWHM of ~4 nm, with low intensity excitation pulses of ~$3x10^{13}$ photons/(cm^2 pulse) in order to avoid saturation effects. Pump and probe pulses were polarized at magic angle to each other. All measurements were performed in a 1 mm cuvette (OD = 2 - 7 /cm in the maximum of absorption) which was moved in a Lissajous scanner during experiments in order to keep the average irradiation per sample volume low. Sample stability was controlled by the absorption spectrum which was the same before and after the measurements.

Data were analyzed by lifetime distribution analysis and are shown as lifetime density maps (LFD maps) (R. Croce et al., 2001). The LFD maps are calculated by an inverse Laplace transformation from the original transient absorption surfaces vs. time and wavelength and represent the amplitudes of the lifetime components in a quasi-continuous lifetime range (analogous to decay-associated difference spectra) (A.R. Holzwarth, 1996). Global target analysis testing various kinetic models was subsequently performed on the LFD maps. White-yellow regions correspond to positive amplitudes and reflect either absorption decay or rise of a bleaching signal. Blue-black regions correspond to negative amplitudes and reflect either absorption rise or decay of the bleaching (R. Croce et al., 2001).

6.2.2 Theoretical Calculations

Equilibrium geometries of the $1A_g^-$ (S_0) and $1B_u^+$ states were taken from our previous work (C.M. Marian et al., 2009). A linearly interpolated excited state relaxation pathway was constructed connecting the Franck-Condon region (reaction coordinate RC=0) and the $1B_u^+$ potential minimum (RC=10). A parallelized version of the combined density functional theory/multireference configuration interaction (DFT/MRCI) method (S. Grimme and M. Waletzke, 1999; M. Kleinschmidt et al., 2009) was used for single-point energy calculations along this pathway. The performance of this method on linear conjugated π-systems (polyenes, α,ω-diphenylpolyenes, and β-carotenes) with experimentally known electronic excitation energies has been carefully investigated (P.O. Andersson and T. Gillbro, 1995; M. Kleinschmidt et al., 2009; J.P. Cerón-Carrasco et al., 2010; D. Pfiffi et al., 2010). As a general trend it is found that this method correctly describes the order of the low-lying $2A_g^-$ and $1B_u^+$ states, in contrast to most other quantum mechanical methods. Moreover, the experimental trends for the energy gap between these states are very well reproduced. Absolute excitation energies for extended π-systems with conjugation length n≥10, on the other hand, are typically underestimated by about 0.3 eV.

In all calculations the SV(P) basis set of the Turbomole library (A. Schäfer et al., 1992) was employed. The configuration state functions (CSFs) in the MRCI expansion are built up from Kohn-Sham (KS) orbitals using the BH-LYP (A.D. Becke, 1993) functional. A common set of reference CSFs was used for all spatial symmetries of the C_{2h} molecular point group. The 1s shells of the carbon atoms were kept frozen in the electron correlation treatment. The initial MRCI reference space was spanned by all single and double excitations from the five highest occupied molecular orbitals (MOs) to the five lowest unoccupied MOs of the ground state KS determinant. Wave functions and excitation energies were computed for six ^1A_g, two ^1A_u, two ^1B_g, and five ^1B_u states as well as five ^3A_g, two ^3A_u, two ^3B_g, and six ^3B_u states. In the second iteration, all configurations with a squared coefficient of at least 0.003 in one of the initial MRCI expansions were included in the final MRCI reference space from which all single and double excitations were allowed.

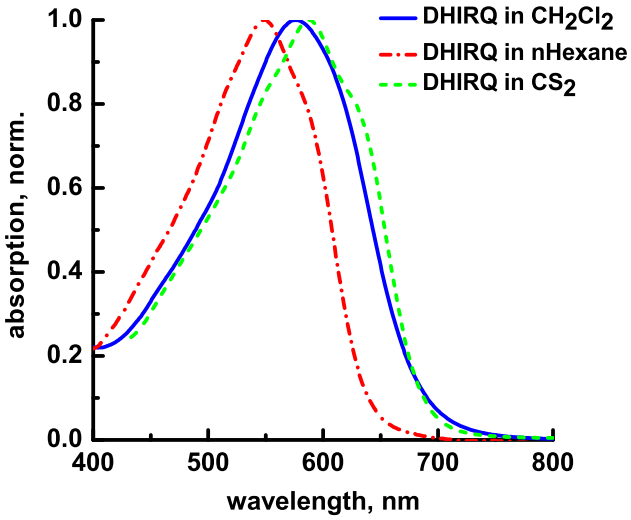

Figure 6.2. Normalized steady-state absorption spectra of DHIRQ in dichloromethane (CH_2Cl_2), n-hexane and carbon disulfide (CS_2).

6.3 Results

6.3.1 Steady-state absorption spectra

Figure 6.2 shows the steady-state absorption spectra of DHIRQ in CH_2Cl_2, n-hexane and CS_2 (for solvent parameters see Table 6.1). Measurements in more polar or higher polarizable solvents were prevented on the one hand by the poor solubility of the compound and on the other hand by its chemical instability in more polar solvents. For this reason the femtosecond measurements were performed only in CH_2Cl_2 and n-hexane. In all three solvents steady-state spectra are extremely red-shifted (~100 nm) in comparison to other

carotenoids with n=10 double bonds in the polyene chain (formally, including the quinone rings, DHIRQ has n=14). DHIRQ shows stronger red shift than even the homolog of β-carotene M19, which has the largest conjugation-dependent shift of the absorption maximum of carotenoids observed so far. M19 has n=17β2 double bonds (for the nomenclature see (IUPAC/IUB, 1975; A.J. Young and G. Britton, 1993)) and its absorption maximum in hexane is located at $\lambda_{(max\ abs)}$ = 530 nm (P.O. Andersson and T. Gillbro, 1995), whereas DHIRQ is much shorter (n=10ϕ2O2, taking into account conjugation in both polyene chain and quinoid rings) but has its absorption maximum in hexane at 550 nm (see Fig. 6.2). Therefore one expects DHIRQ to have a longer effective conjugation length (n_{eff}) than M19. Since no unusual red-shift is observed for DHIR, the reduced di-hydroxy form of DHIRQ (C.M. Marian et al., 2009) (Fig. 6.1), the bathochromic absorbance shift and the high value of n_{eff} of DHIRQ must be due to special characteristics of the quinoid end groups. Additional bathochromic shifts in the absorption of the $1B_u^+$ state are introduced when the polarizability of the solvent increases (B.S. Hudson and B.E. Kohler, 1973; P.O. Andersson and T. Gillbro, 1990; P.O. Andersson et al., 1991). We observed for DHIRQ a ca. 40 nm red shift in CS_2 vs. n-hexane (Fig. 6.2) which is in agreement with the reported spectral shift of spheroidene in the same solvent pair (P.O. Andersson et al., 1991).

Table 6.1. Properties of the solvents used for spectroscopic measurements (taken from http://www.landolt-boernstein.com).

Solvent	ε, dielectric constant	n, refractive index	Polarity $(\varepsilon-1)/(\varepsilon+2)$	Polarizability $(n^2-1)/(n^2+2)$
CH_2Cl_2	9.0	1.424	0.73	0.26
CS_2	2.6	1.67	0.35	0.37
n-hexane	1.89	1.375	0.23	0.23

The substantial broadening of the spectral absorption profile of DHIRQ is likely due to conformational disorder caused by the presence of non-bonded interactions between the methyl side groups of the adjacent quinoid rings and the polyene chain. This is comparable to "normal carotenoids" where this phenomenon is explained by the steric hindrance of the methyl groups with the β-ionone end rings (R.L. Christensen and B.E. Kohler, 1973; R. Hemley and B.E. Kohler, 1977). Indeed a similar broadening is present in DHIR, but is essentially absent in DHHC which lacks the methyl groups attached to the phenyl rings (C.M. Marian et al., 2009) (see Fig. 6.1 for molecular structures of the discussed carotenoids). This broadening is generally further enhanced by carbonyl groups (H.A. Frank et al., 2000) and

becomes more pronounced in more polar solvents like e.g. CH_2Cl_2 (Fig. 6.2). However, the highly polarizable CS_2 apparently stabilizes the molecular conformation leading to a slightly more resolved vibrational structure of the absorption spectrum of DHIRQ (Fig. 6.2).

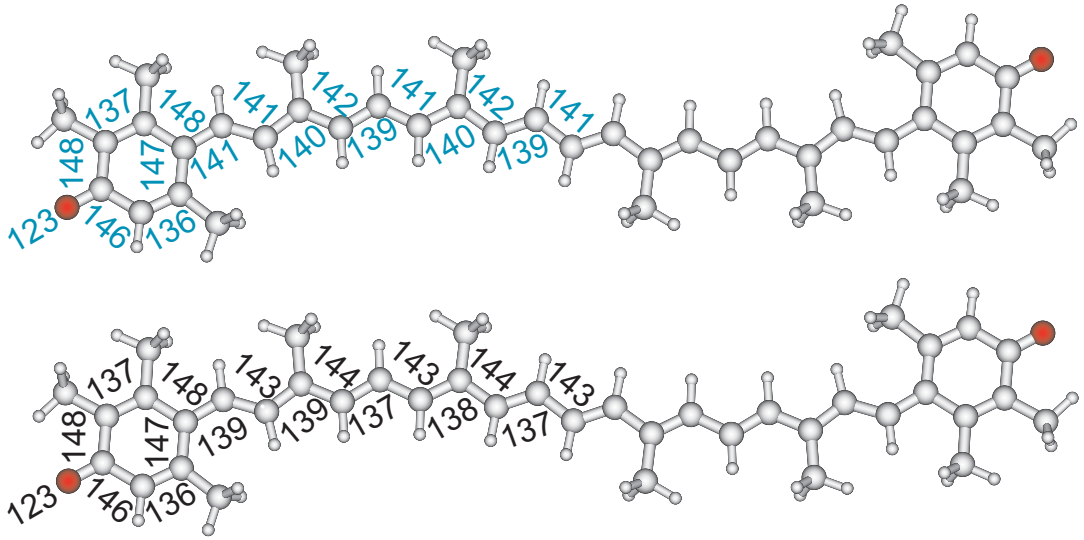

Figure 6.3. Bond lengths of DHIRQ (a) in the excited $1B_u^+$ state and (b) in the ground state geometries.

6.3.2 Theoretical Calculations

In contrast to DHIR which exhibits twisted aromatic end groups, the ground state structure of DHIRQ is characterized by a planar equilibrium geometry. The two carbonyl groups, being part of the conjugated system, cause a reversal of the single- and double-bond pattern with respect to normal carotenoids (see Fig. 6.3 for bond lengths). In particular, the bonds connecting the six-membered rings with the polyene chain adopt double-bond character and force the end groups to be coplanar with the polyene backbone, thus stretching the molecule. The ground state conformation optimization runs were started at various twisted conformations, in particular with regard to the orientation of the end rings. While these tests can not fully replace large scale ground state dynamics calculations, which are beyond the scope of this work, they did not indicate any evidence for the necessity of different ground state conformations. On the C=O groups two high-lying doubly occupied non-bonding orbitals, in the following called *n*-orbitals, are located. It is known that carotenoids carrying carbonyl groups as part of the conjugated system, like peridinin or fucoxanthin, reveal ICT states which profoundly influence the excited state relaxation dynamics (D. Zigmantas et al., 2001; D. Zigmantas et al., 2004; T. Polivka and V. Sundström, 2004).

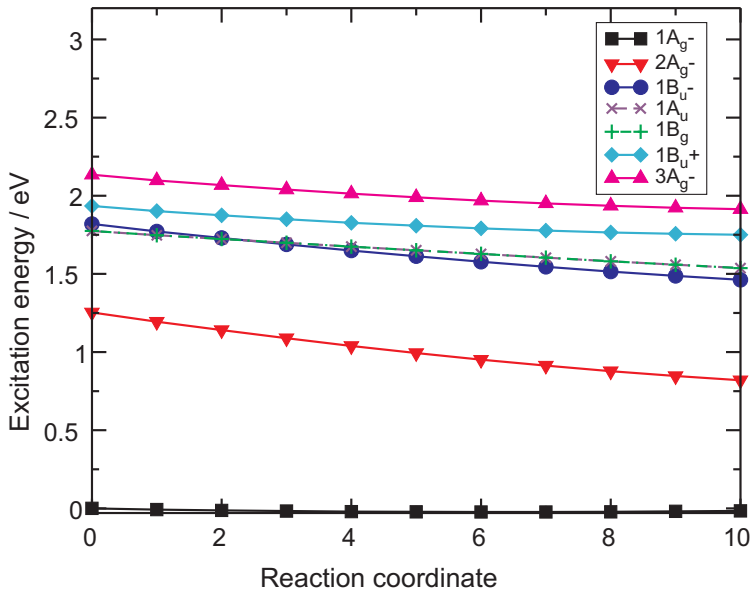

Figure 6.4. Energies of electronic states vs. the conformational relaxation coordinate (labeled as reaction coordinate RC) according to the quantum chemical calculations. Various values between the ground-state minimum geometry (corresponding to the RC value of 0) and the $1B_u^+$ potential minimum geometry (corresponding to the RC value = 10) were calculated. The B_g and A_u states are degenerate. $3A_g^-$, $1B_g$ and $2A_g^-$ are one-photon forbidden states.

Our calculations indicate that indeed excitation of an electron from these in-plane *n*-orbitals to π_{LUMO} and π_{LUMO+1} results in a pair of optically dark ^1A_u and ^1B_g states which carry internal charge-transfer character (ICT) due to the delocalization of π_{LUMO} over the whole polyene chain (Fig. 6.3). Within the accuracy of the calculation these two states are degenerate. The $1B_u^-$ state is calculated to be energetically well below the $1B_u^+$ state and more or less isoenergetic with the ICT states. It may thus be expected to play a pronounced role in the excited state relaxation. This may change however in more polar solvents (the calculations are carried out for vacuum) where the ICT states may be stabilized substantially. The calculated vertical excitation energies of DHIRQ along the linearly interpolated path connecting its ground state and its $1B_u^+$ state minimum geometries are shown in Fig. 6.4. In the Franck-Condon region (RC=0) the $1B_u^-$ state – which is usually considered to be a "dark state" – carries substantial dipole strength. To understand this phenomenon one has to take into account that the Pariser pseudo-parity labels + or – (R. Pariser, 1956) that are typically employed in the nomenclature of carotene electronic states, are only valid in a one-electron approximation and the concomitant selection rules for electronic dipole transitions are not strictly obeyed. In the true C_{2h} molecular point group symmetry both the optically bright $1B_u^+$ and the generally assumed "dark" $1B_u^-$ states transform according to the $1B_u$ irreducible representation. Hence, their configurations are allowed to interact. This kind of interaction is the stronger the closer the two states are in energy. In the Franck-Condon region, where the

energy gap amounts to merely 0.11 eV according to the calculations, the optically allowed ($\pi_{HOMO}\rightarrow\pi_{LUMO}$) single excitation contributes about 11% to the lower ^1B_u state, dubbed $1B_u^-$, while dominating the electronic structure of the upper ^1B_u state ($1B_u^+$) with a squared coefficient of about 0.59. Nuclear geometry relaxation in the $1B_u^+$ potential towards the minimum leads to a near equalization of the C-C bond lengths in the polyene chain (compare Fig. 6.3). The quinoid end groups show no change in the electron density or conformation (i.e. no conformational relaxation) along the reaction coordinate. A stronger geometry dependence of the doubly excited configurations of the $2A_g^-$ and $1B_u^-$ states as compared to the dominantly singly excited leading configuration of the $1B_u^+$ state has been noticed earlier (C.M. Marian and N. Gilka, 2008; M. Kleinschmidt et al., 2009). However, because of the longer conjugation of the molecule and the reversed order of the $1B_u^+$ and $1B_u^-$ states, geometry relaxation in the excited state leads to an increase of the $1B_u^-/1B_u^+$ energy gap in contrast to the shorter conjugation length "normal" carotenoids. At the $1B_u^+$ minimum geometry the DFT/MRCI calculations yield an energy separation of about 0.3 eV between the two ^1B_u states. Here the ($\pi_{HOMO}\rightarrow\pi_{LUMO}$) single excitation contributes less than 2‰ to the $1B_u^-$ wave function and thus its oscillator strength is very low. Note that the $1B_u^-$ state may however borrow substantial transition moment by vibronic coupling to the $1B_u^+$ state. It has been proposed that the $1B_u^-$ state can play an important role in the relaxation of longer-chain carotenoids (T. Sashima et al., 1999; E. Ostroumov et al., 2009); see c.f. (T. Polivka and V. Sundström, 2009) for a review.

6.3.3 Transient absorption

Femtosecond transient absorption (TA) of DHIRQ was measured at room temperature. in n-hexane (Figs. 6.5A,C,E) and CH_2Cl_2 (Figs. 6.5B,D,F). In the VIS range two different excitation wavelengths were used for each solvent: i) excitation on the red side of the absorption band was at 610 nm for n-hexane and 640 nm for CH_2Cl_2; ii) excitation in the maximum of the absorption band was 570 nm for n-hexane and 585 nm for CH_2Cl_2 solution. In addition, measurements in the NIR spectral region (850-1000 nm) were taken for both solvents with excitation in the absorbance maximum.

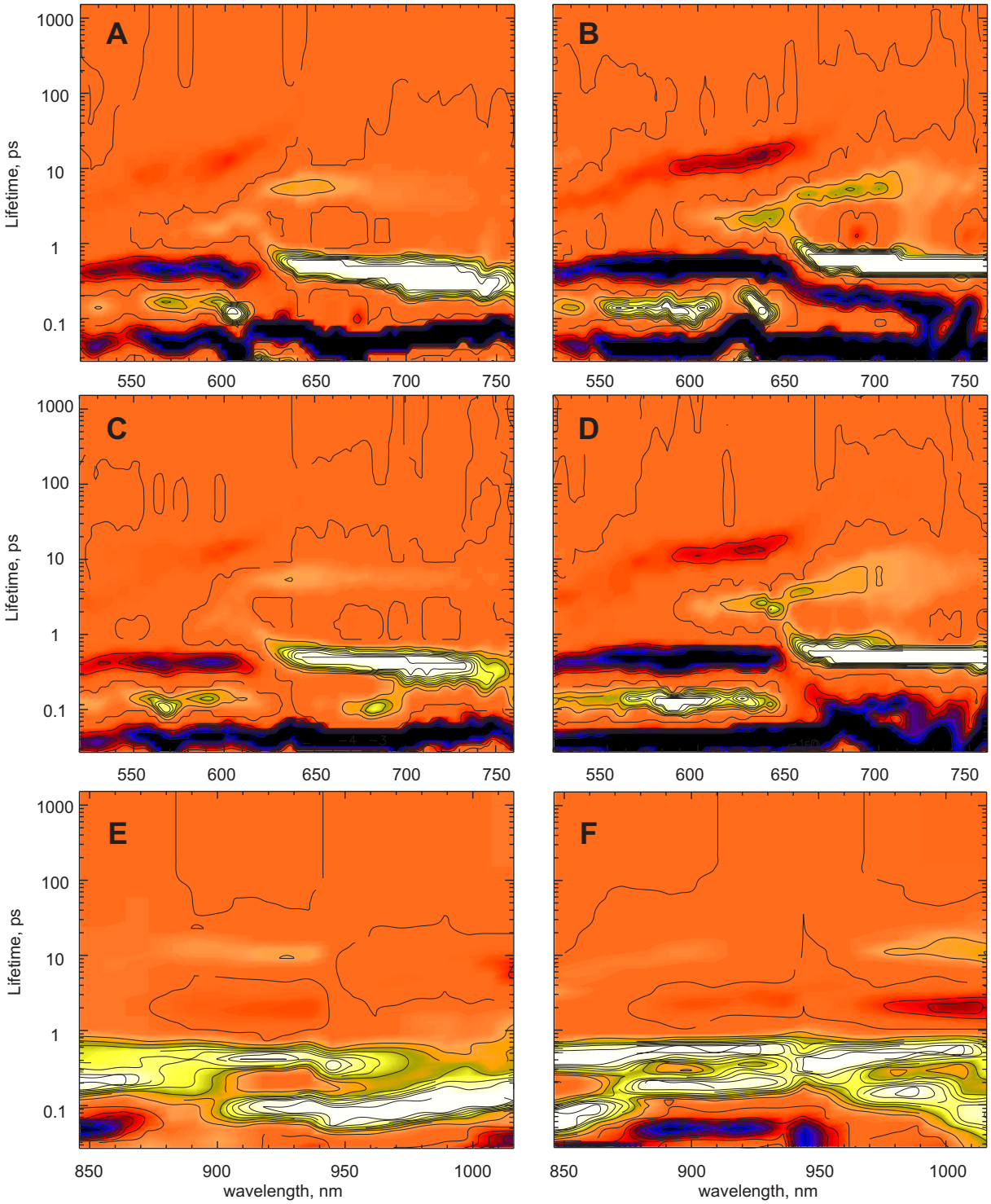

Figure 6.5 Lifetime density maps calculated from the femtosecond transient absorption kinetics of DHIRQ in n-hexane (A,C,E) and CH_2Cl_2 (B,D,F) in the VIS (A-D) and NIR (E-F) spectral ranges. Excitation wavelengths are 640 nm (A), 570 nm (C,E) 610 nm (B) and 585 nm (D,F).

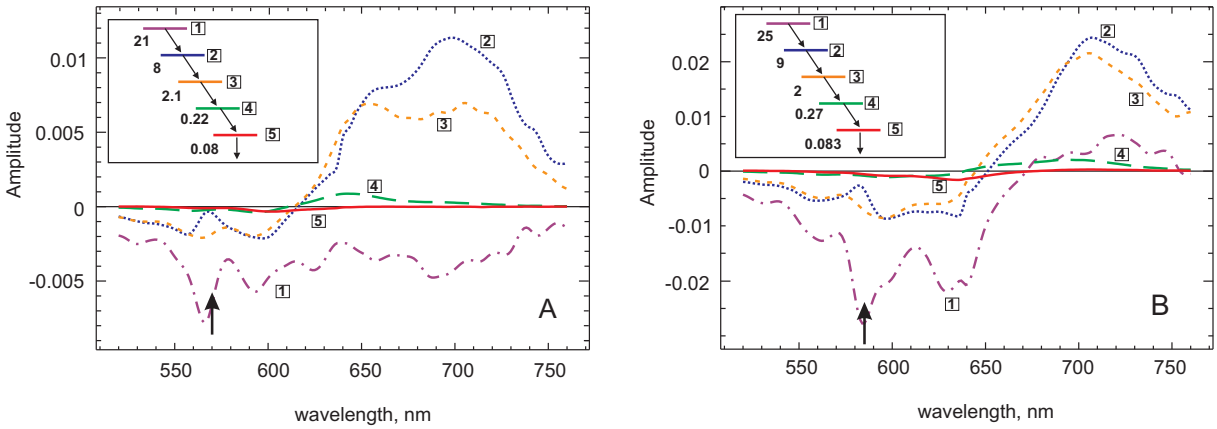

Figure 6.6. Species-associated difference spectra (SADS) of DHIRQ in n-hexane (A) and CH_2Cl_2 (B) in the VIS spectral range. The assumed simple sequential kinetic model (with relaxation rates in ps^{-1}) is shown in the inset. The states (same color for the SADS and the state denomination is used) are shown as boxed numbers. Excitation at 570 nm (A) and 585 nm (B), respectively (as shown by black arrows).

No major changes are observed from the LFD maps for the different excitation wavelengths except for some variations in the ground state bleaching (GB) region on the timescale <70 fs (not shown). These differences will not be discussed any further in this paper since additional measurements and more complex analysis are required in order to meaningfully reveal the variations on the short timescale. However depending on the solvent polarity the relaxation pattern on the time-scale >1 ps changes significantly. Essentially no long-lived components (i.e. ps lifetimes) are observed in n-hexane, whereas in CH_2Cl_2 two components with lifetimes of ~3-4 ps and ~10-15 ps are observed (Fig. 6.5). On the short time scale, DHIRQ shows three lifetime components with lifetimes <70 fs, ~120 fs and ca. 400 fs. These components experience a spectral red shift and a slight increase of their lifetime in the polar CH_2Cl_2 relative to apolar n-hexane solution. The 120 fs and 400 fs contributions show similar spectral features but are of opposite sign in their amplitudes and thus probably correspond to the rise and decay of the same intermediate states. Overall DHIRQ appears to show the shortest excited state decay of all carotenoids that we are aware of.

Global target analysis using a simple sequential kinetic model yields the SADS and rate constants which are shown in Fig. 6.6. Since at this stage nothing can be said about the assignment of the relaxing states they were numbered sequentially (boxed numbers in Fig. 6.6). The initially excited state, which is likely the $1B_u^+$ state, shows a negative amplitude in the SADS reflecting the ground-state bleaching (<600 nm) in CH_2Cl_2 (Fig. 6.6B). In n-hexane this component shows negative amplitude also at long wavelengths (>650 nm) (Fig. 6.6B), which likely represents stimulation emission (SE), possibly from the $1B_u^-$ state (E. Ostroumov et al., 2009). States 2 and 3 (c.f. schemes in Fig. 6.6) reveal spectra with similar ground state

bleaching (GB) signature below 650 nm and a strong excited-state absorption (ESA) band in the 630-760 nm range. The state 2 spectrum shows a small red-shift relative to the state 3 spectrum. For hexane solution the SADS of both states 2 and 3 show a vibrational structure with two bands, whereas only the longer-wavelength band with some small shoulder on the blue side is observed in CH_2Cl_2 (Fig. 6.6). The two longest living states 4 and 5 show very small amplitude, being almost absent in the apolar n-hexane. Since, in the simple sequential model, excitation flows through all states, we expect at least similar GS bleaching amplitude for all states. The resulting small SADS amplitudes in Fig. 6.6 for the two longest-living states must thus be considered as unreasonable. This is a first indication that a simple sequential model is not the correct kinetic description of the excited state dynamics of DHIRQ. Therefore other more complex models are considered in the discussion (see below).

In the NIR region (Fig. 6.5E,F) the LFD maps reveal essentially two (perhaps three in CH_2Cl_2) lifetime components with mostly positive DADS amplitudes, thus reflecting excited state decays. They have rather broad spectra extending out to 1000 nm. Their lifetimes correspond approximately to the two short-lived components observed in the VIS range, i.e. <70 fs and ca. 400 fs.

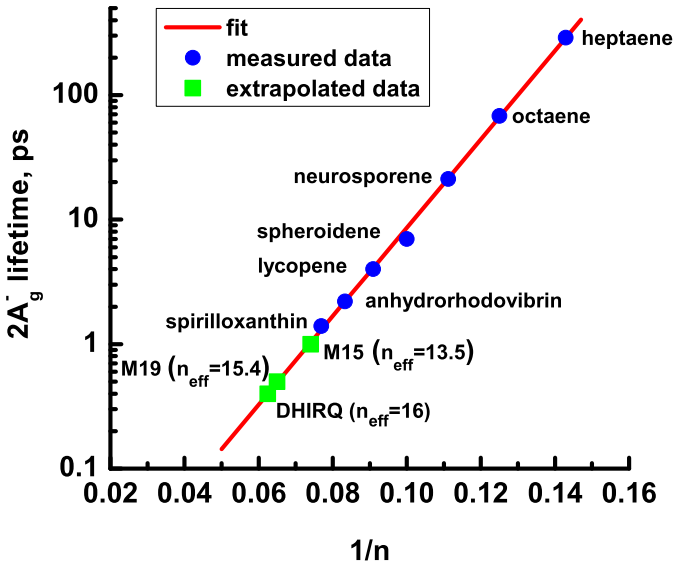

Figure 6.7. Correlation between $2A_g^-$ (S_1) lifetimes [ps] and effective conjugation length 1/n for the polyenes and carotenoids heptaene (H.A. Frank et al., 2002) (n=7), octaene (H.A. Frank et al., 2002) (n=8), neurosporene (J.-P. Zhang et al., 2000) (n=9), spheroidene (J.-P. Zhang et al., 2000) (n=10), lycopene (J.-P. Zhang et al., 2000) (n=11), anhydrorhodovibrin (R. Fujii et al., 2003) (n=12), spirilloxanthin (R. Fujii et al., 2003) (n=13), M15 (P.O. Andersson and T. Gillbro, 1995) (n_{eff}=13.5), M19 (P.O. Andersson and T. Gillbro, 1995) (n_{eff}=15.4), and DHIRQ(n_{eff}=16), this work.

6.4 Discussion

The time-resolved data of DHIRQ show that almost all the excited state decays take place on an ultrafast time scale of <0.5 ps. Comparably fast relaxation rates were reported before for dodecapreno-β-carotene, an M19 homolog to β-carotene (P.O. Andersson and T. Gillbro, 1995). The lifetime of the lowest-lying excited state $2A_g^-$ in this compound is ca. 470 fs, i.e. 15-20% longer than the lifetime of the strong GB/ESA term observed in n-hexane solution of DHIRQ (Fig. 6.5A,C). If one interprets this component in DHIRQ also as the relaxation of $2A_g^-$, then the shorter lifetime indicates a further decrease of the S_0-$2A_g^-$ (S_1) energy gap due to an increase in the conjugation length – in comparison to M19. Figure 6.7 reveals a nearly linear dependence of the lifetime of the $2A_g^-$ state on the conjugation length parameter '1/n' for a number of open-chain carotenoids. By extrapolation of this linear regression, values of n_{eff} for M15, M19 and DHIRQ were estimated as 13.5, 15.4, and 16, respectively. Within the experimental error, the value for M15 is in satisfactory agreement with the value obtained in (D. Kosumi et al., 2009). In that work extrapolating the dependence of the S_0-$1B_u^+$ energy gap on 'n' of open chain carotenoids, the effective conjugation length of M15 was estimated as 14.1. DHIRQ is a blue carotenoid, i.e., it has a very long-wave absorption (Fig. 6.2) and in our view the correlation between effective conjugation length and absorption spectrum is one of the most reliable correlations obeyed by all carotenoids. Therefore this correlation should be used as a strong argument for estimation of the $2A_g^-$ state lifetime and its assignment, when discussing various alternative kinetic models (see section 6.4.3).

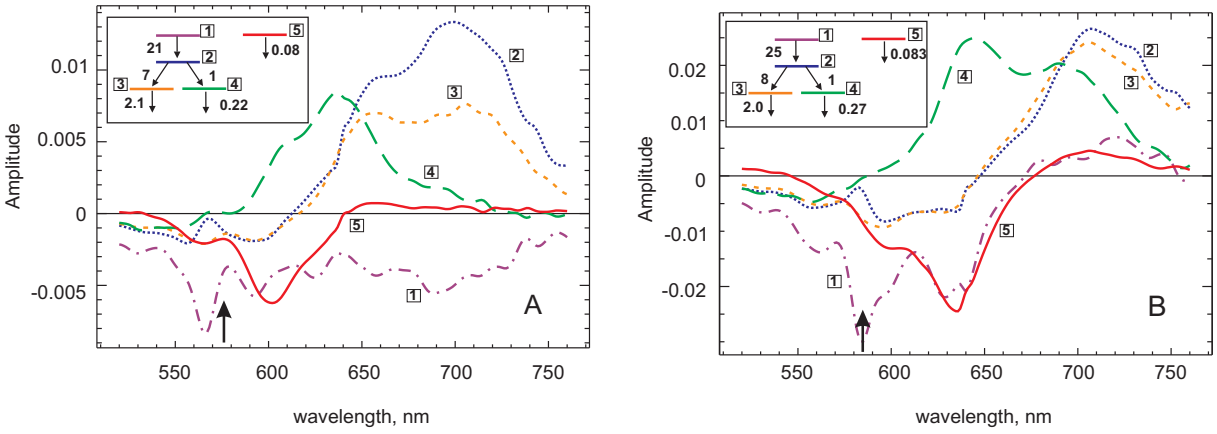

Figure 6.8. Species-associated difference spectra (SADS) of DHIRQ in n-hexane (A) and CH_2Cl_2 (B) in the VIS spectral range. The assumed branching model (with relaxation rates in ps^{-1}) is shown in the inset. The states (same color for the SADS and the state is used) are labeled with boxed numbers. Excitation at 570 nm (A) and 585 nm (B), respectively (shown by black arrow).

Table 6.2. Lifetimes obtained from the sequential (Fig. 6.6) and branching (Fig. 6.8) kinetic models. The lifetimes have errors of ±5 %.

	τ_1	τ_2	τ_3	τ_4	τ_5
Fig. 6.6A / 6.8A (hexane)	47.6 fs	125 fs	476 fs	4.5 ps	12.5 ps
Fig. 6.6B / 6.8B (CH_2Cl_2)	40 fs	111 fs	500 fs	3.7 ps	12 ps

The initially excited state (state 1 in the kinetics schemes of Figs. 6.6 and 6.8) with decay lifetimes of 40-50 fs (Table 6.2), shows in its SADS the typical GB and SE spectra in the absorption region. In hexane solution, the apparent GB signal extends up to about 750 nm, i.e. far beyond the GB and expected "normal" SE region. The red part of the SADS is thus most likely a SE band from a different state. We have observed such a behavior earlier for lutein and β-carotene where we assigned the red SE signal to the $1B_u^-$ state (E. Ostroumov et al., 2009). As pointed out above, the kinetics at very early times (sub 50 fs time range) shows some complexities that require additional studies and thus will not be discussed here. Suffice it to say, there are some indications that the initially excited $1B_u^+$ state may relax in a time faster than the 40-50 fs lifetime to the $1B_u^-$ state from which state 2 (see Figs. 6.6 and 6.8 for states numbering) is populated (Note that we use here a simple numbering nomenclature since electronic assignment of the states is not fully clarified). State 2 as well as state 3 show a strong ESA signal in the red range from 650-750 nm, which characterizes them as either the $2A_g^-$ (S_1) state or as an ICT state (D. Zigmantas et al., 2001; D. Zigmantas et al., 2002; D. Zigmantas et al., 2004). State 2 decays with a lifetime of 110 to 125 fs and state 3 with a lifetime of 475 to 500 fs, depending on the solvent (Table 6.2).

6.4.1 Alternative kinetic schemes

Figure 6.9 shows three alternative electronic level schemes with branching and possible assignment of the states. Note that essentially all of these schemes formally agree with the observed kinetics. However these schemes differ in their electronic level structure and the assignment of the formal intermediates to the actual states. The branching scheme has been introduced in order to solve the problems pointed out above, namely the low amplitude of the SADS of the long-lived states in the sequential model (Fig. 6.6). Application of the different branching schemes for analysis gives the same lifetimes and essentially the same SADS for the corresponding states. For this reason we show the resulting SADS only for the model presented in Fig. 6.8, where branching is introduced from the state 2 to states 3 and 4. It is important to note that these different branching models are not kinetically and spectrally distinguishable for principal reasons: they all formally fit the experimental kinetics equally

well. But the actual situation is even more complex, since the ratio of the decay rates k_{23} / k_{24} is not defined by the kinetic analysis but only their sum $k_{23}+k_{24}$. This leads essentially to an infinite number of possible kinetic solutions. We have chosen in Fig. 6.8 such a ratio of these rates in the branching reaction that the resulting SADS of both states show comparable amplitudes. This is possible since the shape of these SADS depends only weakly on the chosen rates ratio, while the relative amplitudes of the SADS depend very strongly on it. To resolve the ambiguity of the solution either additional kinetic and spectral information on the branching reaction has to be obtained (it is however entirely unclear at present whether and how such additional information can be obtained) or further detailed analysis of the SADS has to be performed in order to allow us to exclude one or more of these schemes. This will be discussed in section 6.4.3. Note that state 5 in all the schemes shown in Figs. 6.8 and 6.9 has been assumed to reflect the kinetics of a separate and independently excited compound, essentially an "impurity" (the reason for this choice is discussed in the following section).

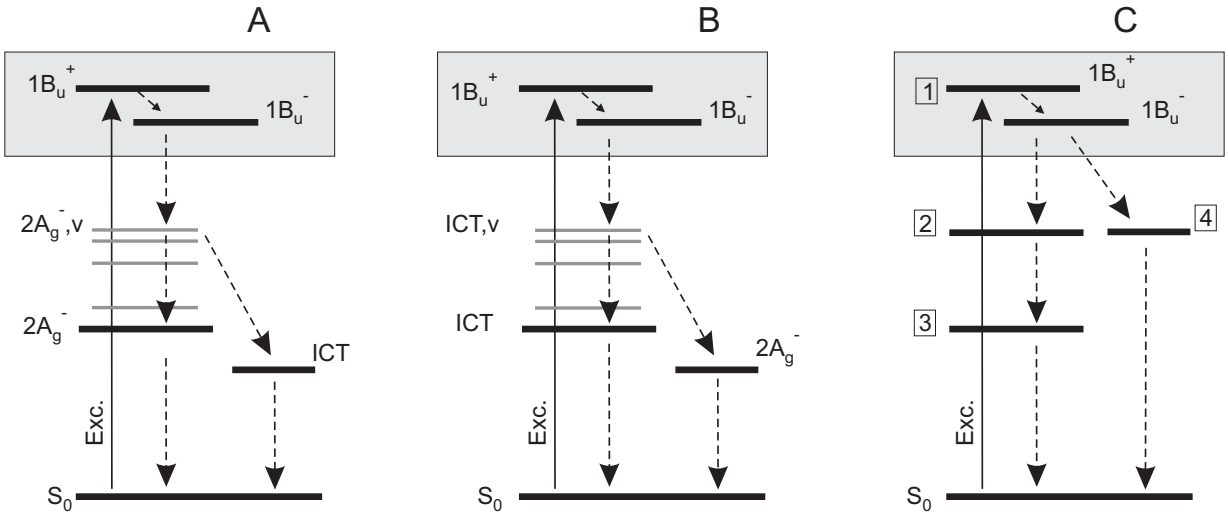

Figure 6.9. Alternative energy level diagrams and excited state energy relaxation schemes for DHIRQ upon initial excitation of the $1B_u^+$ state. In A and B an assignment of the different energy levels to particular states is made. The full line arrow indicates the excitation and the dashed arrows the relaxation processes. In C the energy levels are noted by boxed numbers only referring to the numbering used in Figs. 6.7 and 6.8, since several alternative assignments are discussed in the text. The grey boxes around the $1B_u$ states indicate the fact that we do not discuss in detail the relaxation processes between these levels but rather take the mixed $1B_u$ states as the origin of the first resolved ca. 40 fs relaxation process.

6.4.2 What is the origin of state 5?

We have not discussed so far the origin of state 5 in the kinetic schemes of Figs. 6.6 and 6.8. This state has an extremely small signal amplitude in the LFD maps with lifetimes of 12-14 ps (Table 6.2) and has been assigned to a separate state that does not take part in the

relaxation dynamics of DHIRQ, i.e., it represents essentially a directly excited small amount of "impurity". Presence of an impurity can not be entirely excluded given the fact that DHIRQ is chemically somewhat unstable over longer time periods. The main reason why we treat it in our analysis as an "impurity" is the fact that its TA difference spectrum in the GB region does not seem to agree well with the GB spectrum of SADS of other intermediate states (Fig. 6.8). On the other hand, the overall SADS also does not exclude it to be a carotenoid. At this stage we simply do not have any good reasons to incorporate this state into the relaxation scheme for DHIRQ. This could be done, however, without difficulty if one were to introduce another branching reaction into the kinetic schemes of Fig. 6.9A or 6.9C. We point out that to some extent the SADS of state 5 is reminiscent of the so-called S* state which has been invoked for some carotenoids and so far has been discussed quite controversially (for a review see (T. Polivka and V. Sundström, 2009; N. Christensson et al., 2009)). In the absence of further information we do not comment on the likelihood of such an assignment of state 5 in DHIRQ since we believe that the discussion of the S* state problem requires a wider and more general approach and should be first solved on simpler carotenoids.

6.4.3 Discussion of excited states and relaxation dynamics

We now turn to the discussion of the various alternative kinetic schemes shown in Fig. 6.9. None of these schemes distinguish between the decay of the $1B_u^+$ and the $1B_u^-$ states to the lower-lying states. Note that the schemes shown in Figs. 6.9 are not principally different kinetic schemes. They merely differ in the assignment of the various spectroscopically observed intermediates to different electronic states. Thus these schemes are only shown for simplifying the following discussion of the alternative states assignments. Our theoretical calculations show the $1B_u^-$ to be located well below the $1B_u^+$ state, and thus it is very likely that relaxation occurs via the $1B_u^-$ state, in particular given the fact that these states have essentially identical symmetry. However in this work we do not address the $1B_u^+/1B_u^-$ relaxation and interaction problem explicitly (E. Ostroumov et al., 2009) and consider these two states as a combined $1B_u^+/1B_u^-$ level only. In scheme 9A the relaxation from this combined level occurs initially to a vibrationally excited level of the $2A_g^-$ (S_1) state with a lifetime of 40-50 fs, which finally relaxes to the vibrational ground state of $2A_g^-$ with a lifetime of 110-125 fs. The vibrationally relaxed $2A_g^-$ state has a lifetime of 400-500 fs, depending on the solvent (c.f. Table 6.2). So far, this model reflects the usual relaxation scheme of carotenoids (see (T. Polivka and V. Sundström, 2004) for a review) with the exception of some additional complexity at the early times. The formation of an ICT state occurs by branching from the vibrationally excited $2A_g^-$ state in Fig. 6.9A. The ICT state in

this case would have a lifetime of about 5 ps in hexane and 3.7 ps in CH_2Cl_2, i.e., a significant polarity dependence of lifetime, as has been reported before for ICT states in carbonyl carotenoids (D. Zigmantas et al., 2001; D. Zigmantas et al., 2002; D. Zigmantas et al., 2004). We could alternatively also have the ICT state formed from the vibrationally relaxed $2A_g^-$ state, or have a mixture of both pathways. This would not change the outcome and it would in particular not change the SADS of the involved states.

In the described scenario the $2A_g^-$ state corresponds to the SADS of states 2 and 3 in Fig. 6.8. This implies that the $2A_g^-$ ESA signal would occur above 650 nm with some vibrational structure in case of hexane solution and would have a dominant single band around 710 nm in CH_2Cl_2. Accordingly the ICT state then has to be assigned to state 4 (Fig. 6.8). This means, however, that the ICT state would have a shorter-wavelength ESA than the $2A_g^-$, i.e. in the range of 600-700 nm (see SADS in Fig. 6.8), showing some pronounced dependence of the spectral shape on the solvent polarity, which seems to be reasonable. Thus the ordering of the ESA bands in this assignment would be opposite to the one observed in other carotenoids with an ICT character (D. Zigmantas et al., 2001; D. Zigmantas et al., 2002; D. Zigmantas et al., 2004) where the ICT absorption was reported to be located at longer wavelength. However in the absence of further information on the spectral features of $2A_g^-$ and ICT states we cannot decide which ordering to expect for their ESA bands. The ordering of the ESA bands could easily differ in different carbonyl carotenoids, since the ESA signals do depend on the location of the high-energy end state of the ESA transition. Our scheme also implies that only a fraction of the initial population ends up in the ICT state while the majority of the relaxation occurs through the $2A_g^-$ state directly to the ground state. In the scheme of Fig. 6.8, the percentage of ICT state formed is about 10-15% (Note however the above discussion on the principal inability to uniquely determine the branching ratio). In our view, Fig. 6.9A is the most likely kinetic scheme that reasonably describes the excited state relaxation of DHIRQ without major contradictions. Figure 6.9C represents only a slight variation of this scheme. If we were to assign state 4 in Fig. 6.9C to the ICT state, which in this case would be populated directly from the $1B_u$ states and not via the $2A_g^-$ state, nothing essential would change in the assignment of the states and the population dynamics. One also could imagine a combination of schemes 9A and 9C, where the ICT state could be populated in parallel from both the $1B_u$ states and the $2A_g^-$ state. This would again not change the SADS of the states in any significant manner. The small population of the ICT state in this carotenoid would in this model be simply explained by the very fast decay from the $2A_{g,v}^-$ state which prevents a higher population of the ICT state.

Let us now discuss an alternative state assignment, shown in scheme 9B, where the relaxation from the initially excited $1B_u$ states leads directly to the ICT_v state and the $2A_g^-$ state is formed in a branching reaction from the vibrationally excited ICT_v state. In this case the ICT state would show the ultrafast relaxation (110-125 fs and 400-500 fs) while the $2A_g^-$ state would relax with a lifetime of 3.7-5 ps. Thus very little population would flow through the $2A_g^-$ state. The only advantage of such a scenario would be that the ESA energy ordering would follow the usual order for carbonyl carotenoids possessing ICT states (D. Zigmantas et al., 2001; D. Zigmantas et al., 2002; D. Zigmantas et al., 2004). However, as discussed already above, we do not have any information on the probable location of the ICT ESA band. For this reason we do not consider the same ESA ordering as in other carotenoids to be a strong requirement. The ESA ordering could easily be different in this unusual carotenoid from the previously studied carbonyl carotenoids. Given the extreme long-wavelength absorption of DHIRQ which indicates a very large conjugation length and thus a low-lying $2A_g^-$ (S_1) state, the assignment of the state with shorter lifetime to the $2A_g^-$ state provides a much stronger argument. For these reasons we essentially exclude scheme 9B as a proper assignment of the excited states and relaxation pathways of DHIRQ and suggest scheme 9A as the most likely assignment.

6.5 Conclusions

The quinoid carotenoid DHIRQ reveals complex spectral and temporal properties and combines long carbon-carbon conjugation systems with additional carbonyl groups in special end rings. Because of the resulting long effective conjugation length its absorption band is strongly shifted to the red (the carotenoid solution has a blue color). The early relaxation dynamics of the carotenoid is complicated by low-lying $1B_u^-$ and ICT states below the $1B_u^+$ state, as predicted by the quantum chemical calculations based on the DFT/MRCI method. A model with population of the ICT state from the unrelaxed and/or relaxed $2A_g^-$ state (Fig. 6.9A) or additionally directly from the $1B_u$ states (Fig. 6.9C) is proposed as the most reasonable state assignment that describes the observed kinetics.

Acknowledgements

We gratefully acknowledge Dr. Sebastian Kock for synthesizing the DHIRQ. The present work has been performed as a project of the DFG Sonderforschungsbereich SFB 663 (projects B1, B2 and C1), Heinrich-Heine-Universität Düsseldorf and Max-Planck-Institut, Mülheim a.d. Ruhr, Germany.

Summary

In this work the relaxation dynamics of the electronic excited states of several naturally occurring carotenoids and the synthetic DHIRQ molecule was studied. The investigation of electronic properties of higher lying electronic states with relaxation on the femtosecond time-scale as well of the properties of lower energy electronic states with picosecond relaxation time was performed by means of femtosecond transient absorption spectroscopy combined with quantum chemical calculations and complex kinetic analysis. This allowed to explain the distortion of carotenoid relaxation kinetics and fluorescence spectra and elucidate the controversy of the dark S* state. Furthermore, the unusual properties of the synthetic quinoid carotenoid DHIRQ are reported.

In **Chapter 3** a study of the early relaxation dynamics in lutein (N=10) and β-carotene (N=11) is presented. The transient absorption measurements revealed a strong dependence of the kinetics in the first 400 fs on the solvent polarity and on the excitation wavelength. Strong oscillations have been observed in the 600-700 nm region. The quantum chemical calculations predicted the $1B_u^-$ state to move below the initially excited S_2 ($1B_u^+$) state during the dynamic relaxation from the initially excited state to the potential minimum. Thus an electronic level crossing between the S_2 ($1B_u^+$) and $1B_u^-$ states is proposed for lutein and β-carotene in non-polar solvents. In the crossing region these two states are shown to be strongly coupled and thus electronic quantum beats are proposed to be the source of the oscillatory behavior of the experimental kinetics. It is shown that no conventional lifetime analysis in terms of exponentials can reproduce the observed oscillations. A simple model based on the optical Bloch equation approach describes the essential features of the experimental data and confirms the strong coupling between the S_2 ($1B_u^+$) and the $1B_u^-$ states. The steady-state fluorescence spectra of lutein and β-carotene revealed a strong deviation of the spectrum from the expected calculated fluorescence spectrum. The shift to longer wavelengths of the steady-state fluorescence spectrum is in agreement with the observed red-shifted stimulated emission (SE) observed in the transient spectra. This shift is well in agreement with the shift of the $1B_u^-$ state potential surface along the nuclear coordinate, which has been predicted by quantum chemical calculations. Thus a large part of the fluorescence is due to the $1B_u^-$ state, which is shown not to be a 'dark state'. This study for the first time proves that the $1B_u^-$ state can not be ignored for understanding the relaxation dynamics.

Chapter 4 presents a more elaborate analysis of the same kinetic data of lutein. The Redfield theory approach has been used for analysis of the relaxation kinetics. This approach allows to calculate correct values of the energies of the states of the Hamiltonian and coupling strengths. Furthermore, on the basis of the spectral density function the elements of the relaxation tensor (Redfield tensor) can be calculated. This allowed to assign the species-associated difference spectra (SADS) to the electronic excited states. The SADS have been interpreted in terms of SE and excited state absorption (ESA) from the S_2 ($1B_u^+$) and $1B_u^-$ state as well as ground state bleaching and ESA from vibrationally excited and relaxed S_1 state. Within the Redfield theory approach the kinetics can be reproduced well by means of two vibrational modes – high frequency ω_1=1150 cm^{-1} and low frequency ω_2=330 cm^{-1} modes. The corresponding Huang-Rhys factors have typical values of g_1=0.5 and g_2=1.0. The values of the energies of the states as well as the coupling strengths in the Hamiltonian are located in the expected range and show a reasonable dependence on the excitation wavelength and solvent polarity. Thus it was shown that using the Redfield theory approach one can perform an analysis of the time-resolved data based on a much improved and more realistic physical model, as compared to the optical Bloch equation approach, and the real physical properties of the involved excited states can be calculated. It was shown that the experimental data can not be described without taking into account coherent coupling between these states.

Chapter 5 describes a study of the nature of the 'dark S* state' proposed by other authors. To disclose the origin of the long lifetime component observed in carotenoids β-carotene was measured unpurified and in HPLC purified form. This showed that the longer lifetime component with the S*-reminiscent blue-shifted spectrum originates from an impurity, probably a carotenoid with a short conjugation length. Further experiments performed on β-carotene in various solvents and excitation wavelengths have revealed a ~2 ps lifetime component. Analysis of the excitation wavelength dependent data have shown that a branching kinetic scheme with the parallel population of the S_1 and S* states from the initially excited S_2 state does not give meaningful SADS. In contrary the sequential scheme gave reasonable SADS and the ~2 ps lifetime component, which previously had also been assigned to an S* state, has been assigned to a vibrationally excited S_1 state. This result was confirmed by intensity dependent and low temperature measurements, where only a sequential kinetic scheme was able to reasonably describe the experimental data. Thus the existence of a separate S* electronic state below the S_2 state is excluded.

The dynamics of the recently synthesized quinoid DHIRQ carotenoid was studied in **Chapter 6**. This carotenoid is an oxidation product of the phenolic DHIR carotenoid and

contains two carbonyl groups, which are located on the end rings of the molecule and are a part of the conjugation system. This molecular structure causes a strong deviation of the spectral and kinetic properties as compared to the DHIR carotenoid. A strong bathochromic shift of the absorption spectrum (ca. 100 nm) is observed for DHIRQ as expected for this longer chain carotenoid. The quantum chemical calculations predicted a low lying intra-molecular charge transfer (ICT) state in the electronic structure of the DHIRQ. This theoretical prediction has been confirmed by transient absorption spectroscopy. In contrary to other carbonyl carotenoids, where one lifetime component only is observed for the combined S1/ICT state, two lifetime components have been resolved in the current study. A branching scheme with parallel population of the S_1 and the ICT states describes best the experimental data. The shortest lifetime component (ca. 400 fs) showed no solvent polarity dependence and has been assigned to the S_1 state, whereas the longer lifetime component was observed mostly in polar solvent and was assigned to the ICT state. From the lifetime of the S_1 state the effective conjugation length of the DHIRQ was estimated to be *Neff*=16. Thus the quinoid DHIRQ carotenoid has the shortest lifetime of the S_1 state reported for a carotenoid.

To conclude, in the present work novel information on the origin and dynamics of the reported 'dark states' of carotenoids has been obtained. The unusual phenomenon of electronic coherence in a large molecular system (lutein, N=10) leading to oscillatory behavior of the transient absorption signal is reported. This behavior directly proves for the first time the existence of the $1B_u^-$ state below the $1B_u^+$ state for a typical carotenoid and reveals the importance of the state for understanding the relaxation kinetics from the initially excited S_2 state. Finally the previously proposed existence of the so-called 'dark S* state' has been ruled out for β-carotene (N=11).

Zusammenfassung

In dieser Arbeit wurde die Dynamik der Relaxation der elektronisch angeregten Zustände von einigen natürlich vorkommenden Carotinoiden und dem synthetischen Carotinoid-Molekül DHIRQ untersucht. Die elektronischen Eigenschaften sowohl der energetisch höher liegenden elektronischen Zustände mit Relaxationszeiten im Femtosekunden-Bereich als auch der elektronischen Zustände mit niedrigerer Energie mit Relaxationszeiten im Pikosekunden-Bereich wurden mit Hilfe der femtosekunden-zeitaufgelösten Absorptionsspektroskopie bestimmt und mit einer quantenchemischen Theorie in Verbindung mit einer komplizierten kinetischen Analyse beschrieben. Dadurch wurde es möglich, die Veränderungen in der Carotinoid-Relaxationskinetik und den Fluoreszenzspektren zu erklären und die Kontroverse um den Dunkelzustand S* aufzulösen. Außerdem wurden die ungewöhnlichen Eigenschaften der synthetischen chinoiden Carotinoide DHIRQ charakterisiert.

Kapitel 3 konzentriert sich auf die Untersuchung der frühen Relaxationsdynamik in Lutein (N = 10) und β-Carotin (N = 11). Die transienten Absorptionsmessungen zeigen eine starke Abhängigkeit der Kinetik in den ersten 400 fs von der Polarität des Lösungsmittels und der Anregungswellenlänge. Außerdem waren in der Region um 600-700 nm große Oszillationen zu beobachten. Die quantenchemischen Rechnungen haben vorhergesagt, dass sich der $1B_u^-$-Zustand unter den ursprünglich angeregten S_2-Zustand ($1B_u^+$) während der dynamischen Relaxation vom ursprünglich angeregten Zustand zum Potenzial-Minimum verschieben wird. Daher wird eine Kreuzung der elektronischen Energieniveaus zwischen dem S_2 ($1B_u^+$) und dem $1B_u^-$-Zustand für Lutein und β-Carotin in unpolaren Lösungsmitteln vorgeschlagen. Es wurde gezeigt, dass in der Region der Kreuzung diese zwei Zustände nachweislich stark gekoppelt sind. Daher werden elektronische Quantenbeats als Ursache der Oszillationen in der experimentellen Kinetik vorgeschlagen. Es wurde festgestellt dass keine übliche Lebenszeitanalyse (eine Analyse mit Exponentialfunktionen) die beobachteten Oszillationen nachbilden kann. Ein einfaches Modell auf der Basis der optischen Blochgleichungen beschreibt die Haupteigenschaften der experimentellen Daten und bestätigt die starke Kopplung zwischen dem S_2 ($1B_u^+$) und dem $1B_u^-$-Zustand. Die Fluoreszenzspektren von Lutein und β-Carotin weisen eine starke Abweichung von dem berechneten Fluoreszenzspektrum auf. Die Verschiebung des Fluoreszenzspektrums zu längeren Wellenlängen ist in Übereinstimmung mit der beobachteten Rot-Verschiebung der

stimulierten Emission (SE), die man in den transienten Absorptionsspektren beobachtet. Diese Verschiebung ist auch in guter Übereinstimmung mit der Verschiebung der Potentialfläche des $1B_u^-$-Zustands entlang der Kernkoordinate, die in den quantenchemischen Rechnungen vorhergesagt wird. Demzufolge wird ein großer Teil der Fluoreszenz vom $1B_u^-$-Zustand verursacht, der nachweislich kein 'Dunkelzustand' ist. Diese Untersuchung hat zum ersten Mal bewiesen, dass der $1B_u^-$-Zustand für das Verständnis der Relaxationsdynamik nicht ignoriert werden kann.

Kapitel 4 stellt eine tiefergehende Analyse derselben kinetischen Daten von Lutein vor. Dabei wurde ein Ansatz mit der Redfield-Theorie für die Analyse der Relaxationskinetik verwendet. Dieses Verfahren ermöglicht es, die korrekten Werte der Zustandsenergien in der Hamiltonmatrix und die Kopplungsstärken zu berechnen. Zudem können die Elemente des Relaxationstensors (Redfield Tensor) über die Verwendung der Spektraldichtefunktion berechnet werden. Dadurch können die sogenannten Spezies-assoziierten Differenzspektren (SADS) den elektronischen Zuständen zugeordnet werden. Die SADS wurden unter Berücksichtigung der SE und der Absorption der angeregten Zustände (ESA) aus dem S_2 ($1B_u^+$) und $1B_u^-$-Zustand sowie der Grundzustandsbleichung und der ESA aus dem vibratorisch angeregten und relaxierten S_1-Zustand interpretiert. Innerhalb des Ansatzes der Redfield-Theorie kann die Kinetik mit zwei Schwingungsmoden reproduziert werden: Eine Hochfrequenzmode mit ω_1=1150 cm^{-1} und eine Niedrigfrequenzmode mit ω_2=330 cm^{-1}. Die entsprechenden Huang-Rhys-Faktoren haben typische Werte von g_1=0.5 und g_2=1.0. Die Werte der Zustandsenergien sowie die Kopplungsstärken in der Hamiltonmatrix liegen im erwarteten Bereich und zeigen eine sinnvolle Abhängigkeit von der Anregungswellenlänge und der Lösungsmittelpolarität. Auf diese Weise wurde gezeigt, dass man mit dem Ansatz über die Redfield-Theorie im Vergleich zum Ansatz über die optischen Blochgleichungen eine wesentlich verbesserte Analyse der zeitaufgelösten Daten mit einem realistischeren physikalischen Modell erreichen kann und damit auch die realen physikalischen Eigenschaften der beteiligten angeregten Zustände berechnet werden können. Es wurde weiterhin gezeigt, dass die experimentellen Daten nicht ohne Berücksichtigung der kohärenten Kopplung zwischen diesen Zuständen beschrieben werden können.

Kapitel 5 beschreibt eine Untersuchung über den Charakter des 'Dunkelzustands S*', der von anderen Autoren vorgeschlagen wird. Um die Ursache der Lebenszeit-Komponente mit der langen Lebenszeit, die in Carotinoiden beobachtet wird, aufzuklären, wurde β-Carotin in normaler (verunreinigter) Form und in HPLC-gereinigter Form gemessen. Diese zeigten, dass die längere Lebenszeit- Komponente mit dem S*-typischen blau-verschobenem

Spektrum von einer Verunreinigung erzeugt wird, wahrscheinlich von Carotinoiden mit einer kürzeren Konjugationslänge. Weitere Experimente an β-Carotin in verschiedenen Lösungsmitteln und mit verschiedenen Anregungswellenlängen haben eine ~2 ps Lebenszeit-Komponente nachgewiesen. Die Analyse der Daten von Messungen mit verschiedenen Anregungswellenlängen hat gezeigt, dass ein kinetisches Verzweigungsmodell mit einer parallelen Populierung des S_1 und S*-Zustands aus dem anfänglich angeregten Zustand S_2 keine sinnvollen SADS ergibt. Im Gegensatz dazu ergibt das sequenzielle Modell vernünftige SADS. Die ~2 ps Lebenszeit-Komponente, die vorher einem S*-Zustand zugeordnet wurde, wird nun einem vibratorisch angeregten S_1-Zustand zugeschrieben. Dieses Ergebnis wurde von den intensitätsabhängigen Messungen und Tieftemperatur-Messungen bestätigt, bei denen ebenfalls nur ein sequenzielles kinetisches Modell die experimentellen Daten sinnvoll beschreiben kann. Folglich wird die Existenz eines separaten elektronischen S*-Zustands unterhalb des S_2-Zustands ausgeschlossen.

Die Dynamik des neuerlich synthetisierten chinoiden DHIRQ Carotinoids wurde in **Kapitel 6** untersucht. DHIRQ ist ein Oxidationsprodukt der phenolischen DHIR Carotinoids und enthält zwei Carbonylgruppen, die sich an den Endringen des Moleküls befinden und ein Teil des Konjugationssystems sind. Diese molekulare Struktur bewirkt eine starke Veränderung der spektralen und kinetischen Eigenschaften im Vergleich zum DHIR-Carotinoid. Eine starke bathochrome Verschiebung des Absorptionsspektrums (ca. 100 nm) ist für DHIRQ beobachtet worden, wie sie für solch längerkettige Carotinoide erwartet wird. Die quantenchemischen Rechnungen sagen einen tiefliegenden sogenannten Intra-Molecular Charge Transfer (ICT) Zustand in der elektronischen Struktur des DHIRQ voraus. Dieses theoretische Ergebnis wurde durch die transiente Absorptionsspektroskopie bestätigt. Im Gegensatz zu anderen Carbonyl-Carotinoiden, bei denen nur eine Lebenszeit-Komponente für den kombinierten S_1/ICT Zustand beobachtet wird, wurden in dieser Arbeit zwei Lebenszeit-Komponenten aufgelöst. Ein Verzweigungsmodell mit paralleler Populierung des S_1 und des ICT-Zustands beschreibt die experimentellen Daten am besten. Die kürzeste Lebenszeit-Komponente (ca. 400 fs) zeigt keine Abhängigkeit von der Lösungsmittelspolarität und wird dem S_1-Zustand zugeordnet, während die längere Lebenszeit-Komponente stärker in polaren Lösungsmittel auftritt und wird dem ICT-Zustand zugeschrieben. Aus der Lebenszeit des S_1-Zustands wird die effektive Konjugationslänge des DHIRQ geschätzt auf N*eff* = 16. Demzufolge hat das chinoide Carotinoid DHIRQ die kürzeste S1-Zustandslebenszeit, die für ein Carotinoid berichtet wird.

Als Schlußfolgerung wurden im Rahmen dieser Arbeit neuartige Informationen über den Ursprung und die Dynamik der berichteten ‘Dunkelzustände’ in Carotinoiden erhalten. Über das ungewöhnliche Phänomen der elektronischen Kohärenz in einem großen molekularen System (Lutein, N = 10), die zu starken Oszillationen in den transienten Absorptionssignalen führt, wurde berichtet. Diese Oszillationen beweisen zum ersten Mal direkt die Existenz des $1B_u^-$-Zustands unterhalb des $1B_u^+$-Zustands für ein typisches Carotinoid und demonstriert die Wichtigkeit des Zustands für das Verständnis der Relaxationskinetik aus dem anfänglich angeregten S_2-Zustand. Schließlich konnte die in der Literatur berichtete Existenz des sogenannten ‘S*-Dunkelzustands’ für β-Carotin (N = 11) ausgeschlossen werden.

References

Akimoto, S., I. Yamazaki, S. Takaichi, and M. Mimuro (1999) Excitation relaxation of carotenoids within the S_2 state probed by the femtosecond fluorescence up-conversion method. *Chem. Phys. Lett.* **313,** 63-68.

Akimoto, S., I. Yamazaki, S. Takaichi, and M. Mimuro (2000) Excitation relaxation dynamics of linear carotenoids. *J. Luminesc.* **87-9,** 797-799.

Andersson, P. O., S. B. Bachilo, R.-L. Chen, and T. Gillbro (1995) Solvent and temperature effects on dual fluorescence in a carotenes. Energy gap dependence of the internal conversion rate. *J. Phys. Chem.* **99,** 16199-16209.

Andersson, P. O. and T. Gillbro (1990) Spectral shift of purple bacterial carotenoids related to solvent and protein polarizability. In *Current Research in Photosynthesis. II.*(Edited by M. Baltscheffsky), pp. 117-120. Kluwer Academic Publishers, Dordrecht.

Andersson, P. O. and T. Gillbro (1995) Photophysics and dynamics of the lowest excited singlet state in long substituted polyenes with implications to the very long-chain limit. *J. Chem. Phys.* **103,** 2509-2519.

Andersson, P. O., T. Gillbro, L. Ferguson, and R. J. Cogdell (1991) Absorption spectral shifts of carotenoids related to medium polarizability. *Photochem. Photobiol.* **54,** 353-360.

Barzda, V., V. Gulbinas, R. Kananavicius, V. Cervinskas, H. van Amerongen, R. van Grondelle, and L. Valkunas (2001) Singlet-singlet annihilation kinetics in aggregates and trimers of LHCII. *Biophys. J.* **80,** 2409-2421.

Bautista, J. A., R. E. Connors, B. B. Raju, R. G. Hiller, F. P. Sharples, D. Gosztola, M. R. Wasielewski, and H. A. Frank (1999) Excited state properties of peridinin: Observation of a solvent dependence of the lowest excited singlet state lifetime and spectral behavior unique among carotenoids. *J. Phys. Chem. B* **103,** 8751-8758.

Becke, A. D. (1993) Density-functional thermochemistry. 3. The role of exact exchange. *J. Chem. Phys.* **98,** 5648-5652.

Billsten, H. H., J. Pan, S. Sinha, T. Pascher, V. Sundström, and T. Polivka (2005) Excited-state processes in the carotenoid zeaxanthin after excess energy excitation. *J. Phys. Chem. A* **109,** 6852-6859.

Billsten, H. H., D. Zigmantas, V. Sundström, and T. Polivka (2002) Dynamics of vibrational relaxation in the S_1 state of carotenoids having 11 conjugated C=C bonds. *Chem. Phys. Lett.* **355,** 465-470.

Bloch, F. (1957) Generalized theory of relaxation. *Phys. Rev.* **105,** 1206-1222.

Britton, G., Liaaen-Jensen, S., and Pfander, H.(1998) Carotenoids. Vol.3 Biosynthesis and metabolism. Birkhäuser Verlag AG.

Britton, G., H. Pfander, and S. Liaaen-Jensen (2004) Carotenoids handbook. Birkhäuser Verlag AG.

Brochon, J.-C. (1994) Maximum entropy method of data analysis in time-resolved spectroscopy. In *Methods in Enzymology. Vol.240 Numerical Computer Methods Part B*.(Edited by M. L. Johnson and L. Brand), pp. 262-311. San Diego, Academic Press.

Buckup, T., J. Savolainen, W. Wohlleben, J. L. Herek, H. Hashimoto, R. R. B. Correia, and M. Motzkus (2006) Pump-probe and pump-deplete-probe spectroscopies on carotenoids with N=9-15 conjugated bonds. *J. Chem. Phys.* **125,** 194505-1-194505-7.

Cerón-Carrasco, J. P., A. Requena, and C. M. Marian (2010) Theoretical study of the low-lying excited states of β-carotene isomers by a multireference configuration interaction method. *Chem. Phys.* **in print,** 1-17.

Cerullo, G., D. Polli, G. Lanzani, S. De Silvestri, H. Hashimoto, and R. J. Cogdell (2002) Photosynthetic light harvesting by carotenoids: Detection of an intermediate excited state. *Science* **298,** 2395-2398.

Christensen, R. L. (1999) The Electronic States of Carotenoids. In *The Photochemistry of Carotenoids*.(Edited by H. A. Frank, A. J. Young, G. Britton, and R. J. Cogdell), pp. 137-159. Kluwer Academic Publishers, Dordrecht.

Christensen, R. L., M. G. I. Galinato, E. F. Chu, J. N. Howard, R. D. Broene, and H. A. Frank (2008) Energies of low-lying excited states of linear polyenes. *J. Phys. Chem. A* **112 IS 49,** 12629-12636.

Christensen, R. L. and B. E. Kohler (1973) Low resolution optical spectroscopy of retinyl polyenes: Low lying electronic lebvels and spectral broadness. *Photochem. Photobiol.* **18,** 293-301.

Christensson, N., F. Milota, A. Nemeth, J. Sperling, H. F. Kauffmann, T. Pullerits, and J. Hauer (2009) Two-dimensional electronic spectroscopy of β-carotene. *J. Phys. Chem. B* **113,** 16409-16419.

Chynwat, V. and H. A. Frank (1995) The application of the energy gap law to the S1 energies and dynamics of carotenoids. *Chem. Phys.* **194,** 237-244.

Cogdell, R. J., T. D. Howard, R. Bittl, E. Schlodder, I. Geisenheimer, and W. Lubitz (2000) How carotenoids protect bacterial photosynthesis. *Phil. Trans. R. Soc. Lond. B* **355,** 1345-1349.

Cong, H., D. M. Niedzwiedzki, G. N. Gibson, and H. A. Frank (2008) Ultrafast time-resolved spectroscopy of xanthophylls at low temperature. *J. Phys. Chem. B* **112,** 3558-3567.

Croce, R., M. G. Müller, R. Bassi, and A. R. Holzwarth (2001) Carotenoid-to-chlorophyll energy transfer in recombinant major light-harvesting complex (LHC II) of higher plants. I. Femtosecond transient absorption measurements. *Biophys. J.* **80,** 901-915.

DeCoster, B., R. L. Christensen, R. Gebhard, J. Lugtenburg, R. Farhoosh, and H. A. Frank (1992) Low-lying electronic states of carotenoids. *Biochim. Biophys. Acta* **1102,** 107-114.

Dreizler, R. M. and E. K. U. Gross (1990) *Density functional theory*. Springer-Verlag, Berlin.

Dreuw, A. and M. Head-Gordon (2005) Single-reference ab intio methods for the calculation of excited states of large molecules. *Chem. Rev.* **105,** 4009-4037.

Egorova, D. and W. Domcke (2004) Coherent vibrational dynamics during ultrafast photoinduced electron-transfer reactions: quantum dynamical simulations within multilevel Redfield theory. *Chemical Physics Letters* **384,** 157-164.

Frank, H. A.(1999) The photochemistry of carotenoids. Kluver Academic Publishers, Dordrecht.

Frank, H. A., J. A. Bautista, J. Josue, Z. Pendon, R. G. Hiller, F. P. Sharples, D. Gosztola, and M. R. Wasielewski (2000) Effect of the solvent environment on the spectroscopic properties and dynamics of the lowest excited states of carotenoids. *J. Phys. Chem. B* **104,** 4569-4577.

Frank, H. A. and R. J. Cogdell (1996) Carotenoids in photosynthesis. *Photochem. Photobiol.* **63,** 257-264.

Frank, H. A., A. Cua, V. Chynwat, A. Young, D. Gosztola, and M. R. Wasielewski (1996) The lifetimes and energies of the first excited singlet states of diadinoxanthin and diatoxanthin: The role of these molecules in excess energy dissipation in algae. *Biochim. Biophys. Acta* **1277,** 243-252.

Frank, H. A., J. S. Josue, J. A. Bautista, I. van der Hoef, F. J. Jansen, J. Lugtenburg, G. Wiederrecht, and R. L. Christensen (2002) Spectroscopic and photochemical properties of open-chain carotenoids. *J. Phys. Chem. B* **106,** 2083-2092.

Fujii, R., T. Inaba, Y. Watanabe, Y. Koyama, and J.-P. Zhang (2003) Two different pathways of internal conversion in carotenoids depending on the length of the conjugated chain. *Chem. Phys. Lett.* **369,** 165-172.

Fujii, R., T. Ishikawa, Y. Koyama, M. Taguchi, Y. Isobe, H. Nagae, and Y. Watanabe (2001) Fluorescence spectroscopy of all-trans-anhydrorhodovibrin and spirilloxanthin: Detection of the $1B_u^-$ fluorescence. *J. Phys. Chem. A* **105,** 5348-5355.

Fujii, R., K. Onaka, H. Nagae, Y. Koyama, and Y. Watanabe (2001) Fluorescence spectroscopy of all-trans-lycopene: Comparison of the energy and the potential displacements of its $2A_g^-$ state with those of neurosporene and spheroidene. *J. Luminesc.* **92,** 213-222.

Gai, F., J. C. McDonald, and P. A. Anfinrud (1997) Pump–dump-probe spectroscopy of bacteriorhodosin: Evidence for a near-IR excited state absorbance. *J. Am. Chem. Soc.* **119,** 6201-6202.

Golub, G. H., P. C. Hansen, and D. P. O'Leary (1999) Tikhonov regularization and total least squares. *SIAM J. Matrix Anal. Appl.* **21,** 185-194.

Goodwin, T. W.(1980) The Biochemistry of the carotenoids. Chapman Hall, London,England.

Govindjee (1999) Carotenoids in photosynthesis: An historical perspective. In *The photochemistry of carotenoids*. pp. 1-15. Kluver Academic Publishers, Dordrecht.

Gradinaru, C. C., J. T. M. Kennis, E. Papagiannakis, I. H. M. van Stokkum, R. J. Cogdell, G. R. Fleming, R. A. Niederman, and R. van Grondelle (2001) An unusual pathway of excitation energy deactivation in carotenoids: Singlet-to-triplet conversion on an ultrafast timescale in a photosynthetic antenna. *Proc. Natl. Acad. Sci. USA* **98,** 2364-2369.

Grimme, S. (1996) Density functional calculations with configuration interaction for the excited states of molecules. *Chem. Phys. Lett.* **259,** 128-137.

Grimme, S. and M. Waletzke (1999) A combination of Kohn-Sham density functional theory and multi-reference configuration interaction methods. *J. Chem. Phys.* **111,** 5645-5655.

Gross, E. K. U. and W. Kohn (1990) Time-dependent density functional theory. *Adv. Quant. Chem.* **21,** 255.

Guglielmi, G., J. Lavaud, B. Rousseau, A. L. Etienne, J. Houmard, and A. V. Ruban (2005) The light-harvesting antenna of the diatom *Phaeodactylum tricornutum*. Evidence for a diadinoxanthin-binding subcomplex. *FEBS J.* **272,** 4339-4348.

Hashimoto, H., K. Yanagi, M. Yoshizawa, D. Polli, G. Cerullo, G. Lanzani, S. De Silvestri, A. T. Gardiner, and R. J. Cogdell (2004) The very early events following photoexcitation of carotenoids. *Arch. Biochem. Biophys.* **430,** 61-69.

Hauer, J., T. Buckup, and M. Motzkus (2008) Quantum control spectroscopy of vibrational modes: Comparison of control scenarios for ground and excited states in β-carotene. *Chem. Phys.* **350,** 220-229.

Hemley, R. and B. E. Kohler (1977) Electronic structure of polyenes related to the visual chromophore. A simple model for the observed band shapes. *Biophys. J.* **20,** 377-382.

Herman, P. and I. Barvik (2001) Towards proper parametrization in the exciton transfer and relaxation problem. II. Trimer. *Chemical Physics* **274,** 199-217.

Holzwarth, A. R. (1995) Time-resolved fluorescence spectroscopy. In *Methods in Enzymology. Vol.246 Biochemical Spectroscopy*.(Edited by K. Sauer), pp. 334-362. Academic Press, San Diego.

Holzwarth, A. R. (1996) Data analysis of time-resolved measurements. In *Biophysical Techniques in Photosynthesis. Advances in Photosynthesis Research*.(Edited by J. Amesz and A. J. Hoff), pp. 75-92. Kluwer Academic Publishers, Dordrecht.

Holzwarth, A. R. (2004) Light absorption and harvesting. In *Molecular to Global Photosynthesis*.(Edited by M. D. Archer and J. Barber), pp. 43-115. Imperial College Press, London.

Hsu, C.-P., S. Hirata, and M. Head-Gordon (2001) Excitation energies from time-dependent density functional theory for linear polyene oligomers: Butadiene to decapentaene. *J. Phys. Chem. A* **105,** 451-458.

Hudson, B. and B. Kohler (1974) Linear polyene electronic structure and spectroscopy. *Ann. Rev. Phys. Chem.* **25,** 437-460.

Hudson, B. S. and B. E. Kohler (1973) Polyene spectroscopy: The lowest energy excited singlet state of diphenyloctatetraene and other linear polyenes. *J. Chem. Phys.* **59,** 4984-5002.

Hudson, B. S., B. E. Kohler, and K. Schulten (1982) Linear Polyene Electronic Structure and Potential Surfaces. In *Excited States Vol. 6*.(Edited by E. C. Lim), pp. 1-95. Academic Press, New York.

Ikuta, M., A. Yabushita, F. S. Rondonuwu, J. Akahane, Y. Koyama, and T. Kobayashi (2006) The $1B_u^+$-> $3A_g^-$-> $1B_u^-$-> $2A_g^-$ internal conversion in carotenoids following the energy-gap law identified by 5 fs spectroscopy. *Chem. Phys. Lett.* **422,** 95-99.

IUPAC/IUB (1975) Nomenclature of carotenoids. *Pure Appl. Chem.* **41,** 405-431.

Jailaubekov, A. E., S. H. Song, M. Vengris, R. J. Cogdell, and D. S. Larsen (2010) Using narrowband excitation to confirm that the S* state in carotenoids is not a vibrationally-excited ground state species. *Chem. Phys. Lett.* **487,** 101-107.

Jean, J. M. and G. R. Fleming (1995) COMPETITION BETWEEN ENERGY AND PHASE RELAXATION IN ELECTRONIC CURVE CROSSING PROCESSES. *J. Chem. Phys.* **103,** 2092-2101.

Kleinschmidt, M., C. M. Marian, M. Waletzke, and S. Grimme (2009) Parallel multi-reference configuration interaction calculations on mini-*β*-carotenes and *β*-carotene. *J. Chem. Phys.* **130,** 044708-1-044708-11.

Kohler, B. E. and I. D. W. Samuel (1995) Experimental determination of conjugation lengths in long polyene chains. *J. Chem. Phys.* **103,** 6248-6252.

Kosumi, D., M. Fujiwara, R. Fujii, R. J. Cogdell, H. Hashimoto, and M. Yoshizawa (2009) The dependence of the ultrafast relaxation kinetics of the S_2 and S_1 states in *β*-carotene homologs and lycopene on conjugation length studied by femtosecond time-resolved absorption and Kerr-gate fluorescence spectroscopies. *J. Chem. Phys.* **130,** 214506-1-214506-8.

Kosumi, D., M. Komukai, H. Hashimoto, and M. Yoshizawa (2005) Ultrafast dynamics of all-*trans*-β-carotene explored by resonant and nonresonant photoexcitations. *Phys. Rev. Lett.* **95,** 213601-1-213601-4.

Koyama, Y., F. S. Rondonuwu, R. Fujii, and Y. Watanabe (2004) Light-harvesting function of carotenoids in photo-synthesis: The roles of the newly found $1^1B^-_u$ state. *Biopolymers* **74,** 2-18.

Kühn, O. and H. Naundorf (2003) Dissipative wave packet dynamics of the intramolecular hydrogen bond in *o*-phthalic acid monomethylester . *Phys. Chem. Chem. Phys.* **5,** 79-86.

Landl, G., T. Langthaler, H. W. Engl, and H. F. Kauffmann (1991) Distribution of event times in time-resolved fluorescence: The exponential series approach - algorithm, regularization, analysis. *J. Comput. Phys.* **95,** 1-28.

Larsen, D. S., E. Papagiannakis, I. H. M. van Stokkum, M. Vengris, J. T. M. Kennis, and R. van Grondelle (2003) Excited state dynamics of β-carotene explored with dispersed multi-pulse transient absorption. *Chem. Phys. Lett.* **381,** 733-742.

Liaaen-Jensen, S. and G. Kildahl-Andersen (2008) Blue carotenoids. *Arkivoc* **VI,** 5-25.

Lorenz-Fonfria, V. A. and H. Kandori (2006) Transformation of time-resolved spectra to lifetime-resolved spectra by maximum entropy inversion of the laplace transform. *Appl. Spectrosc.* **60,** 407-417.

MacPherson, A. N. and T. Gillbro (1998) Solvent dependence of the ultrafast S_2-S_1 internal conversion rate of β-carotene. *J. Phys. Chem. A* **102,** 5049-5058.

Marian, C. M. and N. Gilka (2008) Performance of the DFT/MRCI method on electronic excitation of exented π−systems. *J. Chem. Theory Comput.* **4,** 1501-1515.

Marian, C. M., S. C. Kock, C. Hundsdörfer, H.-D. Martin, W. Stahl, E. Ostroumov, M. Müller, and A. R. Holzwarth (2009) Spectroscopic properties of phenolic and quinoid carotenoids: A combined theoretical and experimental study. *Photochem. Photobiol. Sci.* **8,** 270-278.

Marques, M. A. L. and E. K. U. Gross (2004) Time-dependent density-functional theory. *Annu. Rev. Phys. Chem.* **55,** 427-455.

Martin, H. D., S. Kock, R. Scherrers, K. Lutter, T. Wagener, C. Hundsdörfer, S. Frixel, K. Schaper, H. Ernst, W. Schrader, H. Görner, and W. Stahl (2009) 3,3-Dihydroxyisorenieratene, a natural carotenoid with superior antioxidant and photoprotective properties . *Angew. Chem. Int. Ed.* **48,** 400-403.

Maslov, D. and Ostroumov, E. Diagnostics of photosynthesizing organisms by the method of nonlinear fluorimetry (2005). Proc. SPIE **5826**, 315-323, Dublin, Ireland

May, V. and O. Kühn (2000) *Charge and energy transfer dynamics in molecular systems: A theoretical introduction*. John Wiley & Sons, Berlin.

Mimuro, M., U. Nagashima, S. Takaichi, Y. Nishimura, I. Yamazaki, and T. Katoh (1992) Molecular Structure and Optical Properties of Carotenoids for the Invivo Energy Transfer Function in the Algal Photosynthetic Pigment System. *Biochim. Biophys. Acta* **1098,** 271-274.

Mukamel, S. (1995) *Principles of nonlinear optical spectroscopy*. Oxford University Press, New York.

Niedzwiedzki, D., J. F. Koscielecki, H. Cong, J. O. Sullivan, G. N. Gibson, R. R. Birge, and H. A. Frank (2007) Ultrafast dynamics and excited state spectra of open-chain carotenoids at room and low temperatures. *J. Phys. Chem. B* **111,** 5984-5998.

Niedzwiedzki, D. M., D. J. Sandberg, H. Cong, M. N. Sandberg, G. N. Gibson, R. R. Birge, and H. A. Frank (2009) Ultrafast time-resolved absorption spectroscopy of geometric isomers of carotenoids. *Chemical Physics* **357,** 4-16.

Niedzwiedzki, D. M., J. O. Sullivan, T. Polivka, R. R. Birge, and H. A. Frank (2006) Femtosecond time-resolved transient absorption spectroscopy of xanthophylls. *J. Phys. Chem. B* **110,** 22872-22885.

Nybraaten, G. and S. Liaaen-Jensen (1971) Characterization of phenolic carotenoids. *Acta Chem. Scand.* **25,** 370-372.

O'Neill, L. and H. J. Byrne (2005) Structure-property relationships for electron-vibrational coupling in conjugated organic oligomeric systems. *J. Phys. Chem. B* **109,** 12685-12690.

Ostroumov, E., M. G. Müller, C. M. Marian, M. Kleinschmidt, and A. R. Holzwarth (2009) Electronic coherence provides a direct proof for energy-level crossing in photoexcited lutein and β-carotene. *Phys. Rev. Lett.* **103,** 108302-1-108302-4.

Papagiannakis, E., S. K. Das, A. Gall, I. H. M. van Stokkum, B. Robert, R. van Grondelle, H. A. Frank, and J. T. M. Kennis (2003) Light harvesting by carotenoids incorporated into the B850 light-harvesting complex from *Rhodobacter sphaeroides* R-26.1: Excited-state relaxation, ultrafast triplet formation, and energy transfer to bacteriochlorophyll. *J. Phys. Chem. B* **107,** 5642-5649.

Papagiannakis, E., J. T. M. Kennis, I. H. M. van Stokkum, R. J. Cogdell, and R. van Grondelle (2002) An alternative carotenoid-to-bacteriochlorophyll energy transfer pathway in photosynthetic light harvesting. *Proc. Natl. Acad. Sci. USA* **99,** 6017-6022.

Papagiannakis, E., I. H. M. van Stokkum, H. Fey, C. Büchel, and R. van Grondelle (2005) Spectroscopic characterization of the excitation energy transfer in the fucoxanthin-chlorophyll protein of diatoms. *Photosynth. Res.* **86,** 241-250.

Papagiannakis, E., I. H. M. van Stokkum, R. van Grondelle, R. A. Niederman, D. Zigmantas, V. Sundström, and T. Polivka (2003) A near-infrared transient absorption study of the excited-state dynamics of the carotenoid spirilloxanthin in solution and in the LH1 complex of *Rhodospirillum rubrum*. *J. Phys. Chem. B* **107,** 11216-11223.

Papagiannakis, E., I. H. M. van Stokkum, M. Vengris, R. J. Cogdell, R. van Grondelle, and D. S. Larsen (2006) Excited-state dynamics of carotenoids in light-harvesting complexes. 1. Exploring the relationship between the S_1 and S* states. *J. Phys. Chem. B* **110,** 5727-5736.

Pariser, R. (1956) Electronic spectrum and structure of azulene. *J. Chem. Phys.* **25,** 1112-1116.

Parr, R. G. and W. Yang (1989) *Density-functional theory of atoms and molecules*. Oxford University Press, New York.

Perez Lustres, J. L., A. L. Dobryakov, A. R. Holzwarth, and M. Veiga (2007) S_2 ->S_1 internal conversion in β-carotene: Strong vibronic coupling from amplitude oscillations of transient absorption bands. *Angew. Chem. Int. Ed.* **46,** 3758-3761.

Peterman, E. J. G., T. Pullerits, R. van Grondelle, and H. van Amerongen (1997) Electron-phonon coupling and vibronic fine structure of light-harvesting complex II of green plants: Temperature dependent absorption and high-resolution fluorescence spectroscopy. *J. Phys. Chem. B* **101,** 4448-4457.

Peterman, E. J. G., H. van Amerongen, R. van Grondelle, and J. P. Dekker (1998) The nature of the excited state of the reaction center of photosystem II of green plants: A high-resolution fluorescence spectroscopy study. *Proc. Natl. Acad. Sci. USA* **95,** 6128-6133.

Pfiffi, D., B. A. Bier, C. M. Marian, K. Schaper, and C. A. M. Seidel (2010) Diphenylhexatrienes as photoprotective agents for ultrasensitive fluorescence detection. *J. Phys. Chem. A* **114,** 4099-4108.

Pieper, J., M. Rätsep, R. Jankowiak, K.-D. Irrgang, J. Voigt, G. Renger, and G. J. Small (1999) Q(Y)-level structure and dynamics of solubilized light- harvesting complex II of green plants: Pressure and hole burning studies. *J. Phys. Chem. A* **103,** 2412-2421.

Pisliakov, A. V., T. Mancal, and G. R. Fleming (2006) Two-dimensional optical three-pulse photon echo spectroscopy. II. Signatures of coherent electronic motion and exciton population transfer in dimer two-dimensional spectra. *J. Chem. Phys.* **124,** 234505-1-234505-14.

Plakhotnik, T. (2006) Optical Bloch equations and enhanced decay of Rabi oscillations in strong driving fields. *Chem. Phys.* **321,** 337-340.

Polivka, T., R. G. Hiller, and H. A. Frank (2007) Spectroscopy of the peridinin–chlorophyll-α protein: Insight into light-harvesting strategy of marine algae. *Arch. Biochem. Biophys.* **458,** 111-120.

Polivka, T. and V. Sundström (2004) Ultrafast dynamics of carotenoid excited states-from solution to natural and artificial systems. *Chem. Rev.* **104,** 2021-2071.

Polivka, T. and V. Sundström (2009) Dark excited states of carotenoids: Consensus and controversy. *Chem. Phys. Lett.* **477,** 1-11.

Polivka, T., D. Zigmantas, J. L. Herek, Z. He, T. Pascher, T. Pullerits, R. J. Cogdell, H. A. Frank, and V. Sundström (2002) The carotenoid S_1 state in LH2 complexes from purple bacteria *Rhodobacter sphaeroides* and *Rhodopseudomonas acidophila*: S_1 energies, dynamics, and carotenoid radical formation. *J. Phys. Chem. B* **106,** 11016-11025.

Polivka, T., D. Zigmantas, V. Sundström, E. Formaggio, G. Cinque, and R. Bassi (2002) Carotenoid S_1 state in a recombinant light-harvesting complex of photosystem II. *Biochem.* **41,** 439-450.

Redfield, A. G. (1957) On the theory of relaxation processes. *IBM Journal* 19-31.

Renger, T. and A. R. Holzwarth (2008) Theory of excitation energy transfer and optical spectra of photosynthetic systems. In *Biophysical Techniques in Photosynthesis*.(Edited by T. J. Aartsma and J. Matysik), pp. 421-443. Springer, Dordrecht.

Ritz, T., A. Damjanovic, K. Schulten, J.-P. Zhang, and Y. Koyama (2000) Efficient light harvesting through carotenoids. *Photosynth. Res.* **66,** 125-144.

Sander, L. C., K. Epler Sharpless, N. E. Craft, and S. A. Wise (1994) Development of engineered stationary phases for the separation of carotenoid isomers. *Anal. Chem.* **66,** 1667-1674.

Sashima, T., Y. Koyama, T. Yamada, and H. Hashimoto (2000) The $1B_u^+$, $1B_u^-$, and $2A_g^-$ energies of crystalline lycopene, beta-carotene, and mini-9-β-carotene as determined by resonance-Raman excitation profiles: Dependence of the $1B_u^-$ state energy on the conjugation length. *J. Phys. Chem. B* **104,** 5011-5019.

Sashima, T., H. Nagae, M. Kuki, and Y. Koyama (1999) A new singlet-excited state of all-*trans*-spheroidene as detected by resonance-Raman excitation profiles. *Chem. Phys. Lett.* **299,** 187-194.

Sashima, T., M. Shiba, H. Hashimoto, H. Nagae, and Y. Koyama (1998) The $2A_g^-$ energy of crystalline all-trans-spheroidene as determined by resonance-Raman excitation profiles. *Chem. Phys. Lett.* **290,** 36-42.

Schäfer, A., B. Horn, and R. J. Ahlrichs (1992) Fully optimized contracted Gaussian basis sets for atoms Li to Kr. *J. Chem. Phys.* **97,** 2571-2577.

Schulten, K., I. Ohmine, and M. Karplus (1976) Correlation effects in the spectra of polyenes. *J. Chem. Phys.* **64,** 4422-4441.

Siemiarczuk, A., B. D. Wagner, and W. R. Ware (1990) Comparison of the maximum entropy and exponential series methods for the recovery of distributions of lifetimes from fluorescence lifetime data. *J. Phys. Chem.* **94,** 1661-1666.

Stepanov, B. I. (1957) A universal relation between the absorption and luminescence spectra of complex molecules. *Dokl. Akad. Nauk SSSR* **112,** 839-841.

Tavan, P. and K. Schulten (1986) The low-lying electronic excitations in long poylenes: A PPP-MRD-Cl study. *J. Chem. Phys.* **85,** 6602-6609.

Tavan, P. and K. Schulten (1987) Electronic excitations in finite and infinite polyenes. *Phys. Rev. B* **36,** 4337-4358.

van Stokkum, I. H. M., D. S. Larsen, and R. van Grondelle (2004) Global and target analysis of time-resolved spectra. *Biochim. Biophys. Acta* **1657,** 82-104.

Wohlleben, W., T. Buckup, H. Hashimoto, R. J. Cogdell, J. L. Herek, and M. Motzkus (2004) Pump-deplete-probe spectroscopy and the puzzle of carotenoid dark states. *J. Phys. Chem. B* **108,** 3320-3325.

Wohlleben, W., T. Buckup, J. L. Herek, R. J. Cogdell, and M. Motzkus (2003) Multichannel carotenoid deactivation in photosynthetic light harvesting as identified by an evolutionary target analysis. *Biophys. J.* **85,** 442-450.

Young, A. J. and Britton, G.(1993) Carotenoids in photosynthesis. Chapman & Hall, London.

Zhang, J.-P., R. Fujii, Y. Koyama, F. S. Rondonuwu, Y. Watanabe, A. Mortensen, and L. H. Skibsted (2001) The $1B_u$-type singlet state of β-carotene as a precursor of the radical cation found in chloroform solution by sub-picosecond time-resolved absorption spectroscopy. *Chem. Phys. Lett.* **348,** 235-241.

Zhang, J.-P., R. Fujii, P. Qian, T. Inaba, T. Mizoguchi, Y. Koyama, K. Onaka, and Y. Watanabe (2000) Mechanism of the Carotenoid-to-bacteriochlorophyll energy transfer via the S_1 state in LH2 complexes from purple bacteria. *J. Phys. Chem. B* **104,** 3683-3691.

Zhao, Y. and R. S. Knox (2000) A brownian oscillator approach to the kennard-stepanov relation. *Journal of Physical Chemistry A* **104,** 7751-7761.

Zigmantas, D., R. G. Hiller, F. P. Sharples, H. A. Frank, V. Sundström, and T. Polivka (2004) Effect of a conjugated carbonyl group on the photophysical properties of carotenoids. *Phys. Chem. Chem. Phys.* **6,** 3009-3016.

Zigmantas, D., R. G. Hiller, V. Sundström, and T. Polivka (2002) Carotenoid to chlorophyll energy transfer in the peridinin- chlorophyll-a-protein complex involves an intramolecular charge transfer state. *Proc. Natl. Acad. Sci. USA* **99,** 16760-16765.

Zigmantas, D., T. Polivka, R. G. Hiller, A. Yartsev, and V. Sundström (2001) Spectroscopic and dynamic properties of the peridinin lowest singlet excited states. *J. Phys. Chem. A* **105,** 10296-10306.

List of publications

Published:

Ostroumov EE, Müller MG, Hundsdörfer C, Stahl W, Marian CM, and Holzwarth AR. Excited state relaxation dynamics and electronic properties of a quinoid carotenoid. Chem. Phys. (2010), doi:10.1016/j.chemphys.2010.04.030.

Marian CM, Kock SC, Hundsdörfer C, Martin H-D, Stahl W, Ostroumov E, Müller M, and Holzwarth AR. Spectroscopic properties of phenolic and quinoid carotenoids: A combined theoretical and experimental study. Photochem.Photobiol. Sci. (2009), 8:270-278.

Ostroumov E, Müller MG, Marian CM, Kleinschmidt M, and Holzwarth AR. Electronic coherence provides a direct proof for energy-level crossing in photoexcited lutein and β-carotene. Phys. Rev. Lett. (2009), 103:108302.

Ostroumov EE, Fadeev VV, Khristin MS, Pashchenko VZ, and Tusov VB. Fluorescence characteristics and photophysical parameters of light-harvesting chlorophyll *a/b* complex aggregates. Biophysics (Biofizika) (2007), 52:462-467.

Submitted:

Ostroumov EE, Müller MG, Reus M and Holzwarth AR. On the nature of the "dark S*" excited state of β-carotene, (2010).

To be submitted:

Ostroumov EE, Müller MG, and Holzwarth AR. Ultrafast relaxation dynamics of Lutein: The Redfield theory approach, (2010).

Ostroumov EE, Lambrev P, Barros T, Wientjes E, Reus M, Jahns P, Croce R, Kühlbrandt W, and Holzwarth AR. Fluorescent chlorophyll charge transfer states as intermediates in the excited state quenching of light-harvesting complex II, (2010).

Acknowledgements

I would like to express my sincere gratitude to Prof. Alfred Holzwarth for giving me the opportunity to work on the very interesting and diverse topics at the frontiers of science and to thank for giving me a chance to touch the basic research. I am grateful to Michael Reus not only for preparation of all the samples, but also for his help and assistance any time with any problem in the lab. I thank Dr. Marc Muller for the help with the laser systems, always keeping them working, and for the analysis of the data with all possible models.

I sincerely thank Prof. Christel Marian from Düsseldorf University for very fruitful collaboration. All the quantum chemical calculations have been performed in her group and Prof. Marian was always ready to provide the necessary data, proof-read our papers and to discuss problems. I thank our colleagues Dr. Claas Hundsdörfer, Dr. Sebastian Kock and Prof. Wilhelm Stahl from Düsseldorf University for providing the DHIR and DHIR-Q carotenoids. This collaboration resulted in two publications.

A large part of my work on photosynthetic organisms is not included in this thesis. However I would like to thank our collaborators for their help with the samples. Dr. Manuela Nilkens and Prof. Peter Jahns (Düsseldorf University) kindly provided us with the isolated LHCII complexes as well as the whole leaves of *Arabidopsis thaliana*. I gratefully acknowledge Prof. Navasard Karapetyan and Dr. Marina Rakhimberdieva (A.N.Bach Institute of Biochemistry, Moscow) for introducing me into the field of cyanobacteria, providing any possible mutants and for very interesting discussions. I am grateful to Dr. Silke Johanning and Prof. Eckhard Hofmann (Bochum University) for the collaboration on the dinoflagellate algae and providing them in huge amounts and concentrations. I thank Dr. Tiago Barros (formerly Max-Planck-Institute for Biophysics, Frankfurt) for the providing the crystalline LHCII complexes and group of Prof. Markus Motzkus (formerly Philipps-University, Marburg) especially Dr. Tiago Buckup for introducing me into the FWM spectroscopy of carotenoids.

I am very grateful to my M.S. supervisor Prof. Victor Fadeev from M.V. Lomonosov Moscow State University for introducing me into the field of optical spectroscopy and his help and assistance during my studies. I am thankful to my colleagues Dr. Tatiana Dolenko and Dr. Sergei Burikov for sharing our working time, our tea and coffee breaks with relaxing discussions and our joint conference trips.

My special thanks to all my colleagues from Max-Planck-Institute for Bioinorganic Chemistry, Mülheim for their help in the lab and all the fun we had together. Especially to Dr. Jens Niklas and Dr. Alexey Silakov for our joint trips to rocks of the Mediterranean and Citymonkey business.

And finally I am very grateful to my parents for their encouragement, advices, support and patience.